PACIFIC EARTHQUAKE ENGINEERING RESEARCH CENTER

Uncertainty and Correlation in Seismic Risk Assessment of Transportation Systems

Renee G. Lee

and

Anne S. Kiremidjian

Stanford University

PEER 2007/05
JULY 2007

Uncertainty and Correlation in Seismic Risk Assessment of Transportation Systems

Renee G. Lee
Department of Civil and Environmental Engineering
Stanford University, Stanford

Anne S. Kiremidjian
Department of Civil and Environmental Engineering
Stanford University, Stanford

PEER Report 2007/05
Pacific Earthquake Engineering Research Center
College of Engineering
University of California, Berkeley

July 2007

ABSTRACT

This report describes the research and application of ground motion and damage correlation models affecting risk assessment for spatially distributed lifeline systems with specific emphasis on transportation networks. Deterministic and probabilistic seismic risks of the system are assessed for direct structural loss and network reliability. As a result of potentially underestimating system risk, high-cost economic decisions may be conservative.

Two different ground motion correlation models are developed and compared. The sensitivity of loss uncertainty to damage correlation is evaluated. These two different sources of correlation are observed to impact the loss coefficient of variation differently; however, this difference is not significant. It is demonstrated in this study that when ground motion and damage correlation are introduced, the loss distribution becomes increasingly heavy tailed for sample network applications. Furthermore, simulations for dependent link travel times resulted in three different optimal emergency routing configurations for the network application in this report.

Annual seismic risk exceedance curves for system loss and network reliability are developed, with and without correlations. These resulting bounds on risk are more informative to risk decision makers than a single point estimate of the loss.

ACKNOWLEDGMENTS

This work was supported primarily by the Earthquake Engineering Research Centers Program of the National Science Foundation under award number EEC-9701568 through the Pacific Earthquake Engineering Research (PEER) Center.

Any opinions, findings, and conclusions or recommendations expressed in this material are those of the author(s) and do not necessarily reflect those of the National Science Foundation.

We would like to gratefully acknowledge Professor Yue Yue Fan and Mr. Changzheng Liu of the University of California at Davis for their collaboration in the adaptive routing analyses section of this report. This collaborative effort resulted in Figures 4.11–13. We sincerely appreciate Dr. Charles Menun for providing the CARDINAL software. Our gratitude goes also to Ms. Meredith Williams for her extensive assistance with GIS and, in particular, with the development of the map shown in Figure 5.4.

CONTENTS

LIST OF FIGURES

LIST OF TABLES

1 Introduction

1.1 BACKGROUND

This study addresses the effect of spatial ground motion correlation and structure-to-structure damage correlation on seismic risk to spatially distributed transportation systems. In particular, the study focuses on how these sources of correlation impact estimation of structural damage and loss to network bridges, network reliability, and post-even routing. The study incorporates uncertainties in earthquake descriptors to evaluate the effects of correlation on system risk curves.

Currently, no framework for quantifying the correlation parameter in ground motion and in damage exists. Consequently, no systematic methodology exists for incorporating correlation effects into the transportation risk problem. Existing models ignore both variability and correlation on a network, and rely only on first-order estimates of a highly random, highly correlated problem. The methodologies introduced here are intended to overcome this shortcoming.

Seismic risk assessment had been previously based on ad-hoc scenario events, each providing a snapshot of expected system performance. Earthquakes, however, are stochastic in nature. Efficient techniques for representing the uncertainties in earthquake occurrences are developed in this report for use in a full probabilistic seismic risk assessment of the spatially distributed network. In addition, variability in system risk is accounted for by introducing efficient methods for ground motion and damage simulation in the network.

Seismic risk models for spatially distributed transportation systems have generally not taken into consideration correlation between components in their representation of risk. The inclusion of uncertainty and correlation shifts the seismic loss and reliability exceedance curves. This effect is significant in the upper tail of the loss distribution, where risk to civil infrastructure

is of primary interest to insurers, re-insurers, property owners, and urban planners. As a result of underestimating system risk, high-cost economic decisions such as pre-event mitigation strategies or post-event reconstruction and emergency routing are conservatively based. This work demonstrates not only these shifts in the seismic risk curves, but also the effect correlation may have on post-event routing and pre-event mitigation in a case study.

1.2 OBJECTIVE

The objective of this work, focused on a spatially distributed transportation network, is three-fold. The first objective is to provide a systematic methodology for incorporating the spatial ground motion and structure-to-structure damage correlation in a scenario-based seismic risk assessment. The second objective is to model damage dependencies in the network using a computationally efficient approach. The goal of this objective is to be able to extend these risk studies to larger networks, to simulate these analyses for many earthquake scenarios, and to study the effect of dependencies in the network in optimal emergency routing. The third objective is to demonstrate the effects of correlation on system risk curves and the use of importance measures for components in a preliminary retrofit decision-making framework. The study includes the following tasks:

- Review existing methodologies for seismic risk assessment of transportation networks.
- Identify two types of spatial ground motion correlation model and one type of structure-to-structure damage correlation model to be used in this research. Establish an analytical framework and closed form solution to solve first and second-order statistics on direct loss. The framework incorporates both types of correlation into the direct loss assessment.
- Formulate efficient simulation procedures to simulate a correlated random field of ground motion and to model the discrete damage state dependencies between bridges in the network. These simulation techniques are used to study the direct loss distribution for a network, to observe parameter sensitivities in the loss distribution, and to demonstrate the importance of correlation effects in optimal emergency post-event routing.
- Formulate a procedure for identifying a reduced catalog of earthquake events to represent the hazard, i.e., the spatial and temporal uncertainties of earthquake arrivals, for a spatially extended region. Based on this catalog and the procedures outlined previously,

annual seismic risk exceedance curves for system loss and reliability are developed. Bounds on the loss exceedance rate, bounds on the direct aggregate loss for a given level of risk tolerance, bounds on system reliability, and improvements to system risk curve as a result of various retrofit efforts are quantified.

- Consider future research extending applications into operational/network analysis by (1) illustrating the effect of correlation on traveler routing post-event, (2) modeling the transportation system as a stochastic network to capture the redistribution of traffic after bridge failures, and (3) including operational losses in the retrofit framework.

1.3 SCOPE

This research focuses on transportation networks as one class of spatially distributed systems. However, the underlying criteria for spatial ground motion correlation and structure-to-structure damage correlation remain the same when assessing the risk to other types of spatially distributed systems. Although only direct loss is considered for illustrative purposes, the models can be extended to other risk metrics. Life loss and collateral damage are not investigated in this work. Also, damage to structures is assumed to result from ground shaking alone and not also from other modes of failure such as liquefaction or landslides.

Operational loss is discussed through a case study. The study explores the effect of correlation on the shortest-path routing problem for a single origin to a single destination. This study does not attempt to solve the multiple-origin multiple-destination emergency routing problem.

1.4 ORGANIZATION OF REPORT

Chapter 2 is a review of the current methodologies used for risk assessment of spatially distributed systems, with a focus on transportation networks. In Chapter 3, correlation metrics are developed and incorporated in the analytical loss framework. In Chapter 4, efficient simulation algorithms are developed for modeling dependencies in the network components which are then applied to parameter sensitivity studies and post-event optimal routing simulation. Chapter 5 explores the effect of correlation on system risk curves by extending

scenario-based analysis to a full probabilistic seismic risk model. Conclusions and direction of future work are presented in Chapter 6.

2 Review of Seismic Risk-Assessment Methodology and Literature

Modeling of spatially distributed transportation systems is particularly challenging because it requires modeling of a random field of multiple components under multiple earthquakes which occur randomly in time. This entails characterization of the spatial variability of ground motion and spatial variability of damage at multiple sites in a network during any given earthquake event.

This chapter reviews prior research in risk-assessment methodologies for spatially distributed transportation networks, which can be subdivided into two broad categories as described here. These categories include (1) deterministic seismic risk assessment and (2) probabilistic seismic risk assessment. Each of these two major subsections contains a discussion of contributions as well as shortcomings found in previous work. The current work aims to address or resolve many of these shortcomings.

2.1 DETERMINISTIC SEISMIC RISK ASSESSMENT FOR SPATIALLY DISTRIBUTED SYSTEMS

Deterministic seismic risk analysis (DSRA) employs one or more earthquake scenarios to characterize the hazard. The earthquake scenarios are treated as deterministic in magnitude and in location. However, ground motion intensity and structural damage are treated probabilistically. Risk is associated with the impact a disaster has on society and can be described in terms of the following metrics: casualties, damage to civil infrastructure, and downtime loss. This risk may either be deterministically or probabilistically assessed under the influence of the controlling event(s). Because of the interconnected nature of bridges and roadways, the network must be analyzed under each scenario event systematically.

One challenge lies in identifying scenarios for analysis. Scenario selection is typically based on a worst-case scenario or design scenario. Different types of scenarios used in earthquake engineering applications include the maximum credible earthquake (MCE), safe shutdown earthquake (SSE), maximum probable earthquake (MPE), design basis earthquake (DBE), operating basis earthquake (OBE), or seismic safely evaluation earthquake (Kramer 1996).

Much of the prior work in transportation network risk assessment has relied on a deterministic scenario-based approach. DSRA research for highway networks was undertaken in the mid-1990s for Shelby County, Tennessee, an area situated close to the New Madrid fault zone. In Werner et al. (1997) and Werner and Taylor (1995), four scenario earthquakes were used to determine the expected performance of a highway network consisting of 286 bridges.

In Basöz and Kiremidjian (1996), the risk to a transportation network was determined by also considering deterministic scenario events. From the distribution of ground motion at a site, the expectation of the structural damage state and the expected utility of a bridge on the network were assessed for a deterministic scenario event. These values were formulated with the goal of prioritizing bridges for retrofit based on seismic vulnerability, importance on network functionality, and historical significance among other factors. A probabilistic approach was implicitly used in this research by considering the 500-year-return-period intensity measure (IM) from site hazard curves.

In later research by Basöz and Kiremidjian (1998), an advanced classification scheme and improved fragility functions were developed to reduce the uncertainty in risk modeling for highway networks. The intention of these research efforts was to address gross uncertainties in bridge classification systems. Around this time, other improved bridge classification methods and fragility functions were developed (Shinozuka et al. 2000; Basöz and Mander 1999; HAZUS 2002). Kiremidjian et al. (2006) assessed damage and resulting disruption to the San Francisco Bay Region (SFBR) transportation network using four earthquake scenario events based on the HAZUS classification of bridges. Risk assessment on such a large scale was possible through a geographic information systems (GIS) platform. A macro-scale study of the network, which consisted of 2,640 bridges, was undertaken. Under each scenario event, network delays for fixed- and variable-trip demand were reported. Post-event emergency response planning for six hospitals in Alameda County, in the San Francisco Bay Area, was based on expected levels of damage to the components in the network.

Shinozuka et al. (2000) conducted a scenario-based study for the 2,225 bridges in the Los Angeles and Orange County region transportation network. In contrast to Kiremidjian et al. (2006), this study used a Monte Carlo simulation (ten replications) to generate damage states for each bridge on the network. A different classification system for bridges and thus different fragility functions were used in contrast to other DSRA research efforts. The analysis revealed the expected configuration of damaged links to the area networks under the Elysian Park earthquake scenario.

The scenario-based DSRA, while informative, has limitations. First, one seismogenic source is considered at a time, and one event on that source is designated as the scenario under consideration. An event may almost certainly be constructed which contradicts conclusions drawn from another single-event risk assessment. Secondly, the likelihood of the ground motion intensities produced by the selected earthquake scenario is not clear. In contrast, the PSRA takes into consideration different sources and combines their contributions into a frequency of exceeding a risk measure. A discussion of PSRA follows next.

2.2 PROBABILISTIC SEISMIC RISK ASSESSMENT FOR SPATIALLY DISTRIBUTED SYSTEMS

A probabilistic seismic risk assessment (PSRA) for spatially distributed systems takes into consideration all possible earthquakes that may affect the system. This entails characterizing the uncertainties associated with the size and occurrence of earthquakes in a region. The state of current research in PSRA for lifeline systems has been influenced by early works including but not limited to Moghtaderi-Zadeh and Diamantidis (1986), Taylor et al. (1985), Moghtaderi-Zadeh (1990), and Taleb-Agha (1977). Due to computational limitations during that time, Moghtaderi-Zadeh et al. (1982), like others, treated uncertainty in ground motion and in damage as "secondary in importance when compared with the uncertainty in earthquake magnitude and location." However, with improved computing power, these types of uncertainties could be reasonably treated in a full PSRA.

PSRA is rooted in the probabilistic seismic hazard analysis (PSHA) framework, which incorporates the stochastic uncertainties in earthquake processes, thereby defining explicitly the seismic hazard for a site or extended area.

The general PSRA framework is given in Equation (2.1) below:

$$\nu_L = P\left[L > l \mid t \in [0,1]\right]$$

$$= \sum_{\substack{all \\ fault \\ sources,i}} \nu_i \left(\int\int\int\int P\left[L > l \mid D\right] f_{D|IM}\left(d|im\right) f_{IM|R,M}\left(im|r,m\right) f_{R|M}\left(r \mid m\right) f_M\left(m\right) dd\, dim\, dr\, dm \right) \tag{2.1}$$

where,

L = loss (or other risk metric)

t = time (years)

M = magnitude of event

R = distance from source to site (km)

IM = ground motion intensity measure (g)

ν_i = al rate of occurrence of earthquakes generated by source i

$f_X(x)$ = Probability density

For the purposes of PSRA, a catalog of scenarios is compiled or generated so that the uncertainty in earthquake descriptors, or probabilistic hazard, is sufficiently represented in that catalog. It should be noted that in a complete PSRA, risk is now treated by a summation over all possible events generated by all fault sources in a region.

More recent work in seismic risk for transportation networks has incorporated uncertainties of earthquake occurrence into post-event loss assessment. Chang et al. (2000) present a method for identifying a catalog of earthquake scenario events to be used in a PSRA for spatially distributed systems. In their paper, a limited set of scenarios ($\overline{Q}_j, j=1\ldots M$) is identified. The $\overline{Q}_j$'s in this set are chosen in order to reflect different levels of system performance denoted by *S*. Each of the earthquakes in the set is weighted appropriately to best match local site ground motion intensity hazard curves based on all possible earthquakes ($Q_i, i=1\ldots N$) occurring with annual probability, p_i. These weights are referred to as "hazard consistent probabilities." Using their notation, hazard consistent probabilities, $\overline{p}_j$, are adjusted to match the hazard as reflected in Equation (2.2).

$$\sum_{j=1}^{M}\left(S|\overline{Q}_j\right)\cdot\overline{p}_j \approx \sum_{i=1}^{N}\left(S|Q_i\right)\cdot p_i \tag{2.2}$$

Shinozuka et al. (2003), used the catalog generated from Chang et al.'s (2000) hazard matching method, to evaluate performance of transportation networks in the Los Angeles–Orange County area. In a somewhat related work, Campbell and Seligson (2003) presented a method for selecting an earthquake catalog to be consistent with average hazard in a region. However, for every damage level, a different earthquake catalog was identified. Their earthquake catalogs ranged in size from a few earthquakes to as many as 12 earthquakes.

For modeling the earthquake uncertainty, simulation is relied on when analytical solutions are infeasible. With the PSRA, an exhaustive search over all possible earthquakes in a seismic region can be achieved through Monte Carlo methods. Simulation techniques for hazard assessment have been used in many fields with early work by Friedman (1975), Clark (1986), and Steinbrugge (1982). For seismic risk application on transportation networks Taylor et al. (2001) used conventional Monte Carlo simulation to sample earthquakes exhaustively over a finite time horizon. Their research introduced the concept of a "walk-through" table. The table was synonymous with an earthquake catalog representing the hazard in an area. Typically, very long time horizons were used to ensure that a sufficient number of earthquakes were sampled. Though the processes describing seismicity are non-stationary over such time horizons, they are often assumed to be so for simplicity. Time horizons used by previous research in this area include 10,000–50,000 years (Wesson and Perkins 2001; Bazzurro and Luco 2005; Taylor et al. 2001; Cho et al. 2003).

2.2.1 Decision Variable: Loss and System Reliability

The risk to a system is defined in terms of quantities that are meaningful to a decision maker. Decision makers include urban or city planners, government policy makers, emergency planning commissions, private insurers, or property owners. Loss is one form of risk due to seismic hazards, and can be subdivided into two major categories: direct and indirect loss.

Direct loss is defined as the economic cost to repair structural damage to components. The expected damage factor for bridge structures as a function of damage state and structural dimensions are published in HAZUS (2002). Dollar loss per square unit of deck space used herein is based on reported values by Caltrans (2004).

In lieu of using stochastic network analyses to quantify the indirect loss, the reliability of a sub-network is used as a means of describing network operability post-event. Although traffic flow and redistribution are not considered in modeling post-event routes (see Chapter 4), the viability of an origin-to-destination path is assessed via Dijkstra's least-cost path algorithm. Likewise, a reliability assessment for a sample sub-network is based on the viability of an origin-to destination path. Prior research in reliability for transportation network systems have included work by Taleb-Agha (1977), Moghtaderi-Zadeh et al. (1982), Shinozuka et al. (1988), Augusti et al. (1998), and Loh and Lee. (2003).

2.2.2 Spatial Ground Motion and Damage Correlation

Significant levels of ground motion correlation are a known seismic phenomenon (Jeon and O'Rourke 2005; Wang and Takada 2005). The ground motion correlation has been previously considered in risk application by assuming a correlation structure (McGuire 1990; Wesson and Perkins 2001), or by modeling extremes in correlation.

Structure-to-structure damage correlations have been considered in previous literature for portfolios of built structures (Bazzurro and Luco 2005). However for bridge structures on a network, neither closed-form solutions nor data for these correlations exist. It is demonstrated later in this report, however, that assuming a lack of correlation underestimates risk uncertainty. Thus, it is critical to incorporate these ground motion and damage correlation effects into the analysis of network uncertainty for spatially distributed transportation networks, and to consider how various modeling assumptions affect the risk assessment.

3 Spatial Ground Motion Correlation and Structure-to-Structure Damage Correlation: Analytical Framework

3.1 MOTIVATION AND OVERVIEW OF SPATIAL CORRELATION

Economic losses from damage to a lifeline network in the event of a future earthquake are highly uncertain. Uncertainties result from the randomness and correlatedness of the ground motion intensities and structural damage to components on a network. The analytical loss models which incorporate correlation effects have not been previously formulated and are critical for understanding system-wide uncertainty.

The emphasis of this chapter is the development of a framework for ground motion correlation and damage correlation analysis. Such analysis needs to be performed for each scenario event in a probabilistic seismic risk assessment, which is the subject of Chapter 5. Thus, the loss analysis here will be restricted to a single-scenario event without loss of generality. For a given scenario, a magnitude and location of rupture in space are deterministically defined.

In order to simplify risk assessment for a spatially distributed network, modeling assumptions are made which may compromise accuracy in loss analysis. Some commonly used assumptions include generalizing the location of a group of sites to a single site, treating random quantities simply as expectations, ignoring spatial correlation in ground motion intensity between sites, or ignoring the damage correlation that may exist between different network components.

Ground motion correlation is relevant because bridges within a transportation network are affected by the same earthquake. Correlation effects arise not only through source-to-site distances and generic soil classes, but also through the frequency content of earthquake waves

arriving at a site, intervening geologic conditions in the path of propagation, directivity effects, and local site-specific conditions. Two different correlation models for ground motion intensities are discussed in this chapter.

From a damage perspective, there may be structural or geotechnical characteristics specific to a group of bridges that are not captured within very general structural damage models. Additionally, an ensemble of bridges may share similar structural behavior if they were built within the same time frame (Bazzurro and Luco 2005). This is because similar design and build guidelines and similar contractors are used per state department of transportation, federal highway administration, and/or other government and private entities. Similarities are not all explicitly accounted for in the overall structural classification schemes. Bridges are grouped into broad structural sub-types based on shared features such as abutment type, number of spans, type of superstructure and substructure, length and width of the bridge, skew, number of hinges at joints and bents, abutment and column foundation types, and design year (NIBS, 2002; ATC-13, 1985). In California, these structural attributes are obtained from the Structural Maintenance System (SMS) database compiled and managed by Caltrans (1993).

A methodology is presented for analyzing the effects of uncertainty and correlation on direct physical loss to a sample network. The analysis is focused on quantifying levels of risk that any closely spaced network may face given a large scenario event as presented here. The analysis involves preliminary characterization of the ground motion parameters and the bridge fragility function parameters as well as a definition of direct loss. The methodology is illustrated through an application on a transportation network in the San Francisco Bay Area subjected to a scenario earthquake.

The underlying motivation for spatial ground motion correlation and structure-to-structure damage correlation developed in this chapter remains the same when assessing risk to other types of spatially distributed systems. Although only direct loss is considered in this chapter for illustrative purposes, the models introduced here that characterize uncertainty and correlation can be extended to other risk metrics such as operational delay, extent of re-routing for emergency evacuation, and reliability of critical sub-networks.

3.2 ANALYSIS OF DIRECT LOSS

Formulations for the mean and variance of sums of losses for an ensemble of sites are presented in this analysis. The loss metric considered is the damage factor, an expression of the loss normalized by total replacement cost of the structure. The total replacement cost for a given bridge is estimated based on 2004 regional dollar rates per square foot unit of deck. These rates are reported by Caltrans (2004) for different structural types and updated on an annual basis.

The expectation of total loss ($\widetilde{L}_{total}$), given by the sum of the expectations of individual losses at all sites is shown in Equation (3.1), while the total uncertainty is given in Equation (3.2) as follows:

$$E\left[\widetilde{L}_{total}\right]=\sum_{i=1}^{N} a_i E[L_i] \tag{3.1}$$

$$\sigma^2_{\widetilde{L}_{total}} = \left[\sum_{i=1}^{N} a_i^2 \cdot \sigma^2_{L_i} + \sum_{i=1}^{N}\sum_{\substack{j=1 \\ j\neq i}}^{N} a_i \cdot a_j \cdot \rho_{L_i L_j} \sigma_{L_i} \sigma_{L_j}\right] \tag{3.2}$$

L_i is the damage factor for a bridge at site i; $\sigma^2_{L_i}$ is the variance of damage factor at the site; a_i, a_j are *expected* replacement values for structures at sites i and j, respectively; and $\rho_{L_i L_j}$ is the correlation of damage factor for pairs of sites i and j (Vanmarcke 1983). In the formulations of this chapter, the notation $\widetilde{L}$ indicates loss in dollar values, whereas L represents the damage factor, an expression of percentage replacement value between 0 and 1. Section 3.2.1 describes the loss analysis method for uncorrelated sites, while section 3.2.2 is devoted to the characterization of ground motion and structure-to-structure damage correlation in the loss analysis.

3.2.1 Scenario-Based Loss Analysis for Uncorrelated Sites

In order to estimate the physical loss of network components without correlation considerations, single site analysis is sufficient. In this section, the loss formulation for uncorrelated sites is

presented. Treatment of ground motion and structural correlation among multiple sites on a network is introduced in the subsequent section.

The distribution of the logarithm of ground motion intensity (written as U in percent g) at a site follows a normal distribution, with parameters given by an attenuation function of the form given in Equation (3.3).

$$\ln U = f(\theta) + \varepsilon_{\ln U} \tag{3.3}$$

θ represents earthquake descriptors such as the moment magnitude (M_w), the source-to-site distance (R), the shear wave velocity (V_s) averaged over the top most 30 m at the site, faulting mechanism, hanging wall and/or foot wall effects, and directivity parameters among others. $\varepsilon_{ln\ U}$ is the random component of the ground motion intensity, normally distributed with zero mean and standard deviation $\sigma_{ln\ U}$. In the Boore et al (1997) attenuation function referenced throughout this report, θ includes M_w, R, and V_s.

The bridges in a transportation network have been classified into engineering subgroups that make characterization of damage and loss feasible. The HAZUS (2002) fragility functions are based on a 28 bridge type classification system. The bridges are grouped by different combinations of the following criteria listed in Table 3.1.

Table 3.1 Categories used to describe bridge characteristics under HAZUS classification methodology.

Description	Design	State	Year Built
single spanned	seismic	CA	< 1990
multiple column bent, simply supported concrete	conventional	non-CA	< 1975
single column, box girder, continuous concrete			≥ 1990
continuous concrete			≥ 1975
multiple column simply supported steel			
continuous steel			
multiple column bent, simply supported, pre-stressed concrete			
other			

Each fragility function is described as $F_{D|U} = P[D > d|U] = \mathrm{N}(\lambda, \zeta)$, where D is a random variable representing five categorical damage states: none, slight, moderate, major, and collapse, and N represents the normal distribution. U is the ground motion intensity measure (*IM*) random variable represented in this case by the site spectral acceleration (S_a) at the 1.0 s period of the structure. λ is the ground shaking median (S_a) and ζ is the lognormal standard deviation of spectral acceleration at 1.0 sec for which a level of discrete damage state, d, is exceeded by the structure. Only the 1.0 sec spectral acceleration is currently used because in calculating the HAZUS fragility shaking medians, the K_{shape} modifier converts cases for short periods to an equivalent spectral amplitude at T = 1.0 second. The I_{shape} factor in the same calculation serves as an indicator so that bridges that do not require this conversion to a T = 1.0 sec S_a are not treated with a K_{shape} factor. Different fragility functions require different ground motion intensity measures. The methodology is unaffected by the choice of fragility function used because of its modularity.

Table 3.2 Parameters of fragility function for HAZUS bridge class 4.

Damage State	λ	ζ
Slight	0.8000	0.6
Moderate	0.9973	0.6
Major	1.1967	0.6
Complete	1.6953	0.6

For a bridge in HAZUS class 4, the parameters of the fragility function shown in Table 3.2 describe the probability of exceeding damage states of slight (D = 2) to complete (D = 5) as a function of the ground motion intensity.

Then the probability of being *in* a damage state (k) is expressed in Equation (3.4).

$$P\left[D=d^{(k)}\middle|U\right]=\Phi\left(\frac{\ln u-\ln\lambda}{\zeta}\right)_k-\Phi\left(\frac{\ln u-\ln\lambda}{\zeta}\right)_{k+1} \tag{3.4}$$

$\Phi(\cdot)$ is the standard normal cumulative distribution function.

Following the total probability theorem, the product of the probability distribution of ground motion at a given site and the bridge fragility function is sufficient in characterizing the probability distribution of damage and hence the expectation of loss for a given bridge at a site (Equation (3.5)). The subscript i from Equation (3.1) is now included to represent the site.

$$E[L_i]=\sum_k\int_{u_i}E\left[L_i|D_i=d_i^{(k)}\right]\cdot P\left[D_i=d_i^{(k)}\middle|U_i\right]\cdot f_{U_i}du_i \tag{3.5}$$

D_i is a discrete random variable represented by the different damage states at a site i given by, $D_i=\left\{d_i^{(k)},\quad \begin{matrix}k=1\ldots5\\ i=1\ldots n\end{matrix}\right.$ where n = number of sites, and k = damage state. f_{U_i} is the probability density function of ground motion at site i, and L_i is the term describing the damage factor for the structure at site i.

The variance, given by the first term on the right-hand side of Equation (3.2) is expanded in Equation (3.6):

$$\sigma_{L_i}^2=E\left[L_i^2\right]-E[L_i]^2 \tag{3.6}$$

Equation (3.6) can be further expanded as follows:

$$\sigma_{L_i}^2=\sum_k\int_{u_i}E\left[L_i^2\middle|D_i=d_i^{(k)}\right]\cdot P\left[D_i=d_i^{(k)}\middle|U_i\right]\cdot f_{U_i}du_i \tag{3.7}$$

$$-\left[\sum_{k}\int_{u_i} E\left[L_i|D_i=d_i^{(k)}\right]\cdot P\left[D_i=d_i^{(k)}\middle|U_i\right]\cdot f_{U_i}du_i\right]^2$$

where,

$$E\left[L_i^2\middle|D_i=d_i^{(k)}\right]=\sigma^2\left[L_i|D_i=d_i^{(k)}\right]+\left[E\left[L_i|D_i=d_i^{(k)}\right]\right]^2 \tag{3.8}$$

If bridge losses are assumed to be uncorrelated, then Equation (3.7) is sufficient to calculate the variance of the expected aggregate loss.

3.2.2 Scenario-Based Loss Analysis for Multiple Sites

In a given event, the ground motion at all sites will be correlated because they are affected by the same earthquake and some of them may have similar local geologic site conditions depending on their respective separation distances. The joint probability of non-exceedance, $P\left(\left[U_i\le u_i|M_w,R_i,V_{si}\right],\left[U_j\le u_j\middle|M_w,R_j,V_{sj}\right]\right)$ for pairs of sites i and j are conditioned on deterministic earthquake parameters, which are subsequently excluded for notational clarity. The ground motion intensity at sites i and j has been assumed to follow a bivariate normal distribution, ϕ, (Wesson and Perkins 2001) as given in Equation (3.9).

$$f_{U_i,U_j}(u_i,u_j)=N\left(\frac{\ln(u_i)-\mu_{\ln U_i}}{\sigma_{\ln U_i}},\frac{\ln(u_j)-\mu_{\ln U_j}}{\sigma_{\ln U_j}},\rho_{ij}\right) \tag{3.9}$$

From the bivariate normal cumulative distribution function, $F_{(i,j)}=P\left(U_i\le u_i,U_j\le u_j\right)$, calculated using algorithms from Hill (1973) and Thomas (1986), a discrete approximation is computed by the differencing operator in Equation (3.10) (Abramowitz and Stegun 1964), where i and j represent site indices.

$$f_{U_iU_j}(u_i,u_j)du_idu_j=P\left(U_i=u_i,U_j=u_j\right)=F_{(i,j)}-F_{(i,j-1)}-F_{(i-1,j)}+F_{(i-1,j-1)} \tag{3.10}$$

The accuracy of Equation (3.10) depends on the discretization of ground motion bins used in the differencing operator. Thus, several spacings for these bins were tested ranging from 0.001 g–0.30 g. It was found that the variation in final estimation of the loss standard deviation was negligible when considering a bin size up to but not larger than 0.10g for the sample networks presented at the end of this chapter. A disaggregation of loss by ground motion revealed that 3.0 g was a sufficient upper bound on loss. Loss contributions from ground motion

higher than 3.0 g were found to be negligible. The binning of ground motions at 0.10g intervals also ensured that $\sum_{i,j} f_{ij} \cong 1$.

3.2.2.1 Ground Motion Correlation Model

Ground motion correlation has not previously been taken into consideration or is at best bounded between perfectly correlated or perfectly uncorrelated cases in prior seismic risk models for spatially distributed systems. According to Franchin et al. (2006), this is because a vector-valued attenuation law that accounts for spatial dependence between sites has not yet been developed. Wesson and Perkins (2001) present a correlation model that partitions the ground motion error into zero-mean Gaussian interevent and intraevent terms. In that model, a function of the two error terms designated by ε_r and ε_e (inter and intraevent terms) determines a constant correlation parameter. The correlation parameter is not a function of separation distance between sites or their epicentral azimuths. Research on isotropic macrospatial ground motion correlation has recently been undertaken by Wang and Takada (2005). Their model, based on attenuation functions published in Japan, considers logarithmic deviations in predicted versus recorded ground motion intensity measures, and determines correlation lengths ranging from roughly 20 to 50 km.

In the analysis that follows, two different isotropic ground motion correlation models are considered. The first model assumes dependencies are invariant to spatial separation distances. Thus, the sensitivity of the loss standard deviation to a constant level of ground motion correlation between all sites is determined. This kind of model can be used to draw conclusions on the loss standard deviation when separation between sites is unknown.

A second type of isotropic ground motion correlation model is presented which accounts for spatial dependence and identifies other sources contributing to the ground motion correlation. This model is based on isotropy and homogeneity of a random field, wherein the joint probability distribution functions are unchanged through translations or rotations in space and depend only on the separation distances between sites. These assumptions are motivated by McGuire's (1990) framework. Two sources contributing to the variability in ground motion intensities are taken into account here: that arising from similar earthquake effects and that arising from similar site conditions.

It should be noted that a third model, an anisotropic model which accounts for the directional effect on the correlation, is not addressed here. Sites experiencing forward directivity effects, or forward wave propagation, may experience very different ground motion attenuation from sites at a similar distance away from the fault located behind the direction of propagation.

The first isotropic ground motion correlation model, also referred to here as the non-distance-dependent model, is given by an equi-correlated matrix (i.e. $Corr(U_i, U_j) = \rho$ for $\rho \in [0,1]$ and $i \neq j$) (Ditlevsen 1981). The sensitivity of this parameter on loss standard deviation is accomplished by varying ρ_{ij}. The second isotropic ground motion correlation model, which is also referred to as the distance-dependent model, requires further discussion and is described here. The ground motion *IM* between pairs of sites can be modeled as jointly normal with linear correlation. Thus it is sufficient to consider pairwise covariances between sites. From Equation (3.3), the ground motion intensity at two sites, U_i and U_j, with earthquake parameters M_w, R, and V_s, are expressed as shown in Equation (3.11):

$$\begin{aligned} \ln U_i &= f(M_w, R_i, V_{s,i}) + \varepsilon_i \\ \ln U_j &= f(M_w, R_j, V_{s,j}) + \varepsilon_j \end{aligned} \tag{3.11}$$

where residuals at sites i and j are given by,

$$\begin{aligned} \varepsilon_i &= \varepsilon_e + \varepsilon_{s,i} + \varepsilon_{r,i} \\ \varepsilon_j &= \varepsilon_e + \varepsilon_{s,j} + \varepsilon_{r,j} \end{aligned} \tag{3.12}$$

All $\varepsilon_e, \varepsilon_s, \varepsilon_r$ are assumed to be mutually uncorrelated zero-mean normally distributed random residual terms where,

ε_e = earthquake error term

ε_s = distance-dependent correlated site error term

ε_r = uncorrelated random error term

and,

$$\begin{aligned} Var(\varepsilon_e) &= \sigma_e^2 \\ Var(\varepsilon_s) &= \sigma_s^2 \\ Var(\varepsilon_r) &= \sigma_r^2 \\ Cov(\varepsilon_{s,i}, \varepsilon_{s,j}) &= \rho_{i,j}^s \sigma_{s,i} \sigma_{s,j} = \exp\left\{-(r_{ij}/r_o)^2\right\} \sigma_s^2 \end{aligned} \tag{3.13}$$

The correlation term between site errors (ε_s) decays exponentially with separation distance, which implies that closely spaced sites will tend to be more highly correlated through

their respective site conditions. The site correlation term with standard correlation distance r_o and separation distance between sites r_{ij} is modeled as $\rho^s_{i,j} = \exp\{-(r_{ij}/r_o)^2\}$. This model belongs to a class of Gaussian covariance models, which is further discussed in Ripley (1981). Two of these models are shown below in Figure 3.1.

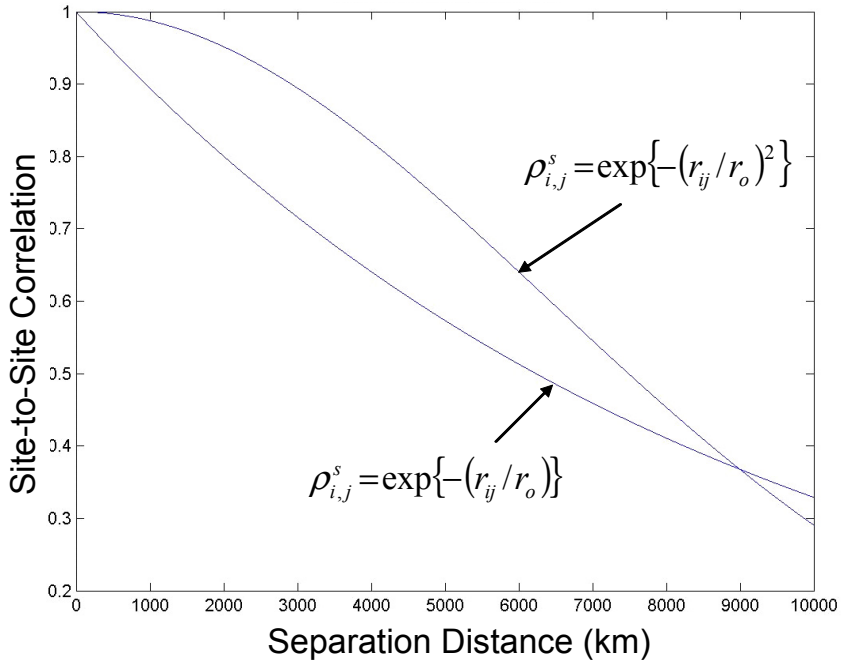

Fig. 3.1 Two Gaussian correlation models.

Because the $\varepsilon_e, \varepsilon_s, \varepsilon_r$ terms are mutually uncorrelated, the cross terms (i.e., $Cov(\varepsilon_e, \varepsilon_s)$, $Cov(\varepsilon_{ri}, \varepsilon_{rj})$, etc.) equal zero. Then, from Equation (3.15), letting $\varepsilon_i = A$ and $\varepsilon_j = B$,

$$Var(A-B) = Var(\varepsilon_{s,i} + \varepsilon_{r,i} - \varepsilon_{s,j} - \varepsilon_{r,j}) \tag{3.14}$$

Because ε_s and ε_r terms are statistically independent, Equation (3.14) can be rewritten as:

$$\begin{aligned} Var(A-B) \quad &= Var(\varepsilon_{s,i}) + Var(\varepsilon_{s,j}) - 2Cov(\varepsilon_{s,i}, \varepsilon_{s,j}) \\ &\quad + Var(\varepsilon_{r,i}) + Var(\varepsilon_{r,j}) - 2Cov(\varepsilon_{r,i}, \varepsilon_{r,j}) \end{aligned} \tag{3.15}$$

Furthermore, the $\varepsilon_{r,i}$ and $\varepsilon_{r,j}$ terms are statistically independent, thus Equation (3.15) can be simplified:

$$Var(A-B) \quad = 2\sigma_s^2 - 2\rho^s_{i,j}\sigma_s^2 + 2\sigma_r^2 \tag{3.16}$$

The $Var(A-B)$ term can also be expressed in terms of the covariance of the residuals at two sites given by Equation (3.17).

$$Var(A-B) = Var(A) + Var(B) - 2Cov(A,B)$$

$$= \left[\sigma_e^2 + \sigma_s^2 + \sigma_r^2\right] + \left[\sigma_e^2 + \sigma_s^2 + \sigma_r^2\right] - 2Cov(A,B) \tag{3.17}$$

Combining the expressions for $Var(A-B)$ from Equations (3.16) and (3.17) into Equation (3.18) and solving for $Cov(A,B)$ results in Equation (3.19):

$$2\sigma_s^2 - 2\rho_{i,j}^s \sigma_s^2 + 2\sigma_r^2 = 2\left[\sigma_e^2 + \sigma_s^2 + \sigma_r^2\right] - 2Cov(A,B) \tag{3.18}$$

$$\begin{aligned} Cov(A,B) &= \sigma_e^2 + \rho_{i,j}^s \sigma_s^2 \\ &= \sigma_e^2 + \exp\left\{-\left(r_{ij}/r_o\right)^2\right\}\sigma_s^2 \end{aligned} \tag{3.19}$$

Then, the final form of the correlation in ground motion residuals at sites i and j where $i \neq j$ is given in Equation (3.20).

$$\rho_{A,B} = \frac{Cov(A,B)}{\sqrt{Var(A)}\sqrt{Var(B)}} = \frac{\sigma_e^2 + \exp\left\{-\left(r_{ij}/r_o\right)^2\right\}\sigma_s^2}{\sigma_e^2 + \sigma_r^2 + \sigma_s^2} \tag{3.20}$$

For ($i = j$), the ground motion is perfectly correlated (i.e., the univariate ground motion distribution at the site).

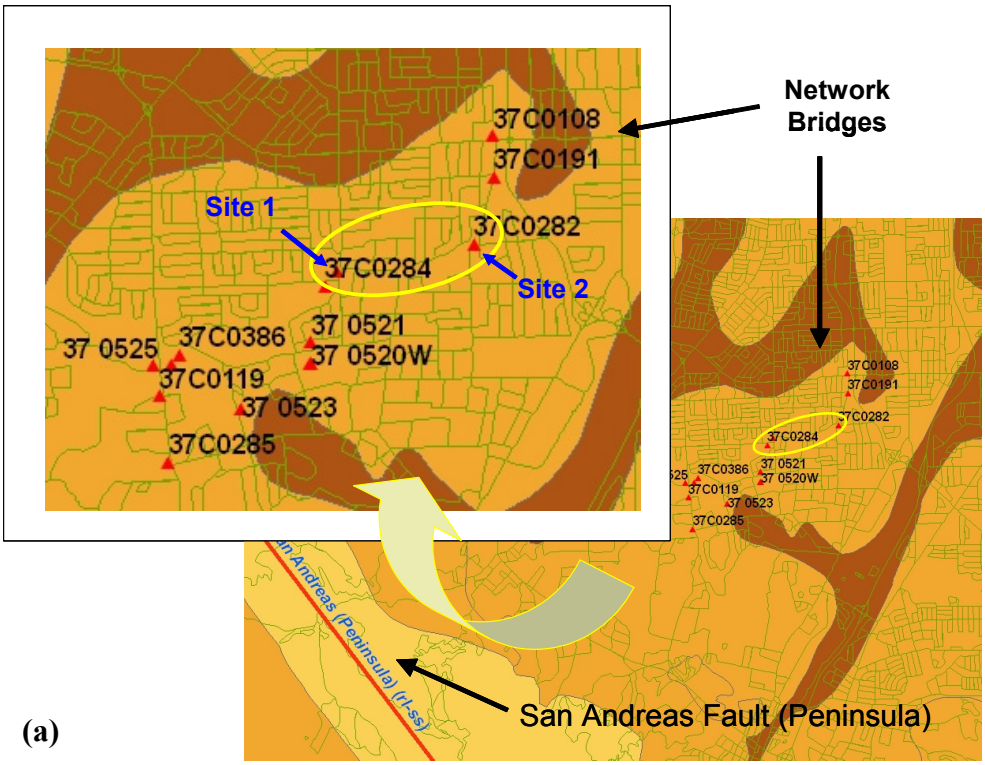

(a)

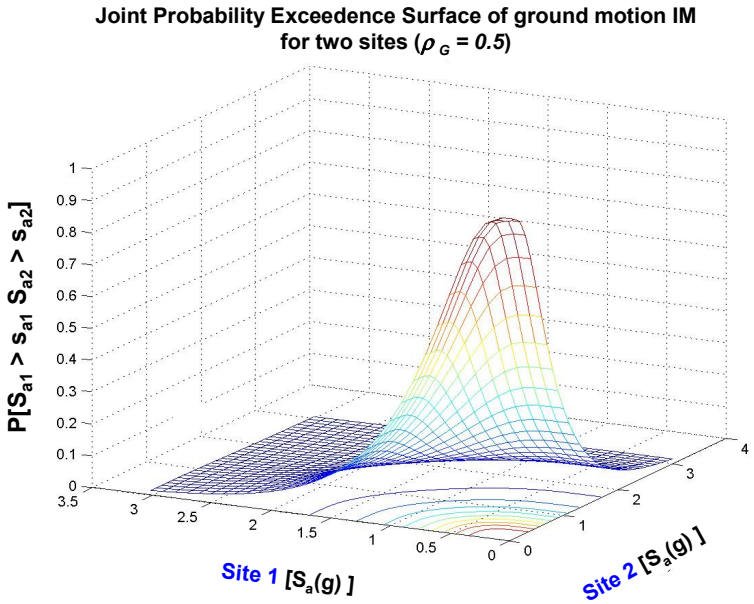

(b)

Fig. 3.2 (a) Map of sample network subject to scenario event on San Andreas fault. Bridges identified by Caltrans-ID and (b) joint probability exceedance surface $P[S_{a1} > s_{a1}, S_{a2} > s_{a2}]$ of ground motion intensity S_a (T = 1.0s, ξ = 5%) for two locations denoted Site 1 and Site 2.

Because the variance terms in $\rho_{A,B}$ are not explicitly known, the following modeling assumptions about the contribution of each of these three terms to total variance (i.e., $\sigma_{Total}^2 = \sigma_e^2 + \sigma_s^2 + \sigma_r^2$) are made: $\sigma_e^2 = \sigma_s^2 = 0.40\left(\sigma_{Total}^2\right)$ and $\sigma_r^2 = 0.20\left(\sigma_{Total}^2\right)$. The weighting of each of the contributors to ground motion covariance is the most realistic physical representation of possible weighting combinations. The random error constitutes the smallest portion of the total ground motion variance, while earthquake and local site effects are known (physical) contributors to spatial ground motion correlation and thus take a larger percentage of the total variance. It should be noted that although the Boore et al. (1997) attenuation model is used, the partitioning of error as reported by their model was not used here. Furthermore, the correlation model here is restricted to values of ρ_{ij} between 0.4 and 0.8 for $i \neq j$, and 1.0 for $i = j$, whereas Wang and Takada (2005) report correlation values less than or equal to 1.0 for all i, j.

For the equi-correlated assumption described earlier in this section, the site-error contribution is excluded from Equation (3.20). The contributions of σ_e^2 and σ_r^2 are weighted in varied amounts such that they sum to σ_{Total}^2.

3.2.2.2 Damage Correlation Model

Structural characteristics such as the abutment and deck types, as well as a broad class of materials differentiating bridge types by steel or concrete construction, are already accounted for by the fragility function. One can make the assumption that bridges sharing the same bridge category type are fully correlated through their fragility functions, while those of dissimilar bridge type are independent through their different fragility functions. This would be the most basic assumption made when modeling structure-to-structure damage correlation. In this case, all bridges are classified according to a general design class with an expected level of performance (given a level of ground motion intensity) and some uncertainty around that level of performance. From Equation 3.4, the probability of being in a damage state *k* is given by the difference in probabilities of exceedance for a damage state *k* and its next higher damage state *k+1* at a level of ground motion intensity.

The structural performance of an individual bridge may differ from the prescribed fragility because the unique stochastic response of each structure may not be fully explained by

its performance at a T = 1.0 sec ground motion spectral acceleration at the site. This variability may be due to the unique construction workmanship per bridge as design and build methods differ by contractor. The material quality is prone to natural fluctuations over a long range of construction years due to variability of manufacturing practices. Bridges of the same class grouped by design method, contractor/construction crews, and/or design year may help explain various contributions to the fragility dispersions (which is constant at 0.6 for HAZUS functions). The aleatory uncertainty, which cannot be explained by further data, accounts for the remaining error in the fragility dispersion. Thus, a model describing the similarity (or dissimilarity) of bridge performance in terms of these shared (or unrelated) qualities can be postulated. This motivates the need to define partial correlation *within* a bridge class. For bridges of different classes, grouping the structures by these same attributes suggests a non-zero correlation *across* bridge types.

The data required for such a correlation model are not currently available. Therefore, the equi-correlated assumption (i.e., $Corr(D_i, D_j) = \rho$ for $\rho \in [0,1]$ and $i \neq j$) is used to provide an upper bound on the variance. The correlation is assumed to be conditionally independent of the ground motion intensity level. A sensitivity analysis of the variance of total loss is used by varying levels of damage correlation.

The information needed to assess the covariance of $L_i L_j$ is contained in Equations (3.21–23). The Markovian property in which the probability of a random variable depends only on the previous random variable is assumed to hold. As a result, the loss depends only on the damage states of the bridges. That is, $L_i L_j$ in Equation (3.22) is conditioned directly on $D_i D_j$ and not also on $U_i U_j$. Thus, the covariance of loss, $L_i L_j$, is simplified as follows:

$$\sigma_{L_i,L_j} = E[L_i L_j] - E[L_i]E[L_j] \tag{3.21}$$

$$E[L_i L_j] = \sum_{k_i=1}^{5}\sum_{k_j=1}^{5}\int_{u_j}\int_{u_i}\Big[E\big[L_i L_j | D_i = d_i^{(k_i)}, D_j = d_j^{(k_j)}\big]\cdot P\big[D_i = d_i^{(k_i)}, D_j = d_j^{(k_j)}\big|U_i, U_j\big] \times f_{U_i U_j}(u_i, u_j)du_i du_j\Big] \tag{3.22}$$

$$E\big[L_i L_j | D_i = d_i^{(k_i)}, D_j = d_j^{(k_j)}\big] = \rho_{L_i L_j | D_i D_j}\sigma_{L_i|D_i}\sigma_{L_j|D_j} + E\big[L_i\big|D_i = d_i^{(k_i)}\big]\cdot E\big[L_j\big|D_j = d_j^{(k_j)}\big] \tag{3.23}$$

It is important to recognize that $E[L_i L_j | D_i D_j]$ in Equation (3.23) can be reduced to the product of two conditionally independent expectations of damage factor *(L)* at sites *i* and *j* if the

damage factor conditioned on damage at a site is considered to be independent of damage factor conditioned on damage at a different site. After making the appropriate substitutions from Equations (3.5) and (3.21–3.23), the expression for covariance of $L_i L_j$ (3.24) is developed:

$$\begin{aligned}\sigma_{L_iL_j} = \sum_{k_i=1}^{5}\sum_{k_j=1}^{5}\int_{u_j}\int_{u_i} E\left[L_i|D_i = d_i^{(k_i)}\right]\cdot E\left[L_i|D_j = d_i^{(k_i)}\right]\cdot P\left[D_i = d_i^{(k_i)}, D_j = d_j^{(k_j)}\middle|U_i, U_j\right]\cdot f_{U_iU_j}(u_i,u_j)du_i du_j \\ -\left[\sum_{k_i=1}^{5}\int_{u_i} E\left[L_i|D_i = d_i^{(k_i)}\right]\cdot P\left[D_i = d_i^{(k_i)}\middle|U_i\right]\cdot f_{U_i}(u_i)\,du_i\right] \\ \times\left[\sum_{k_j=1}^{5}\int_{u_j} E\left[L_j|D_j = d_j^{(k_j)}\right]\cdot P\left[D_j = d_j^{(k_j)}\middle|U_j\right]\cdot f_{U_j}(u_j)\,du_j\right]\end{aligned} \tag{3.24}$$

The mean damage factor conditioned on damage state, as provided in HAZUS, is used in this analysis and listed in Table 3.3.

Table 3.3 HAZUS mean damage factor for given damage state.

Damage State	Mean Damage Factor
Slight	0.03
Moderate	0.08
Major	0.25
Complete	2/x x ≥ 3*
	1.00 x < 3*

* x = no. spans

The univariate distributions in Equation (3.24) can be computed by straightforward numerical procedures. The remaining joint probability of damage can be exactly solved in the (i) independent and (ii) fully correlated cases, while it must be numerically approximated in the (iii) partially correlated case.

The case of full correlation, $\rho = 1$, is unique in that it occurs if the ground motion at two sites and the structural type at the two sites are identical. Otherwise, the discrete joint probability is zero for non-identical bridge classes, and zero for identical bridge classes when $u_i \neq u_j$. The discrete joint probability reduces to Equation (3.25).

$$P\left[D_i = d_i^{(k_i)}, D_i = d_i^{(k_j)}\middle|U_i, U_j\right] = \begin{cases} P\left[D_i = d_i^{(k_i)}\middle|U_i\right] = P\left[D_j = d_j^{(k_j)}\middle|U_j\right] & class_i = class_j,\ u_i = u_j \\ 0 & otherwise \end{cases} \tag{3.25}$$

If the damage correlation is pairwise independent, $\rho = 0$, then the joint discrete distribution conditioned on ground motion becomes the product of two univariate distributions as shown in Equation (3.26).

$$P\left[D_i = d_i^{(k_i)}, D_j = d_j^{(k_j)} \middle| U_i, U_j\right] = P\left[D_i = d_i^{(k_i)} \middle| U_i\right] \times P\left[D_j = d_j^{(k_j)} \middle| U_j\right] \tag{3.26}$$

For partial correlation, a closed-form solution does not exist. A method that can fit the 5x5 matrix representing the joint probability that two different sites are in damage states (d_i, d_j) is sought. The available inputs include the marginal probabilities of being in damage states one through five at each of two sites, and the level of damage correlation between the two sites. A least-squares adjustment can be used to find the optimal solution for P_{ij} while satisfying ten constraints, corresponding to every marginal probability at the two sites. This would require ten Lagrange multipliers. This part of the formulation then becomes an optimization problem.

The solution to $P\left[D_i = d_i^{(k_i)}, D_j = d_j^{(k_j)} \middle| U_i, U_j\right]$ requires identifying expected damage and variance of damage for one site as shown in Equations (3.27–3.28) (univariate site subscripts are excluded here):

$$E[D|U] = \sum_{k=1}^{5} k \cdot P\left(D = d^{(k)} \middle| U\right) \tag{3.27}$$

$$\text{let } \mu = E[D|U]$$

$$\begin{aligned} \sigma^2[D|U] &= E\left[(D-\mu)^2 \middle| U\right] = E\left[D^2 \middle| U\right] - 2\mu \cdot E[D|U] + \mu^2 \\ &= \sum_{k=1}^{5} k^2 \cdot P\left(D = d^{(k)}\right) - \mu^2 \end{aligned} \tag{3.28}$$

After solving Equations (3.29–3.31) below,

$$\rho_{[D_i, D_j | U_i, U_j]} = \frac{\sigma_{[D_i, D_j | U_i, U_j]}}{\sigma_{[D_i|U_i]} \sigma_{[D_j|U_j]}} \tag{3.29}$$

$$\sigma_{[D_i, D_j | U_i, U_j]} = E[D_i, D_j | U_i, U_j] - E[D_i | U_i] \cdot E[D_j | U_i] \tag{3.30}$$

$$E[D_i, D_j | U_i, U_j] = \sum_{k_i, k_j} k_i \cdot k_j \cdot P\left[D_i = d_i^{(k_i)}, D_j = d_j^{(k_j)} \middle| U_i, U_j\right] \tag{3.31}$$

let $P_{ij} = P\left[D_i = d_i^{(k_i)}, D_j = d_j^{(k_j)} \middle| U_i, U_j\right]$. Then the following objective function in Equation (3.32) is minimized

$$= \min_{P} \left(\left(\frac{\sum_{i,j} i \cdot j \cdot P_{ij}}{\sigma_{[D_i|U_i]}\sigma_{[D_j|U_j]}} - \frac{E[D_i|U_i] \cdot E[D_j|U_j]}{\sigma_{[D_i|U_i]}\sigma_{[D_j|U_j]}} \right) - \rho \right)^2 \tag{3.32}$$

subject to the following constraints.

The first condition is that the marginal probabilities must be preserved (3.33).

$$\begin{aligned} P\left[D_i = d_i^{(k_i)}\right] &= \sum_j P_{ij} \\ P\left[D_j = d_j^{(k_j)}\right] &= \sum_i P_{ij} \end{aligned} \tag{3.33}$$

The second condition is that cell probabilities must be $0 \le P_{ij} \le 1$ for $\forall\ i, j \in \{D_i, D_j\}$, which is automatically satisfied by the above constraint.

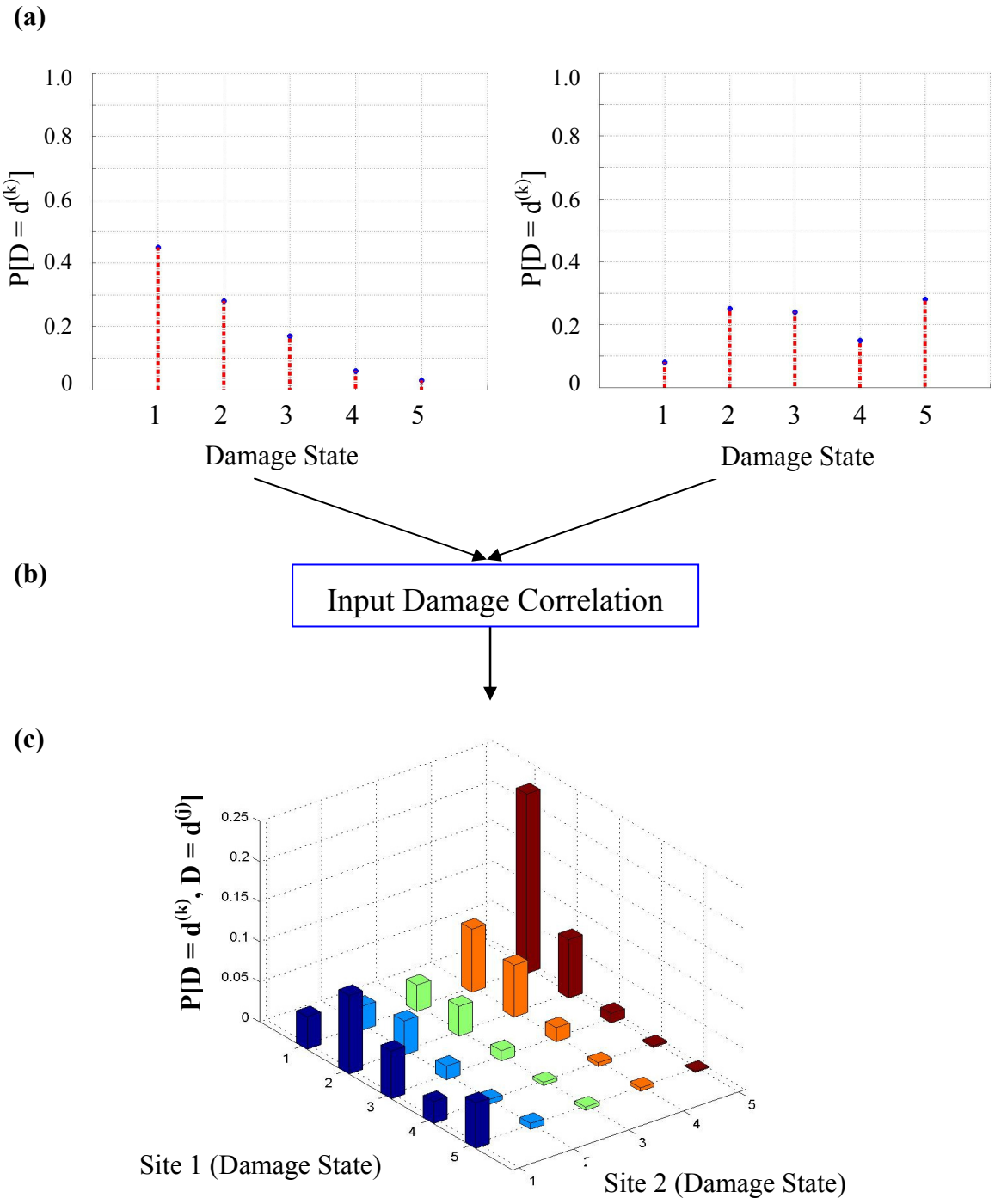

Fig. 3.3 Approach for solving joint probability of damage at Sites 1 and 2. Given (a) marginal distributions for damage and (b) an input correlation, ρ_D, (c) joint probability of damage is determined by minimizing objective function in (3.32).

The estimation of $P\left[D_i = d_i^{(k_i)}, D_j = d_j^{(k_j)}\right]$ in cases of partial damage correlation is a necessary component of seismic risk evaluation for a transportation network, not only in assessing direct loss uncertainty, but also in determining the effect on routing optimization as discussed in Chapter 4.

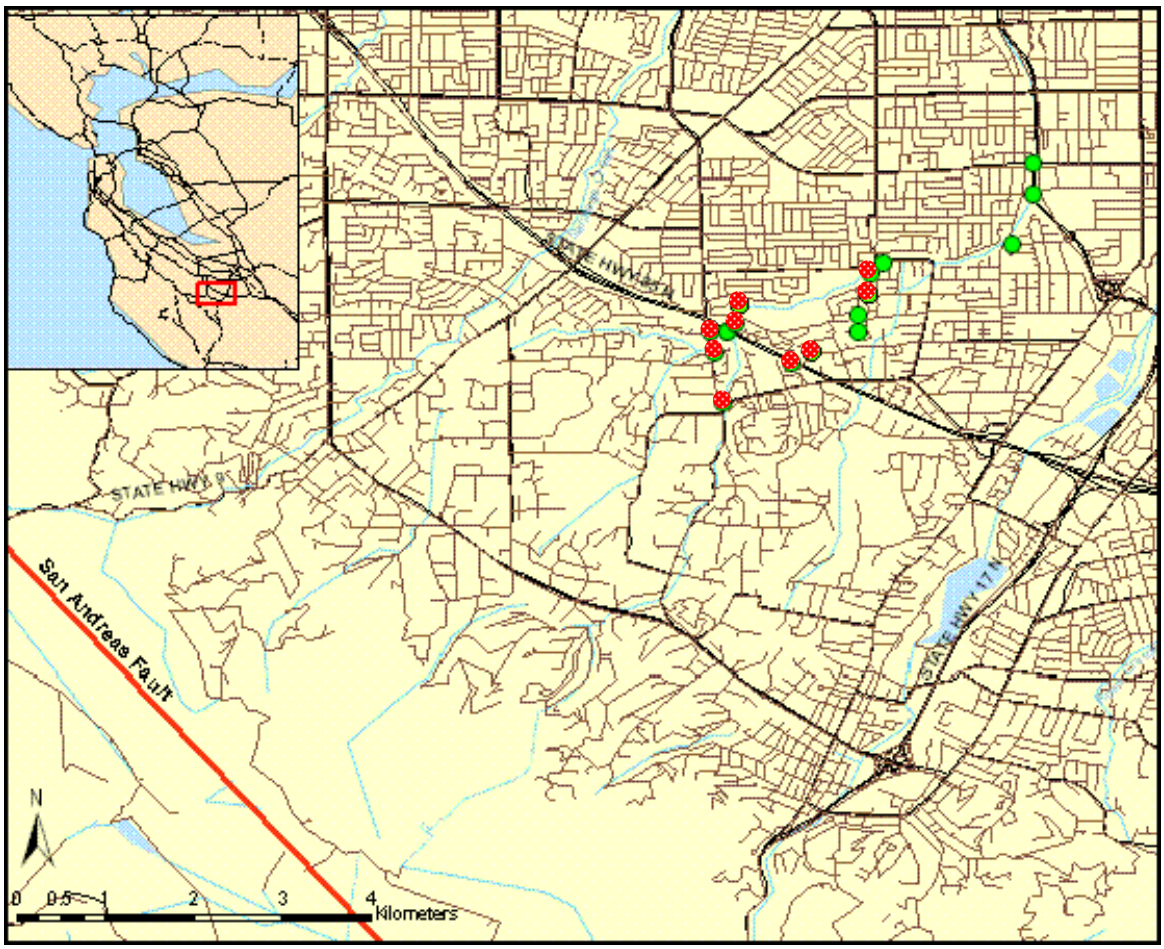

Fig. 3.4 Location of 9 bridges (hatched circles) and 16 bridges (hatched and filled circles) in San Francisco Bay test area. Insert identifies location of the sub-network within the San Francisco Bay region.

3.3 APPLICATION

Two sample networks, one consisting of 16 bridges, another consisting of a subset of 9 from the original 16, are shown in Figure 3.4 and used in this application. The bridges are located within

7–11 km of the peninsula segment of the San Andreas fault. A M_w = 8.0 event on the San Andreas fault is used for illustrative purposes in this analysis.

The attenuation relationship by Boore et al. (1997) is used to determine the distribution of ground motion intensity (e.g., spectral acceleration at T = 1.0 sec), at each site on the network. Source-to-site distances are calculated as defined in Boore et al. (1997). For two sites on the network, the ground motion joint probability density is solved as shown in Figure 3.5. The discrete joint probability of damage for two cases of ground motion and damage correlation inputs is shown in Figure 3.6 for two sites on the network.

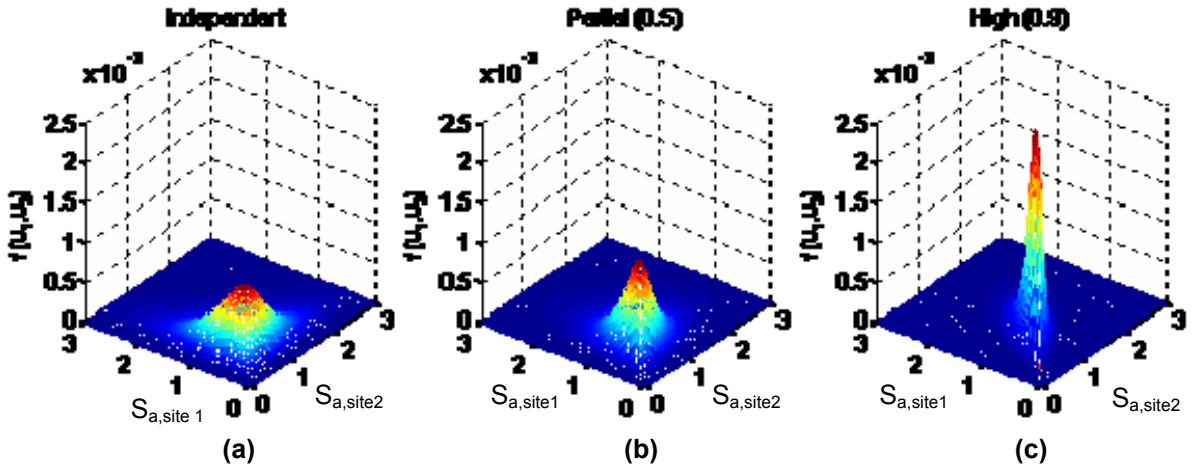

Fig. 3.5 Ground motion (S_a, T = 1.0 sec) joint probability density for two sites on network assuming varying levels of pairwise ground motion correlation: (a) $\rho_G = 0$; (b) $\rho_G = 0.5$; (c) $\rho_G = 0.9$.

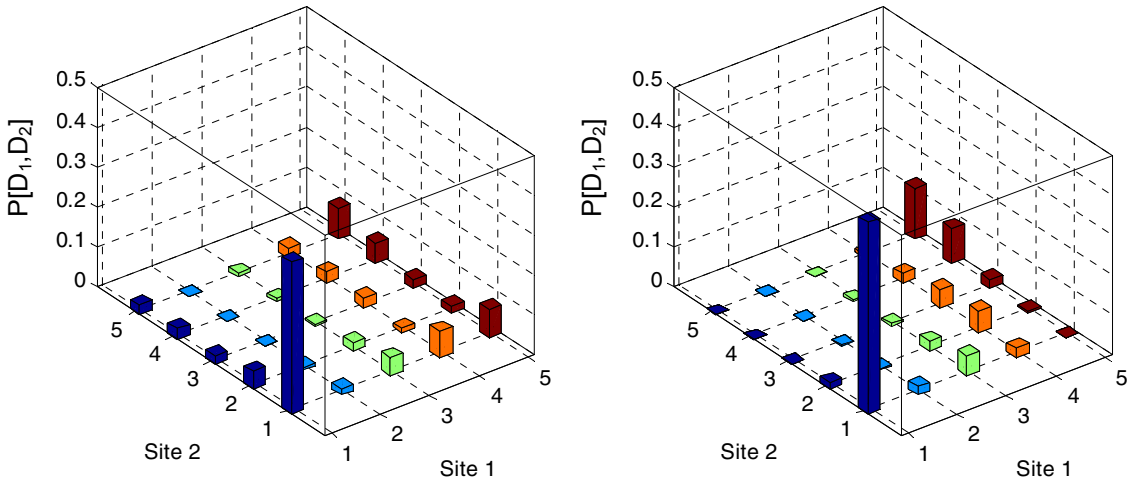

Fig. 3.6 Discrete joint probability mass function of damage for two sites on network under (a) $\rho_G = \rho_D = 0.5$ and (b) $\rho_G = \rho_D = 0.9$.

The results from the application of the analytical framework to the two sample networks are plotted in Figures 3.7–3.8. In Figure 3.7, the coefficient of variation of total loss (CoV,δ) is bounded for the two networks using the equi-correlated assumption for ground motion and for damage. The loss is bounded between $\delta_L = [0.7, 1.6]$ for the larger network (Fig. 3.7a) and $\delta_L = [0.8, 1.5]$ for the smaller network (Fig. 3.7b). The range of δ_L is comparable between the two different sized networks. When assuming no correlations, the loss CoV is 0.6 for the large network and 0.7 for the small network.

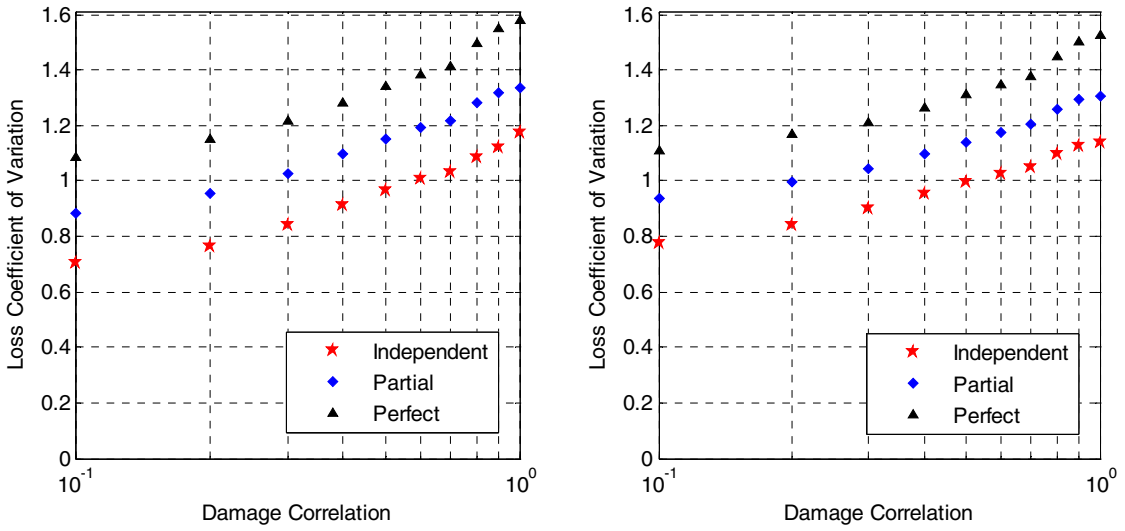

Fig. 3.7 Loss coefficient of variation for two networks, (a) N = 16 and (b) N = 9 (b). Lowest marker points (☆) result from independent ground motions. Highest marker points (△) result from perfect ground motion correlation.

The results from the distance-dependent ground motion correlation model showed CoV in the range of $\delta_L = [1.0, 1.4]$ for both networks. The similarity in results for the two sized networks is partially due to the fact that the smaller network consists of a subset of the same bridges contained in the larger network consisting of 16 sites. The range of the loss CoV is narrower than in the non-distance-dependent case and lies on the high end of loss CoV because it has been assumed in the distance-dependent model that a large portion of the correlation between sites is explained by the earthquake error term, constituting 40% of σ^2_{Total}. Consequently, even if the distance-dependent site error term (σ^2_s) approaches zero, or sites are fairly far apart, the minimum correlation between sites is still moderate at 0.4. Thus, a distance-dependent site error term equal to zero results in the equi-correlated model, with off-diagonal terms of 0.4.

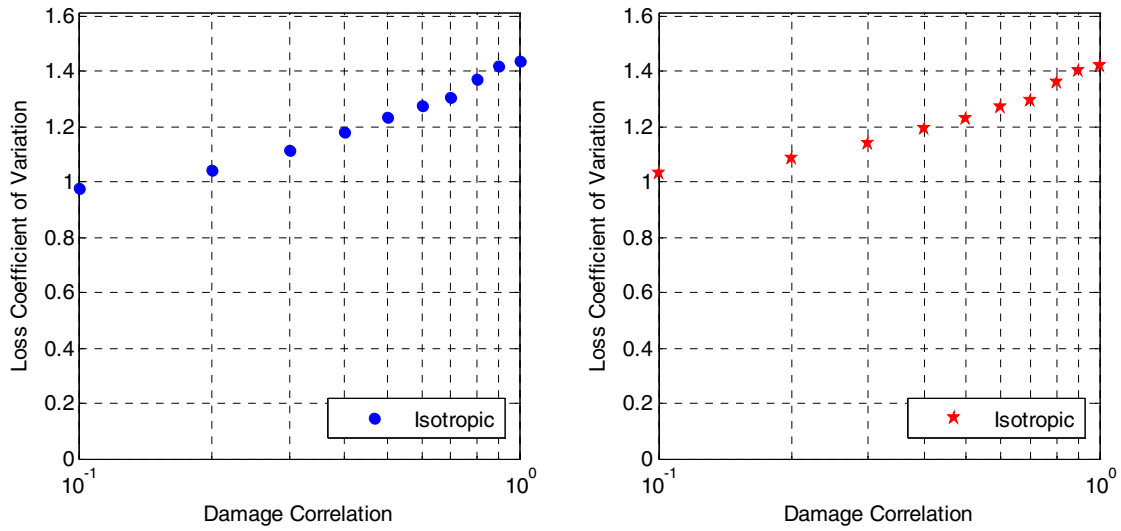

Fig. 3.8 Loss dispersion for two different networks (a) N = 16 (a) and (b) N = 9, assuming distance-dependent ground motion correlation.

In the equi-correlated or non-distant-dependent model, the sensitivity of ground motion correlation, ρ_{ij}, on CoV is carried out under three possible conditions. First, the earthquake error (σ_e^2) and site error terms (σ_s^2) are weighted each as 0% of σ_{Total}^2, or $\rho_{ij}=0$. Second, the earthquake error (σ_e^2) and residual error terms (σ_r^2) are treated each as 50% of σ_{Total}^2, or $\rho_{ij}=0.5$. Third, the earthquake error term (σ_e^2) is treated as 100% of σ_{Total}^2, or $\rho_{ij}=1.0$. The effect of these varying cases of ground motion correlation on δ_L is plotted in Figure 3.8. When holding the ground motion correlation constant, the loss CoV is sensitive to changes in damage correlation between sites. When holding damage correlation constant between components, the loss CoV is still sensitive to changes in ground motion correlation, but to a lesser degree. However, it should be emphasized that neither correlation effect dominates the other completely in terms of the contribution to the overall uncertainty.

In the distance-dependent model, the sensitivity of ground motion correlation on CoV is explained as follows. If the earthquake error term is reduced, and more of the error is explained by the distance-dependent site error term, the standard correlation distance r_o is extremely important. For shorter standard correlation distances, the overall loss CoV will be highly dependent on the proximity of sites to each other on the network. Parameters of this model require further investigation, limiting its application.

It is expected that a larger network will be spread over a larger seismic area. If the same scenario event were applied to this larger network, the CoV is expected to change depending on the proximity of all sites to the fault, their separation distances, and the bridge types that are represented in the network. Large separation lengths between sites and a presumably more varied population of bridges will lessen correlation effects in these two particular instances. However, further study is required to more completely assess the effects of the network size on the risk.

3.4 SUMMARY

Quantifying the expected value of loss or damage, while important, may not adequately describe the risk to a suite of bridges in a spatially distributed transportation network. This is because quantifying uncertainty is an important aspect of the risk assessment. In order to accurately assess the uncertainty in the overall risk, it is important to consider the effects of both spatial ground motion correlation and structure-to-structure damage correlation. This research formulates a methodology for incorporating these correlation effects in the risk assessment of spatially distributed systems. Although a demonstration is performed for a transportation network, the analytical framework applies to any spatially distributed system.

This chapter seeks to demonstrate that neglecting correlation underestimates the direct loss CoV by between 20% and 170% for the networks studied here. A sensitivity analysis of both spatial ground motion correlation and structure-to-structure damage correlation is used to show the importance of including these effects. Ground motion correlation and damage correlation effects impacts the loss CoV differently. However, this difference is not extremely significant. The sensitivity study shows that when moderate levels of damage correlation ($\rho_D = 0.5$) are considered, loss CoV is higher by as much as 30–60%. These results are on the same order as the effects from considering moderate levels of ground motion correlation ($\rho_G = 0.5$). When moderate levels of both effects are considered together the loss CoV increases by 90%. Thus, the impact of the individual types of correlation as well as the combined effect of both correlations on the loss uncertainty is critical.

A ground motion correlation model is developed and used to assess the loss CoV as a function of separation distance between sites. This correlation model generally yields a higher range of loss CoV values compared to results based on the equi-correlated non-distance-dependent model for the application in this chapter. This is because sites on the application

network are closely spaced. For a network whose sites are farther apart, a lower range of loss CoV is expected when using this distance-dependent isotropic correlation model presented here.

The effect of correlation is later shown in this report to have a notable impact on emergency routing in the transportation system and in development of system risk curves. Decisions based on risk curves that do not incorporate correlation may result in conservative pre-event mitigation planning or emergency response strategies.

4 Scenario-Based Seismic Risk Assessment: Parameter Sensitivity Study and Network Routing Application

The analytical framework presented in Chapter 3 forms the basis for the simulation techniques introduced in this chapter. The analytical approach for incorporating non-zero or non-unity damage correlation is infeasible for large networks. Where an analytical solution is impractical or impossible, Monte Carlo techniques are used instead. Monte Carlo methods are used to model statistical dependencies in risk assessment for a transportation network, to report sensitivities of the loss distribution to truncation of the random replacement cost and damage factor, and to demonstrate variations in optimal emergency routing due to ground motion and damage correlations in the network.

The organization of this chapter is as follows. Section 4.1 discusses several techniques used to simulate a random field of correlated ground motion intensities. These techniques are tested for speed, precision, and simplicity of implementation. Methods for inducing correlation in both a distribution free form and in an approximate Pearson form are tested using the different sampling methods. Section 4.2 introduces a recent functional model for handling dependencies when joint distributions are a priori unknown. This approach is used to model discrete damage state dependencies in the network. It is presented here as a computationally efficient alternative to the optimization procedure used in Chapter 3. This increased efficiency makes it possible to extend the modeling application to larger sized networks, to analyze the network under suites of earthquakes in a catalog, and to expand correlation studies into applications for transportation network analyses. In Section 4.3, simulation results are compared with results from Chapter 3. In Section 4.4, the loss distribution sensitivity to the damage factor and replacement cost random variables is tested. The results point to the importance of defining the truncation bounds on both

random variables. Emergency routing is currently based on minimizing the expected travel time from an origin to a destination given post-disaster closures and damage in the network in the absence of correlations. In Section 4.5, a standard shortest-path algorithm is used to demonstrate the variability of optimal routing paths in the presence of correlations.

4.1 EFFICIENT SIMULATION OF CORRELATED GROUND MOTION INTENSITIES

4.1.1 Introduction

When an exact solution is infeasible with traditional numerical approaches, Monte Carlo (MC) simulation provides an effective alternative. The performance of MC is typically measured by ease of use, accuracy, efficiency, memory requirements, and generality of technique (Walker 1977). Limited memory size or excessive run-time occasionally prohibits large sample sizes. In modeling the network routing problem, for example, a large number of network analyses replications cannot be practicably accommodated by standard network algorithms. As a result, expected values of damage and link travel times are used for simplicity with uncertainty treated as an afterthought. This results in a crude first-order approximation of optimal routes.

Modeling a correlated random field involves a two part approach. First, realizations are sampled from the underlying multivariate distributions with the aid of a pseudorandom number generator and inverse transform methods. Second, realizations are ordered to match the target correlation matrix. Methods for improving efficiency of both stages are summarized in this section.

Variance reduction techniques take advantage of what is already known about the problem in order to improve efficiency. In comparing two methods, "efficiency" is defined as a function of compute time and variance of the random variable estimator using a given method (Rubenstein 1981). If performed correctly, fewer samples are required to achieve the same statistical accuracy as compared to standard MC. Various techniques include updated Latin hypercube samples (Florian 1992), the spectral representation approach (Shinozuka and Deodatis 1996), stratification, and others (i.e., control variates, antithetic variates, importance sampling).

The other aspect of simulating correlated random variables that requires some discussion is correlation control. In particular, two different types of correlation parameter are discussed here: rank (non-distribution-dependent) and Pearson types. In Chapter 3, distribution dependent

correlations were assumed for both ground motion and damage correlation parameters. However, because of the ease of using rank correlations and because in practice, the correlation parameter is generally not precisely known, using rank correlations is worth consideration. The Spearman rank correlation and Pearson correlation are given respectively in Equations (4.1) and (4.2).

$$\rho = 1 - \frac{6\sum_i d_i^2}{n\left(n^2 - 1\right)} \tag{4.1}$$

$$\rho = \frac{E[(X - \mu_X)(Y - \mu_Y)]}{\sigma_X \sigma_Y} \tag{4.2}$$

d_i = the difference between ranks of corresponding values of X and Y

n = the number of pairs of values

ρ = correlation parameter between X and Y

The matrix method is the standard method for enforcing a target rank correlation in randomly generated samples (Iman and Conover 1982). However, a shortcoming of using the matrix method is that randomly generated samples are oftentimes not independent to begin with, especially for cases of small sample size and a large number of variables. This results in large errors for the resulting rank correlation. Removing random correlations in the randomly generated samples that naturally result when sample sizes are small was the focus of Florian's (1992) updated LHS method. The updating method is based on the same principles found in Iman and Conover's (1982) paper. However, random samples are first placed into a pre-specified ordering which reduces randomly generated correlations. This is done before attempting to induce correlation.

An alternative approach to correlation control was introduced by Huntington and Lyrintzis (1998). They proposed minimizing these large correlation errors by using a single switch algorithm. The algorithm matches Pearson correlations instead of rank correlations by applying an approximate Gaussian transformation on the data and checking for convergence to a specified correlation matrix. The method relies on switching sample points one at a time and checking how well correlation is matched after each iteration. While its precision is superior to matrix method precision, the algorithm had two potential issues. The first issue was speed. For high-dimensional problems and large sample sizes, the authors reported day-long run-times. The second issue was that unless stratification resulted in fairly uniform projections, the procedure

iterates to a solution which matched correlation through outliers. This phenomenon is more noticeable for small sample sizes.

To address this problem, discrepancy-controlled samples can be used to ensure uniformity in samples. Doing so decreases the prevalence of correlation through outliers. Discrepancy can be defined as a measure of the samples' deviation from the uniform distribution (Niederreiter 1992). Rather than using simple random samples, selectively choosing deterministic samples or quasi-random sequences (QMC) shows significant improvement over standard Monte Carlo.

4.1.2 Sampling Random Variables

Selecting a method by which to sample random variates will often depend on the problem type and/or computing constraints. The most rudimentary choice for sampling is simple random sampling. However, other methods can be used to improve the efficiency of the solution. Simple random sampling is used in the applications presented in Sections 4.3 and 4.4. For the emergency routing problem in Section 4.5, quasi-random sequences are used instead of simple random samples because of its improved uniformity. This is especially advantageous for controlling correlation in small sample sizes. These sample types are summarized briefly here, with further details in the Appendix, Section 4.6.

4.1.2.1 Simple Random Sampling

Simple random samples are uniform numbers drawn at random using any number of random number generators. Standard Monte Carlo methods are based on inverse transformation of simple random samples to reflect some parent distribution. Doing so allows a practical solution to problems that are impossible to formulate analytically.

4.1.2.2 Latin Hypercube Sampling

For a one-dimensional problem, sampling from equal spaced intervals is an effective way of assuring uniformity in the domain of a variable. This is the motivation behind Latin hypercube

sampling (LHS). McKay, Beckman, and Conover (1979) introduced Equation (4.3) for LHS in computing experiments.

$$y_{ik} = F_i^{-1}\left(\frac{\pi_k(i) - U_{ik}}{n}\right) \tag{4.3}$$

where,

n = number of samples

d = total number of input random variables

π_k = independent uniform random permutations of $i = 1, \ldots, n$

$U_{ik} \sim U[0,1)^d$ = independent uniform random number for $k = 1 \ldots d$

F_i^{-1} = inverse cumulative distribution function

The benefit of using LHS over standard MC is that fewer samples are required to solve the integrand in Equation (2.1). Similarly, fewer samples are required for characterizing *IM* and *DS* when assessing optimal emergency routing paths. In considering multiple sites in the network, LHS is associated with stratification on all $k = 1 \ldots d$ dimensions (i.e., sites) simultaneously (Owen 2005).

A variation on the LHS method by McKay et al. (1979) is a method of sampling section means (Huntington and Lyrintzis 1998) according to the following rules:

$$x_{i,k} = \frac{1}{n}\int_{y_{i,k-1}}^{y_{i,k}} x\, f_i(x)\, dx \tag{4.4}$$

$$y_{i,k} = F_i^{-1}\left(\frac{k}{n}\right) \qquad k = 1, \ldots, n \tag{4.5}$$

where $x_{i,k}$ is the sample, $y_{i,k}$ are the bounds of integration, n is the total number of samples, F_i^{-1} is the inverse cumulative distribution function of the random variable, while f_i is the probability density function for the i^{th} random variable. The motivation for the sampling section means is to improve precision in matching marginal moments.

4.1.2.3 Quasi-Random Sequences

Quasi-random sequences offer major advantages over MC. One of the benefits of using QMC over standard MC is improved discrepancy, or uniformity of samples in low-dimensional projections (unit hypercube or hypersquare plots). As will be shown in Section 4.1.4, the

uniformity of QMC points is especially useful in controlling linear correlation for very small sized samples. The sub-network routing analysis is one example for which QMC methods are well suited because of constraints on run-times and simulation cycles for network solvers. Efficient simulations are required for characterizing the random hazard and risk at multiple sites on the sub-network, incorporating several layers of dependencies in these models, and assessing the interdependencies in network flows. A discussion of QMC points follows in Section 4.6.

4.1.3 Incorporating Correlation in Sampled Data

Rank correlation in randomly generated samples can be achieved by applying basic matrix properties to the data. The main motivation for using rank correlation over Pearson correlation is that computations on non-normal data or raw data, especially in the presence of outliers, may not be meaningful (Iman and Conover 1982).

Iman and Conover (1982) introduced a non-distributional approach to incorporating correlation in data. Van der Waerden data scores $\left(\Phi^{-1}(i/[N+1])\ \ i=1\ldots N\ samples\right)$ or raw data ranks suffice in the matrix operations. Given a matrix X with identity correlation matrix I and some positive definite correlation matrix C with lower triangular matrix P, the matrix X is transformed to have correlation C by XP^t. This procedure relies on the assumption that random generation of X results in linearly independent columns. For small sample sizes, this assumption is weak. This random source of correlation error may be diminished by performing the matrix operations iteratively until all variables are nearly uncorrelated. It should be noted, however, that this procedure may still converge to a solution with correlation errors. After this is done, the matrix algorithm for inducing a target rank correlation C (where $C \neq I$) can be used only once with no further iterations.

If however, distribution specific correlations are known, target correlations on raw data may be important to consider. Several methods have been proposed for achieving target correlations in small samples with known distributional dependence (e.g., directional sampling, genetic algorithms, simulated annealing). The single switch operator (Huntington and Lyrintzis 1998) is one method that offers precision and is simple to execute. Because the single switch algorithm operates directly on transformed data rather than on ranks, Pearson correlations are considered instead. The single switch algorithm for inducing correlation (Fig. 4.1) is more precise than the matrix method previously discussed, at the cost of slightly longer run-times.

The operator requires a search over all pairs of switches in each column, which minimizes the error in the correlation. The operator works on a *sample number* row by *variable number* column of data. The method begins by operating on the second column of data. Values are switched within the second column, and a Pearson correlation between the first and second column is computed for each switch between i and j, where $(i = 1 \ldots N; j = 1 \ldots N; \text{ for } i \neq j)$. After iterating through all possible pairs of switches between elements of a data column and making switches to minimize correlation errors, the algorithm operates on the next column and so forth until all columns have been adjusted. The algorithm works with raw data that have been standardized. The resulting data consist of columns representing zero mean, unit standard deviation variables. This is an approximate transformation of non-normal variables to the standard normal space. After the switching algorithm is completed, standardized data are transformed back into their original space.

4.1.4 Comparison of Sampling Methods

The stratification methods discussed in Section 4.1.2 and the methods for inducing correlation from Section 4.1.3 are now applied in this section to determine the number of ground motion samples required to reach a threshold square-root of sum of squares error (SRSS) for a network, with the error recorded as shown in Equation (4.6),

$$\underset{\substack{i=1\ldots N, j=1\ldots N \\ i \neq j}}{} \qquad Error_{SRSS} = \sqrt{\frac{\sum_{i,j} \left(\hat{C}_{i,j} - C_{i,j}\right)^2}{N(N-1)}} \tag{4.6}$$

where,

$\hat{C}_{i,j}$ = observed correlation

$C_{i,j}$ = target correlation

N = total number of sites in the network

For smaller sample sizes, Figure 4.1 shows a comparison of the two correlation control techniques, with matrix methods used on LHS and Fauré samples, while the single switch operator is used on randomly permuted section means according to Equations (4.4) and (4.5). The results using LHS are presented for an approximate 15–18 percentile. Fauré points are deterministic, thus percentiles are not plotted. It should be noted that although the correlation

parameter types being measured are different, the SRSS error measures the absolute deviation of the resulting correlation parameter from the target correlation parameter. The single switch operator results in much lower errors than the matrix methods for small sample sizes because the algorithm searches for an optimal ordering of samples until the correlation error is a minimum.

Although the single switch operator provided better correlation control than traditional matrix methods for both section means and Fauré points, experimental tests showed that the fastest way to establish target correlations is through outliers. The result is shown in Figure 4.2a. These types of outliers are less likely to occur when the discrepancy is controlled, as shown in Figure 4.2b.

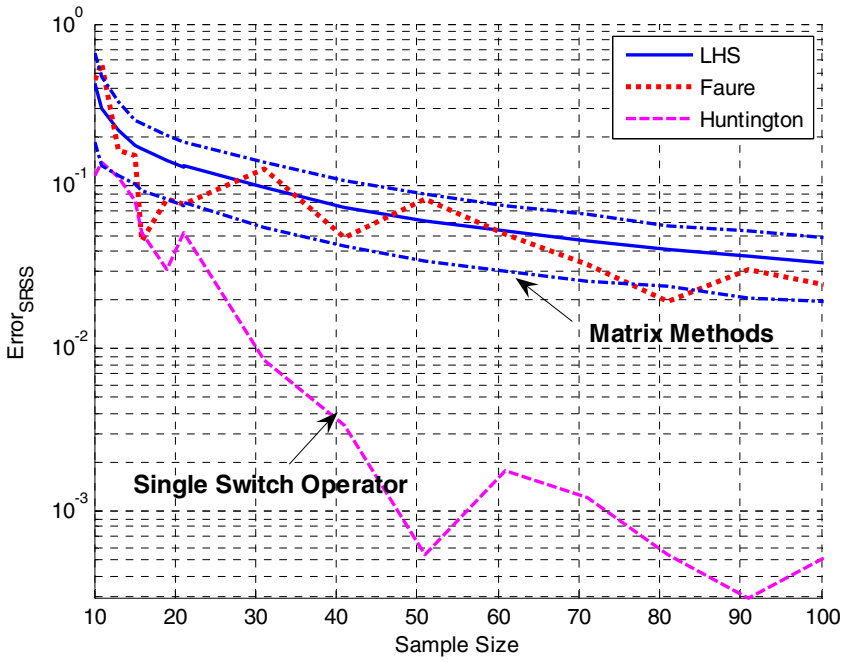

Fig. 4.1 Huntington and Lyrintzis (1998) single switch with sample means versus matrix methods with other sample values.

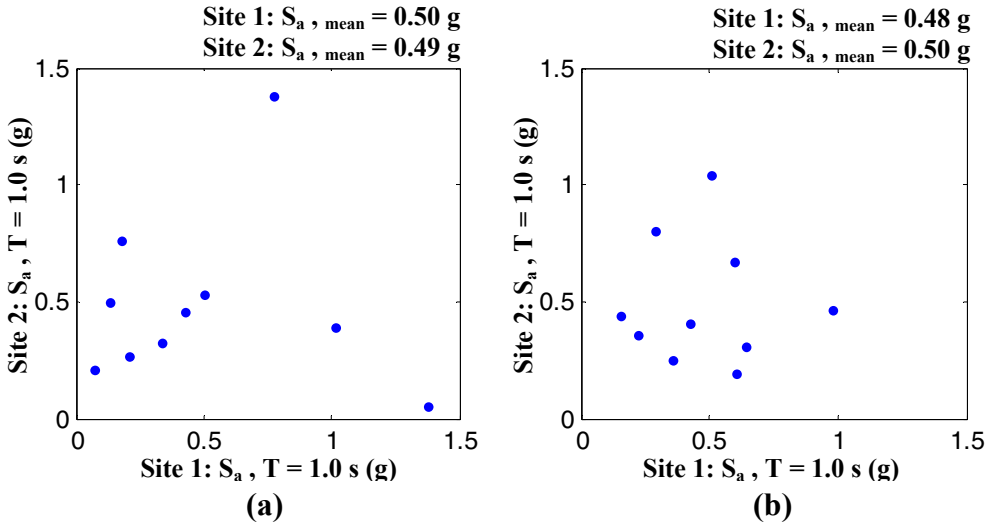

Fig. 4.2 (a) $\rho = 0$, Section mean samples (several outliers); (b) $\rho = 0$, QMC samples (no outliers). Sample means are exact in (a) and approximate in (b), and are indicated in upper right corner of each plot.

In sampling a very small number of ground motion intensities, the single switch operator provides better correlation control than standard matrix methods only if the presence of outliers is checked. The effect of outliers can be reduced by using QMC samples instead of simple random samples or section mean samples.

4.2 SAMPLING OF CORRELATED DISCRETE BRIDGE DAMAGE STATES

The marginal distributions of damage and their known correlation structure (**R**) do not together define their joint distribution. As a result, no unique solution exists for choosing a model from which to sample the joint discrete damage states. Ferson (2004) discusses in greater detail the possible approaches one may take to characterize the dependencies between several variables. One approach in dealing with dependent variables is to transform them into independent variables. Another approach is to consider stochastic models of dependence by assuming a particular dependence function such as the copula.

A copula function ties together the marginal distributions and **R** to define their multivariate distribution. In general, the correlation parameter from the MC simulation will not be equivalent to the correlation parameter used in the linear least-squares optimization approach. However, a linear correlation structure is assumed for sensitivity study purposes and general

comparisons between the two methods can be made. The Gaussian copula used in Sections 4.3–4.5 is expressed as follows (Embrechts 2003):

$$C_R^{Ga}(u) = \Phi^n\left(\Phi^{-1}(u_1), \Phi^{-1}(u_2), ..., \Phi^{-1}(u_n)\right) \tag{4.7}$$

The copula models correlated bridge performance realizations where Φ^n is the jointly distributed n-variate standard normal with correlation matrix **R**, Φ^{-1} is the inverse standard normal, $C_R^{Ga}(u)$ is the n-variate Gaussian copula with the same correlation matrix **R**, and u is a uniform variate. The algorithm for sampling is given in Table 4.1.

Table 4.1 Algorithm for simulating correlated damage states.

- Sample an independent n-variate standard normal (z_i) for $i=1..n$, where n is equal to the number of sites in the network.
- Factorize using Cholesky decomposition $\mathbf{R} = \mathbf{L}\mathbf{L}^T$
- Solve $\mathbf{x} = \mathbf{L}\mathbf{z}$
- Take the probability-integral transform of **x** by $u_i = \Phi(x_i)$, where $u_i \sim uniform(0,1)$
- For a given ground motion intensity level (the independent variable), inverse transform the uniform realizations from the probability of exceedance space to the discrete damage state space.
- Return damage state, $d_i^{(k)}$ where $\{k = 1 \ldots 5\}$

4.3 SCENARIO-BASED LOSS UNCERTAINTY FOR MULTIPLE CORRELATED SITES

The two sub-networks shown in Section 3.3 are tested here using simple random sampling of ground motion intensities and a Gaussian copula for modeling damage dependencies between components in the networks. A scenario-based analysis (M_w = 8.0 event, San Andreas fault zone) identical to the one presented in Chapter 3, is used here for illustrative purposes. The joint ground motion intensities are sampled in this section using a standard Monte Carlo approach where n = 10,000 random numbers in [0,1] are generated in Matlab. Figure 4.3 is a contour of sampled points for a pair of sites in the sub-network. These sampled data are used with the multinomial damage sampling algorithm presented in Section 4.2. A comparison of the discrete joint probability of damage for several cases of ground motion and damage correlation based on an optimization procedure and based on the Gaussian copula is shown in Figure 4.4.

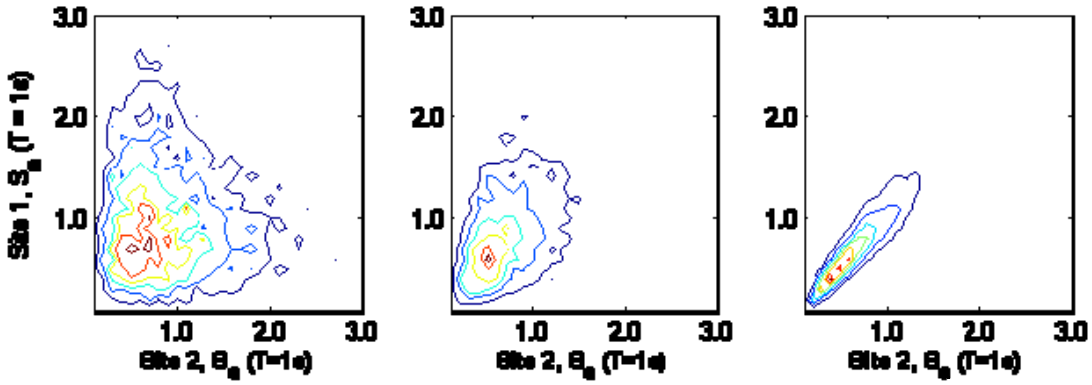

Fig. 4.3 Contours of standard MC sampled joint ground motion intensity realizations where intensity measure is spectral acceleration (S_a) at period T = 1 sec. Cases of ground motion correlation considered are (a) ρ_G = 0; (b) ρ_G = 0.5; (c) ρ_G = 1.0.

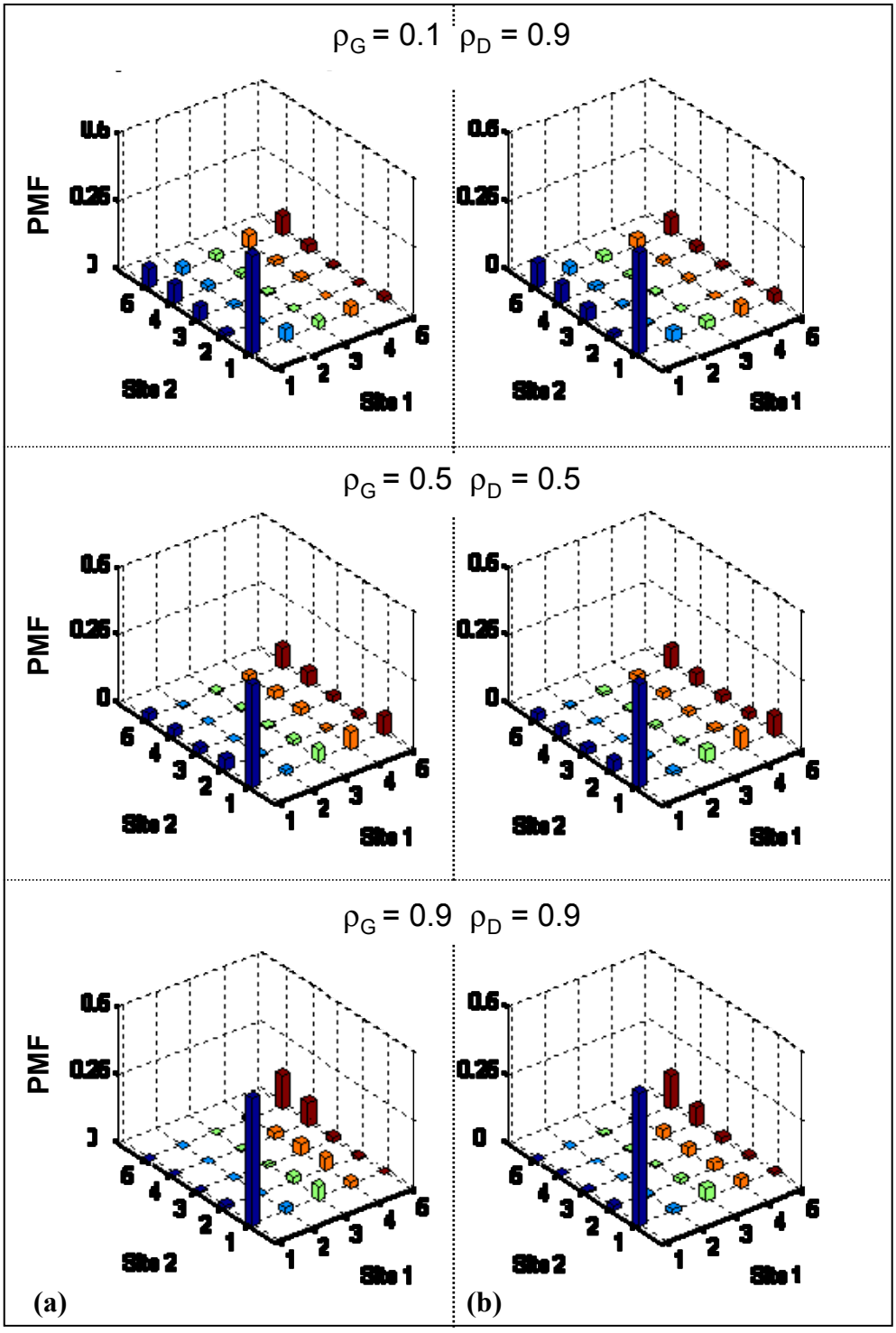

Fig. 4.4 Discrete joint probability mass function (PMF) of damage for two sites under varying cases of ground motion correlation (ρ_G) and damage correlation (ρ_D). Column (a) is optimized discrete PMF. Column (b) is sampled PMF by a Gaussian copula.

The results from the analytical framework are plotted in Figures 4.5–4.6 as open-faced markers. Simulation results are plotted as points with error bars. The standard error is estimated by drawing 1000 bootstrap samples for a 95% confidence interval (Efron and Tibshirani 1993). A comparison of the results from Chapter 3 and results based on standard Monte Carlo techniques reveal good agreement when ground motion correlation levels are high. However, for the smaller network, the MC results do not agree as well when ground motion correlation levels are low.

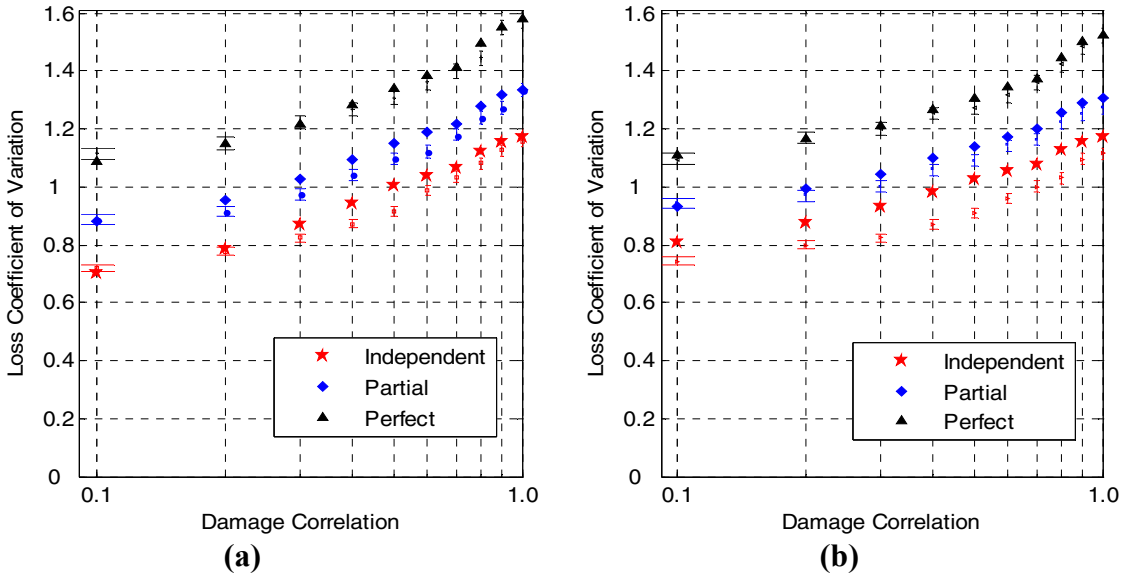

Fig. 4.5 Loss coefficient of variation (CoV) for two networks, (a) *N = 16* sites and (b) *N = 9* sites. Highest marker points ( ) from perfect ground motion correlation; lowest marker points ( ) from independent ground motions.

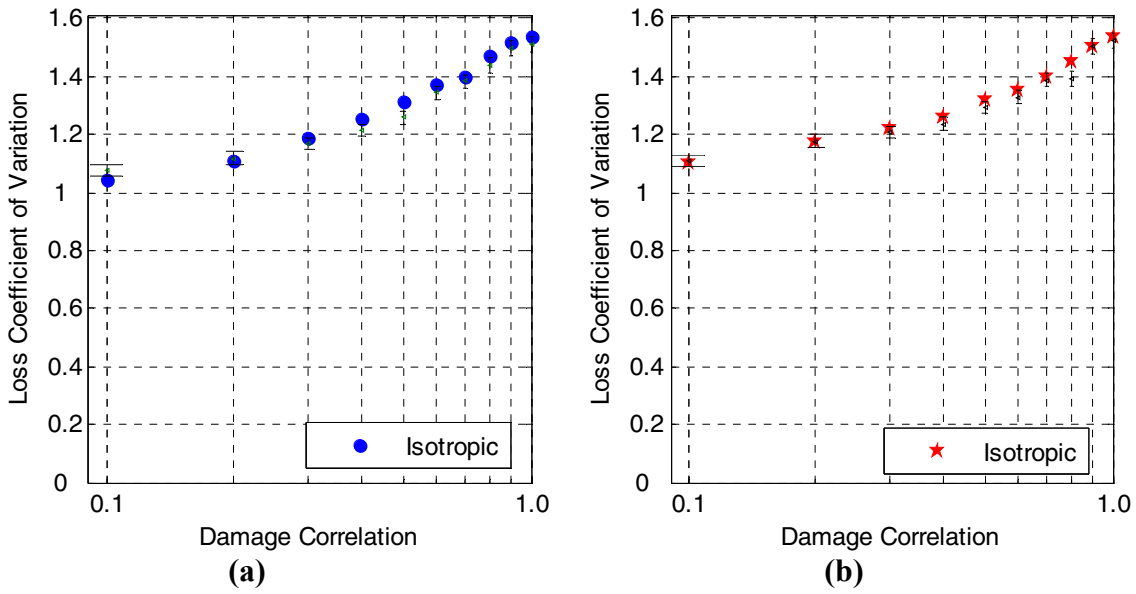

Fig. 4.6 Loss coefficient of variation (CoV) for two different networks, (a) N = *16* sites and (b) *N* = *9* sites assuming distance-dependent isotropically correlated ground motions.

There are several explanations for the differences found in those two figures. One explanation for the differences at low levels of ground motion correlation is that the modeling of damage state dependencies is approximate in both approaches. Thus, they are not identical and as a result, the sensitivity of the loss coefficient of variation when ground motion correlation is low is due to damage state modeling uncertainty. The agreement in the two methods at higher levels of ground motion correlation is because the joint ground motion distribution has a known closed form which is readily captured by standard MC methods. The propagation of modeling uncertainties in multinomial damage states is significant if damage correlations are high and spatial ground motion correlation is low. If, however, ground motion correlation is high, the uncertainty in modeling multinomial damage states is not as significant. This is evident in the distance-dependent case (Fig. 4.6) where ground motion correlations are high for this application. It is nevertheless demonstrated that the influence of the damage correlation parameter is a necessary aspect of characterizing loss uncertainty.

4.4 LOSS DISTRIBUTION

The aggregate loss ($\widetilde{L}$) distribution provides a fully probabilistic representation of direct loss in the network. However, the distribution is not trivial to solve numerically and does not generally fit into any closed-form solution. In such cases, a MC approach is feasible. Uncertainties in damage factor and replacement cost, in addition to uncertainties in ground motion intensity and structural damage, are considered in the loss distribution here. The total component repair cost uncertainties here are assumed to be completely described by uncertainties in damage factor (L) and uncertainties in replacement cost (A).

The loss ($\widetilde{L}_i$) distribution for a single site i is shown below in Equation (4.8), while the sum of their distributions is given in Equation (4.9):

$$f_{\widetilde{L}}\left(\widetilde{l}_i\right) = \int_{L_l}^{L_u} \sum_{d=1}^{5} \int_{-\infty}^{\infty} f_A(a)\, f_{L|D}(l\,|d)\, f_{D|U}(d\,|u)\, dl\, du \tag{4.8}$$

$$f_{\widetilde{L}}\left(\widetilde{l}\right) = f_{\widetilde{L}_1} * f_{\widetilde{L}_2} * \cdots * f_{\widetilde{L}_n} \tag{4.9}$$

where,

U = Spectral Acceleration at T = 1.0 sec

i = component on network consisting of n sites

D = Damage state where, $D \in$ [1, 2, 3, 4, 5]

L = Damage factor given by $L \sim N_{tr}(\mu_t, \sigma_t)$ with truncation bounds in Table 4.2

A = Replacement cost of structure given by $L \sim N_{tr}(\mu_t, \sigma_t)$ with truncation bounds of 40% and 160% of the expected replacement cost

$\widetilde{L}$ = Loss in dollars

$f(\bullet)$ = Probability density function

$*$ = Convolution

L is a damage factor distributed as a Gaussian random variable truncated between an upper (L_u) and lower limit (L_l) from Table 4.2. ρ_G indicates ground motion correlation, ρ_D indicates damage correlation, and an unsubscripted ρ refers to correlation in *both* damage and ground motion.

Table 4.2 Damage-factor bounds from HAZUS and for sensitivity studies (Cases 1–3).

	HAZUS			Case 1		Case 2		Case 3	
Damage State	Mean	L_l	L_u	L_l	L_u	L_l	L_u	L_l	L_u
None	0.01	0.00	0.01	0.00	0.01	0.00	0.03	0.00	0.01
Slight	0.03	0.01	0.03	0.02	0.08	0.03	0.08	0.01	0.03
Moderate	0.08	0.03	0.15	0.05	0.20	0.08	0.20	0.03	0.10
Major	0.25	0.15	0.40	0.20	0.50	0.20	0.60	0.10	0.30
Complete	2/x $x \geq 3$* 1.00 $x < 3$*	0.40	1.00	0.50	1.00	0.60	1.00	0.30	1.00

* x = no. spans

The expected replacement cost $E(A)$ is based on bridge deck area and regional rates of construction. Though no standard metric currently exists to quantify the replacement cost variability, the consensus among experts is that repair cost variation is high and bridge repair efforts must be conducted on an ad-hoc basis (Caltrans 2004).

To understand the impact of these uncertain parameters on the loss distribution, sensitivity tests are carried out. First, the standard MC approach is used to test the sensitivity of the loss distribution to various sources of dependencies in the network. Next, uncertainties in the damage factor and the replacement cost are accounted for and the truncation parameters for both random variables are subject to sensitivity study. In characterizing both L and A, it is assumed that both are normal, centered at their mean values, and symmetrically truncated. It is assumed that a central area under the normal distribution equal to 0.95 is represented in the truncated range. Finally, these approaches are useful in determining whether the truncation estimates of the damage factor as prescribed by HAZUS (2002) are reasonable and how the uncertainty in range of replacement costs affect these loss distributions.

Table 4.3 Sensitivity study (Cases 1–3) for replacement cost truncation.

	L_u	L_l
Case 1	$0.4\mu_A$	$1.6\mu_A$
Case 2	$0.8\mu_A$	$1.2\mu_A$
Case 3	$0.7\mu_A$	$1.3\mu_A$

These questions are investigated by inspecting changes in the aggregate loss distribution due to (1) ground motion and damage correlation and (2) changes in truncation of the distributions on L and on A. Figure 4.7 is a plot of the empirical direct loss PDF under varying

ground motion and damage correlation levels, using a normal kernel smoothing window of varying widths. The y-axis represents the smoothed densities with dollar loss indicated on the x-axis.

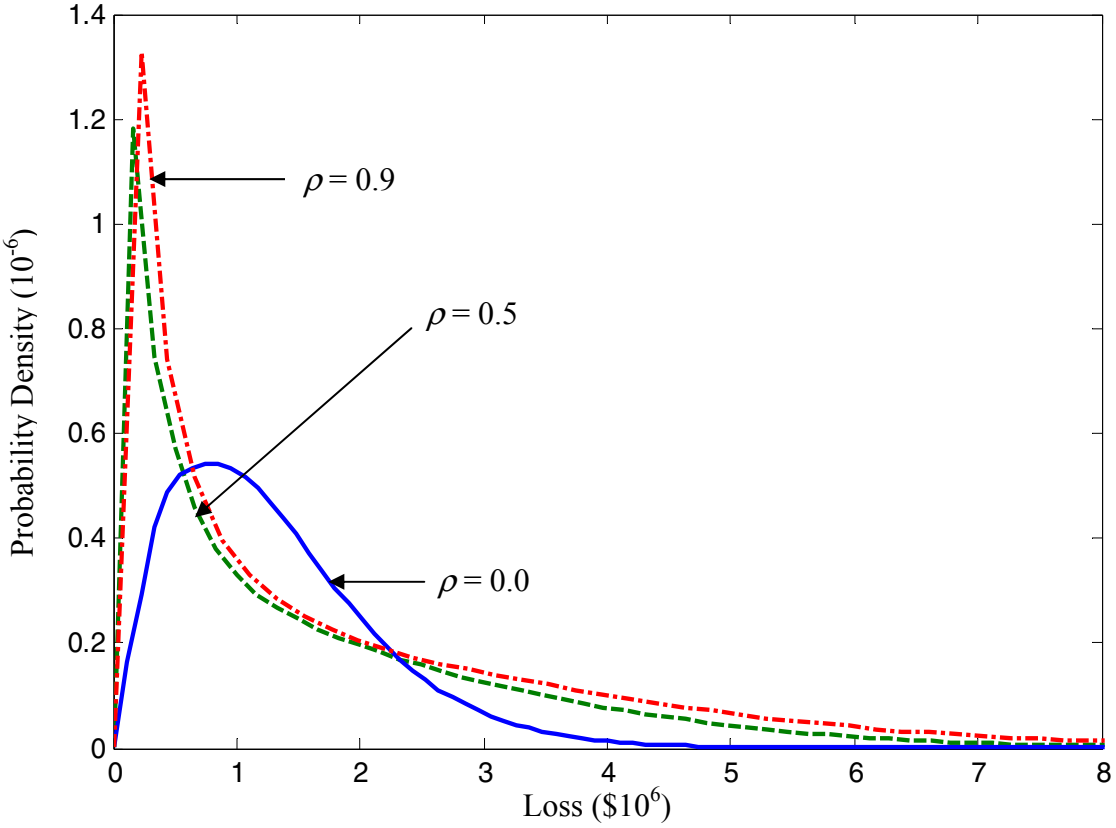

Fig. 4.7 Empirical PDF of aggregate network direct loss.

The effect of correlation on the empirical direct loss PDFs is demonstrated in Figure 4.7. Several observations can be made. First, for uncorrelated sites, the aggregate distribution is well behaved (i.e., not characterized by heavy tails). Second, as higher levels of both ground motion and damage correlation are introduced, the loss distribution becomes increasingly heavy tailed. The implication is that by ignoring correlation, the chance of higher loss levels is significantly underestimated. For example, in Figure 4.7, the differences between ignoring correlation and considering correlation are notable for aggregate loss values above $2.3MM. Fourth, while the means are roughly the same, the standard deviation of the losses becomes higher.

The effect of variations on the truncation bounds for damage factor (L) (see Table 4.2) and the replacement cost (A) (see Table 4.3) were tested next. The damage-factor bounds were varied under the condition that the mean damage factor was within the tested range.

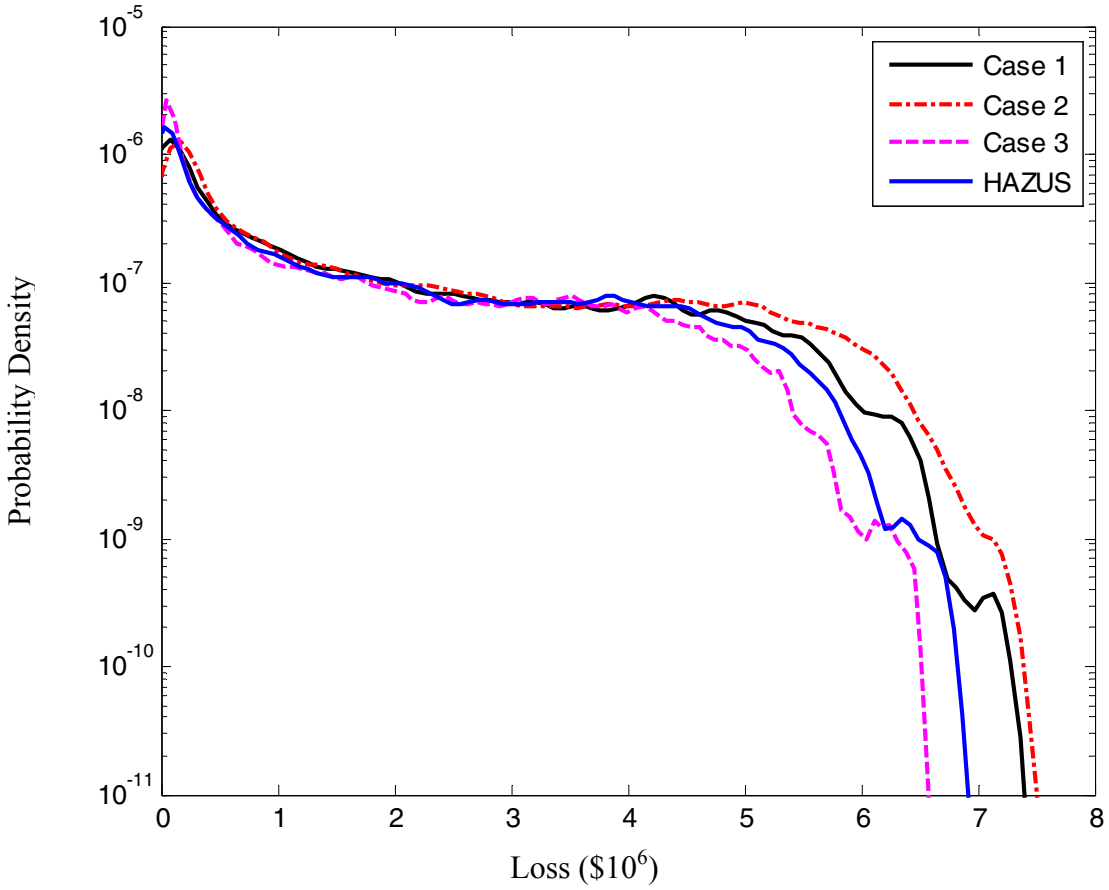

Fig. 4.8 Sensitivity of PDF to damage-factor truncation bounds ($\rho = 0.9$).

The upper tails of the empirical PDF curves highlight the important differences between the damage-factor truncation bounds. The differences are more visible when plotted in log-linear scale. These variations reflect a range of possible low probability, high consequence losses. More importantly, the HAZUS (2002) suggested truncation bounds are shown to be more conservative than one of the cases tested here, but less conservative than two other cases considered.

The replacement cost truncation bounds were then tested for ranges listed in Table 4.3. The results in Figure 4.9 show large differences in the upper tail region of the loss curve, depending on the range of truncation.

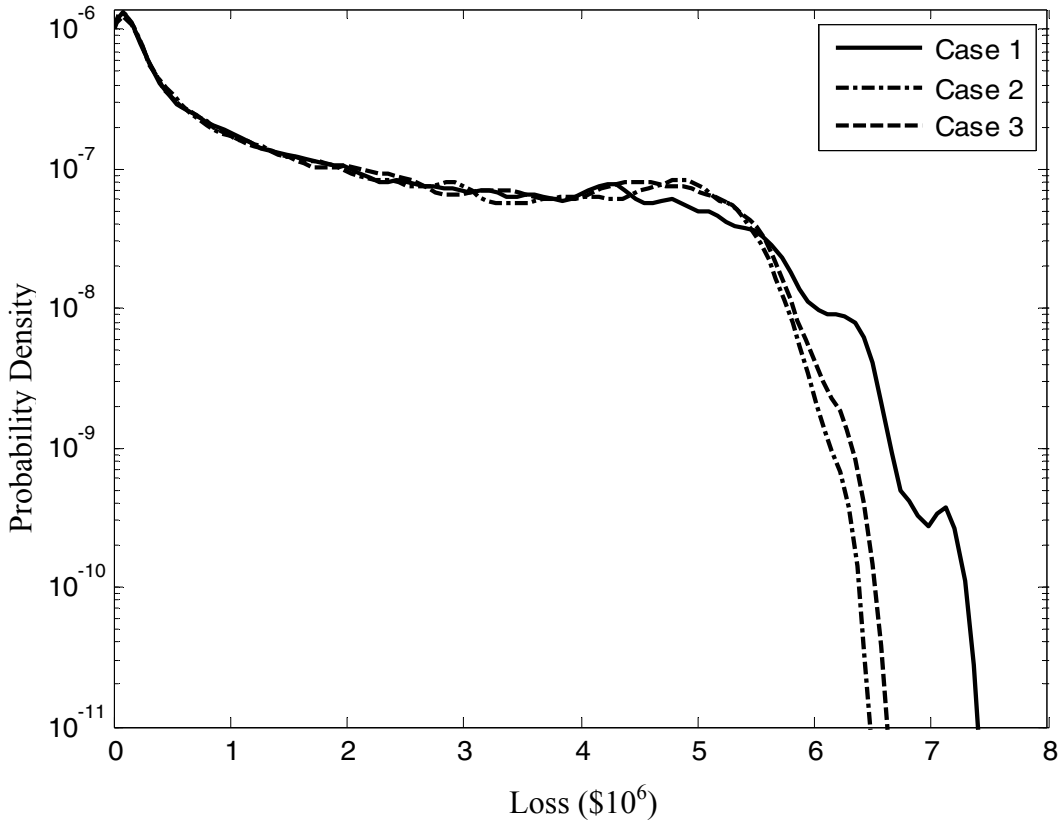

Fig. 4.9 Sensitivity of PDF to truncation bounds on *A*.

In this section, sensitivity studies of the loss PDF to correlation and sensitivity studies related to damage factor and replacement cost truncation were carried out. The motivation of this section was to demonstrate the impact of uncertainty sources to the loss distribution. In doing so, a rational basis for identifying which uncertainties are most critical in the determination of scenario-based risk is developed. These studies may be extended to larger networks or to a portfolio of building structures.

4.5 SCENARIO-BASED EMERGENCY ROUTING WITH CORRELATION: ADAPTIVE ROUTING

The loss decision variable considered in this report has thus far referred to bridge specific direct loss. In the previous section, standard MC methods were used to study the effect of dependencies on the loss distribution and to study the sensitivity of the loss to uncertainties in the damage factor and the replacement cost of bridge structures. Operational loss has not yet been discussed in this research. Its importance, however, has been emphasized in Kiremidjian et al. (2006),

which showed that a more significant portion of the expected total loss was due to delays on the transportation system.

After an earthquake, emergency vehicles must be quickly routed and distribution of relief goods transported from a given origin to a destination. Post-event information about the damage status of bridges on major networks is limited. Repair crews and inspection teams must assess how much of the roadway can safely remain open. Thus, identifying emergency routes on major transportation networks is important for emergency preparedness and planning purposes.

Correlation is applicable in the network analysis because of interdependencies of bridges and roadways in a transportation network. In this section of the report, the effect of correlation on optimal emergency routing for a single origin to single destination problem is demonstrated.

4.5.1 Dijkstra Shortest-Path Algorithm for Emergency Routing Based on Uncorrelated Sites

Various network routing algorithms have been developed to solve the problem of identifying the optimal or least cost path. Two such commonly used algorithms include the Floyd-Warshall (1962) algorithm and Dijkstra's (1959) shortest-path algorithm. Currently, the post-event shortest path is modeled by assuming uncorrelated link travel times that are based on the bridge damage probability. The different bridge damage states correspond to different travel costs for traversing the bridges.

The search for an optimal path is demonstrated in a sample sub-network as shown in Figure 4.10, where closed circles represent bridges and lines represent links on the network. The relevant bridges studied in this network are indicated in Table 4.4 below. It should be noted that a single bridge is associated with multiple links; however each link is associated with a single bridge. The sub-network located in Contra Costa County, CA is subjected to a scenario $M_w = 7.0$ event along the entire length of the Hayward fault.

Table 4.4 Caltrans bridge and link IDs for test network.

Bridge ID	Link ID					
28-0121	4857	4860	4861	5071	5072	5075
28-0122	4967	4968	4984	4990	4991	5061

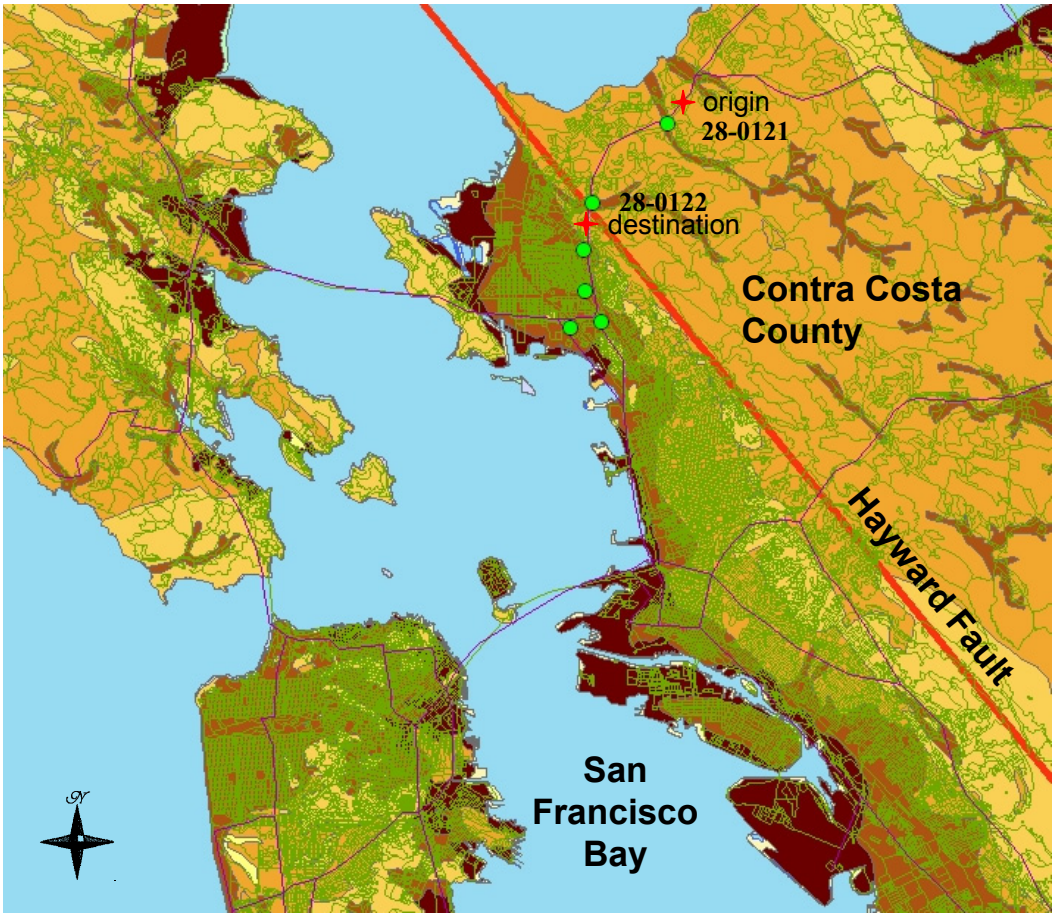

Fig. 4.10 Test sub-network in Contra Costa County for adaptive routing problem; bridge locations marked by filled markers.

4.5.1.1 Methodology

Dijkstra's algorithm is used to find the shortest path between two nodes (e.g., indicated by *"origin"* to *"destination"* in the above example). In determining the shortest path, a connections matrix and a backnode matrix must be initialized. The connections matrix is initially based on the cost of traversing from node j to node k in a directed graph. This cost is denoted c_{jk}. For cases where traversing from j to k is not possible because roadways do not exist, this cost is assigned a very large value. The backnode matrix stores the node-ID for the node last traversed. This matrix provides a means of tracing the optimal path.

The method is based on a tree-branching algorithm. A path that links j to k is compared against a path that links (j to m) to (m to k). If the latter path is the minimum of the two, it is

selected for branching and node m is added to set V as a visited node. If V is the set of nodes already visited, then the algorithm stops once V contains all nodes. All link costs, measured in units of time to traverse, are assumed to be positive.

In the sub-network above, each bridge is associated with a link in the sub-network. Each link, q, in the network is associated with an expected link travel time, $E[T_q]$. For simplicity, link travel times are dependent only on the post-event damage state of the bridge. Link travel times are below, where $k \in [1,2,3,4,5]$ indicates the damage state.

$$T_q^{(k)} = [1.0 \quad 1.5 \quad 3.0 \quad 10.0 \quad 10.0] \times E[T_q] \tag{4.10}$$

For a bridge in a damage state of four or higher, the associated link cost is assigned a large number (i.e., it cannot be traversed). For a bridge in a damage state of three, link costs are increased to three times the expected link cost, while for a damage state of two link costs are increased by 50%. Bridges experiencing no damage (D = 1) will not result in any lane closures or increases in link costs (Kiremidjian 2006).

Only two bridges are considered in the simple demonstrations that follow in the remainder of this section. This small network is chosen to illustrate how conventional emergency routing performs in a single earthquake scenario. The links associated with a bridge consist of roadways that approach the bridge, roadways that depart from the bridge, and exit and entrance ramps to the bridge. Links not associated with any of the bridges are assumed to remain unaffected by the earthquake event. As a result, local roads and highway roads not immediately connected to a bridge are assumed to be fully operational in the event of an earthquake. The transportation network is thus characterized by a high level of redundancy and resilience for connectivity despite bridge failures or road closures.

4.5.1.2 Results

If the ground motion intensities and bridge damage states in the network shown in Figure 4.10 are considered to be uncorrelated, then the optimal path in Figure 4.11 is obtained using Dijkstra's shortest-path algorithm. The expected link travel times, assuming bridges are uncorrelated, are found by multiplying Equation (3.4) by Equation (4.10). The resulting path does not bypass any of the major highway bridges. Thus, small local roads do not provide support in this least cost path.

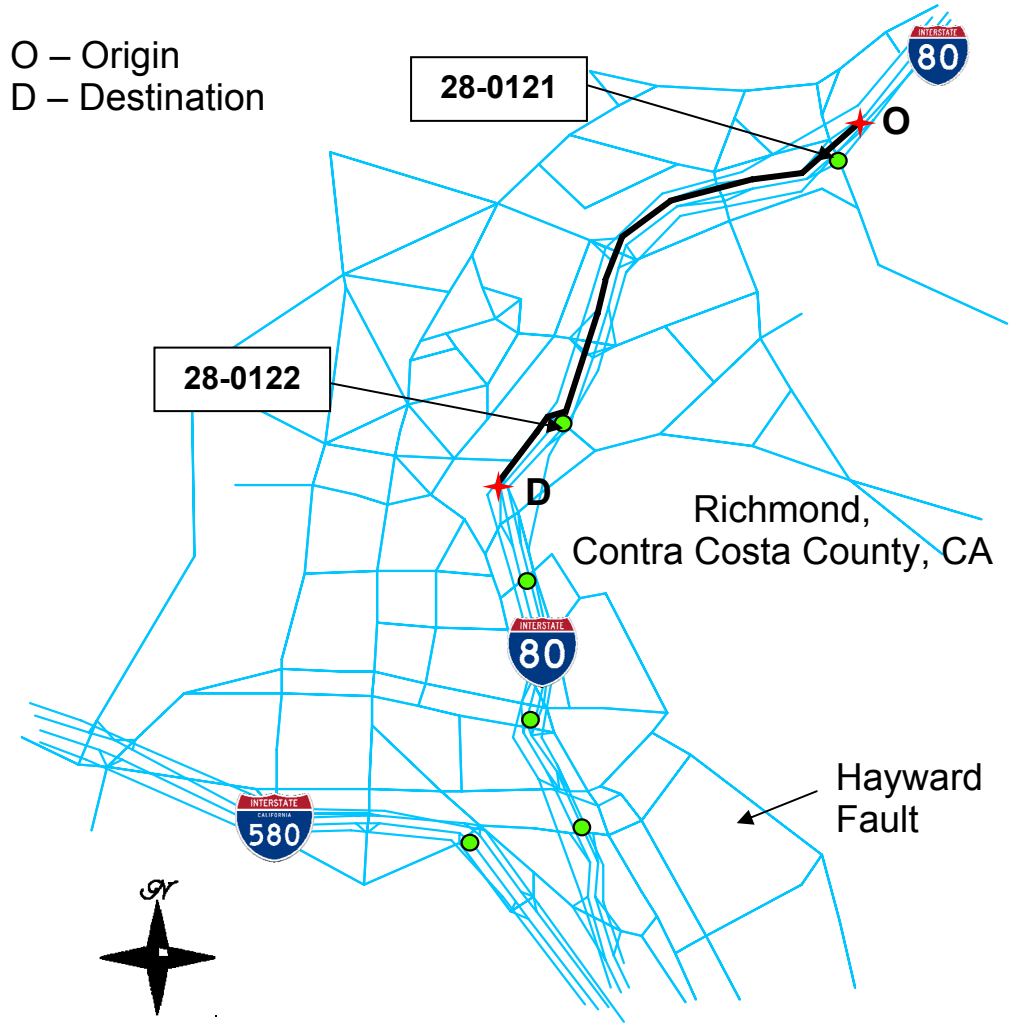

Fig. 4.11 Standard path using uncorrelated link travel times; network located in Contra Costa County, California, subject to characteristic earthquake event on Hayward fault.

4.5.2 Dijkstra Shortest-Path Algorithm for Emergency Routing Based on Correlated Sites

4.5.2.1 Methodology

In demonstrating the impact of ground motion correlations in the network routing problem, the same procedure used for the uncorrelated bridge case is followed, however, with different results. Conventional correlation control using simple random samples were shown in Section

4.1 to have potentially large errors for very small sample sizes. Thus, for the small sample sizes used in the network application, a single-switch operator is used on QMC points to control correlation in ground motion samples. It is demonstrated through application that optimal routing paths will vary depending on the level of ground motion correlation between sites in a network. Though preliminary results show small differences in the optimal path as a result of ground motion uncertainties and correlation, the differences are nonetheless significant for real-time decision making and highlight the variability in routing choices.

An efficient ground motion sampling approach is used to scale down the number of runs required to identify the variations in optimal paths from origin to destination. First, ten realizations of correlated ground motion intensities are sampled using QMC points, and ordered to match a target correlation of 0.5. The damage state for each bridge, conditioned on the ground motion realization, is assessed based on Equation (3.27). Conditional probabilities of damage are used to update the link travel times en-route as an optimal path is found.

The problem is initialized by considering the damage state from the first sample for the first bridge encountered on the path. The conditional probability of bridge $i+1$ being in a damage state of $k \in [1,2,3,4,5]$ given that the damage state at the bridge i is $j \in [1,2,3,4,5]$ is given by Equation (4.11).

$$P\left[D_{i+1}^{(k)} \middle| D_i^{(j)}\right] = \frac{no.of\ samples\left(D_{i+1}^{(k)} \bigcap D_i^{(j)}\right)}{no.of\ samples\left(D_i^{(j)}\right)} \tag{4.11}$$

Expected link travel times for each of the links en-route are assigned according to Equation (4.12) below, where q is the link associated with bridge $i+1$, and ' indicates transpose:

$$E[T_q] = P\left[D_{i+1} \middle| D_i\right] T_q' \tag{4.12}$$

Each of ten damage realizations is used to simulate the possible bridge damage states for the sub-network examples in this section. The first bridge on the route is initially assigned a damage state according to the simulated data. The optimal path is thereafter identified by updating the expected link travel times through conditional damage probabilities. The resulting optimal paths from the correlated bridge damage data are then compared against the least-cost path shown in Figure 4.11. Alternative optimal path configurations are still determined using Dijkstra's algorithm, and are referred to as adaptive paths through the remainder of this section.

4.5.2.2 Results

The optimal routing path found previously was based on uncorrelated bridge damage states. Consideration of spatial ground motion correlation and uncertainties in ground motion intensities results in random realizations of dependent link travel times. In the following example, experiments for each of the link travel time realizations based on the M_w = 7.0 event on the Hayward fault resulted in three different adaptive shortest-path configurations. One of the adaptive path configurations is identical to the path assuming uncorrelated link travel times in Figure 4.11. The two other realizations of adaptive paths are shown below in Figure 4.12 and Figure 4.13.

The configuration for both (two) of these paths is described as follows. In the first configuration shown in Figure 4.12, the damage reported for the first bridge [28-0121] results in a low conditional probability of being in moderate to severe damage states for the second bridge [28-0122]. As a result, link travel times are approximately unchanged from their expected link travel times when ignoring correlation. Upon reaching the second bridge, the bridge damage state realization is determined to be severe (i.e., damage state of four). The other links associated with the second bridge [28-0122] are updated to accommodate this damage information. A detour is taken by bypassing links associated with bridge [28-0122]. The links traversed in this adaptive path configuration are listed in Table 4.5. The links on the left column of Table 4.5 are equivalent to those traversed in the uncorrelated link travel time shortest-path configuration. The links on the right column of Table 4.5 represent those links taken on the detour, after link travel times are adjusted to reflect the realized damage at bridge [28-0122].

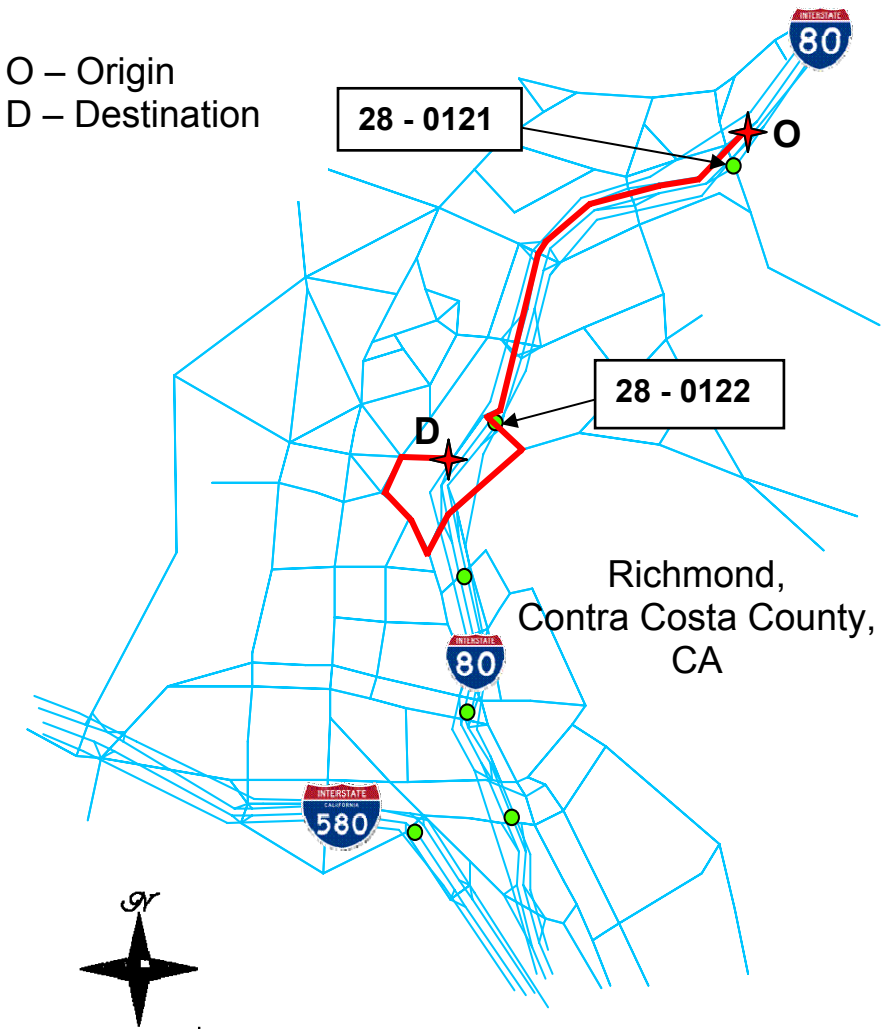

Fig. 4.12 One realization of adaptive shortest path considering correlation in ground motion and in damage, where *O* indicates origin and *D* indicates destination.

The second of these two adaptive configurations differed from both Figure 4.11 and Figure 4.12. In the second configuration shown in Figure 4.13, all roadways associated with bridge [28-0122] are avoided. This occurs because damage information of the bridge [28-0121] results in a high conditional probability of bridge [28-0122] being in one of the more severe damage states ($D \geq 3$). Thus, link travel times are increased according to Equation (4.10) to reflect this higher likelihood of damage.

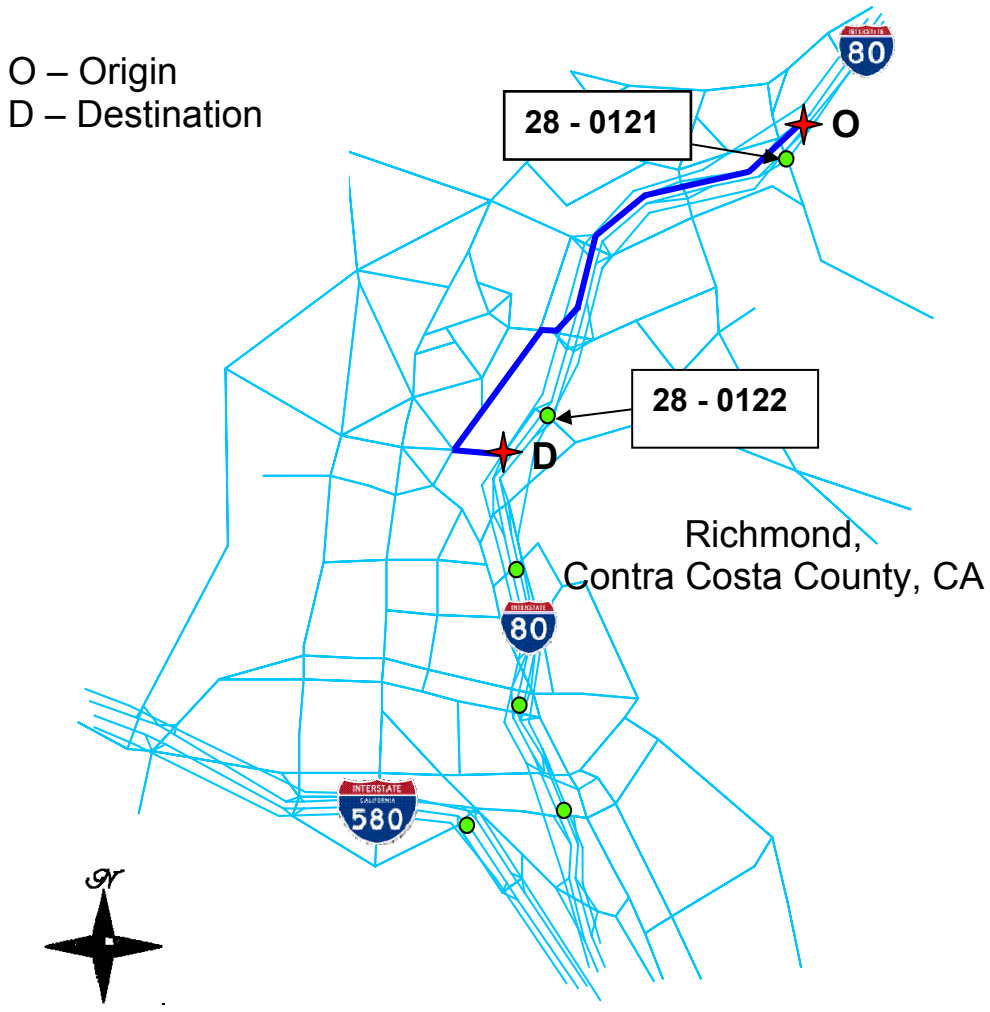

Fig. 4.13 One realization of adaptive shortest path considering correlation in ground motion and in damage, where *O* indicates origin and *D* indicates destination.

These variations on the shortest-path route under uncorrelated bridges results in shorter travel times than the travel time associated with Figure 4.11 route.

Table 4.5 ID for links traversed in adaptive path configuration shown in Fig. 4.12. Arrow to right column indicates where adaptive route deviates from route under assumption of uncorrelated link times.

Link ID	Adaptive Route Link ID
4860 – Bridge 28-0121	4985
4855	5062
4853	5093
4915	24993
5028	4954
4952	4983
4925	5020
4993	25067
4968 – Bridge 28-0122	25063
	24987

Table 4.6 ID for links traversed in adaptive path configuration shown in Fig. 4.13. Arrow to right column indicates how adaptive route deviates from route under assumption of uncorrelated link times.

Link ID	Adaptive Route Link ID
4860 – Bridge 28-0121	4926
4855	4997
4853	24982
4915	24987
5028	
4952	

4.6 APPENDIX: QUASI-RANDOM SEQUENCES

In order to illustrate the concept of discrepancy, Figure 4.14a shows fewer empty areas in the square than Figure 4.14b. In general, QMC achieves improved equi-distribution in lower-dimensional problems (see Figure 4.15) involving small-sized samples when compared to standard MC and LHS. However, in very high dimensions QMC has been shown to under-perform compared to standard MC (see Fig. 4.16). Moreover, it is not possible to estimate the accuracy of the samples themselves without the use of randomized QMC (RQMC) methods,

which are not discussed here. Interested readers are referred to Owen (1998). The motivation and formulation of QMC sampling follows in the remainder of this subsection.

The discrepancy is a measure of the uniformity of a sample of random points. It is defined as the supremum over all differences between the fraction of points lying in the interval [a, b) and the volume enclosed in [a, b). Several measures of discrepancy exist, with the general form given by:

$$D_n(x_1,\ldots,x_n) = \sup_{a<b,a,b\in[0,1)^d} \left| \frac{1}{n}\sum_{i=1}^{n} 1_{a\le X_i<b} - \prod_{k=1}^{d}\left(b^k - a^k\right) \right| \tag{4.13}$$

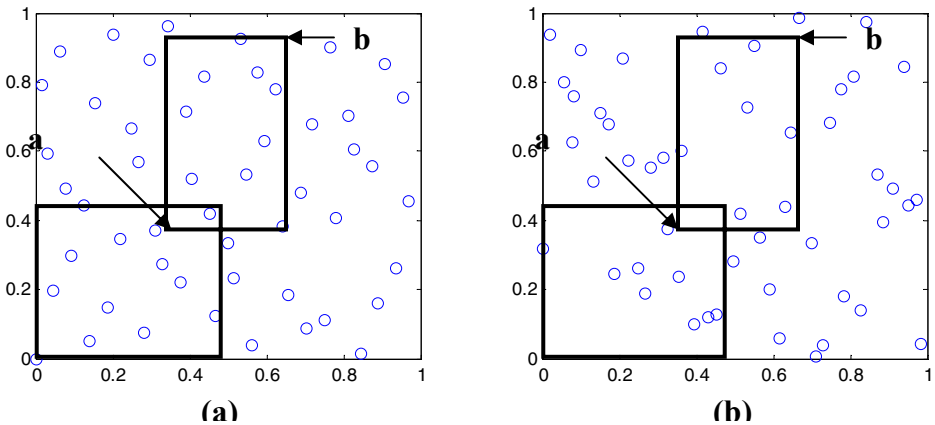

Fig. 4.14 (a) Halton samples and (b) unbiased Latin hypersquare samples.

The second term on the right-hand side represents the volume (i.e., expected number of points) in the box bounded by [*a* , *b*), whereas the first term is the actual number of points that are counted in the box. The box may be grounded to (*a* = 0) or it may float within any *b*-ary box.

The simplest form of quasi-random sampling is the Halton sequence. The radical inverse function, $\phi_b(n)$, forms the basis of the deterministic number generation algorithm for Halton sequences. Here, the n^{th} number of the sequence is written in radix *b*, where *b* > 2, as shown in Equation (4.14) below, then re-expressed back in base 10 as shown in Equation (4.15).

$$\text{for } 0 \le a_k < b \qquad n = \sum_{k=0}^{m} a_k\, b^k = a_0 + a_1 b + a_2 b^2 + \ldots + a_m b^m \tag{4.14}$$

$$\phi_b(n) = \sum_{k=0}^{m} a_k(n) b^{-k-1} = \frac{a_0}{b} + \frac{a_1}{b^2} + \ldots + \frac{a_m}{b^{m+1}} \tag{4.15}$$

Converting *n* base 10 into base *b* requires finding *m*, where *m* is given by one subtracted from the integer result of the logarithm of *n* divided by the logarithm of *b* in base 10 rounded

toward infinity. The value for a's are solved by finding the maximum number of times that the b^m's factor into n. These numbers are then reflected across the decimal point in the radical inverse function and converted back to base 10. The base b is given by the i^{th} prime number (e.g., if $i = 4$, $b = 7$), where i represents one of the bridges in the network.

4.6.1 Halton Sequence

The sequencing of quasi-random vectors (one $n \times 1$ vector for each dimension d) is based on prime bases. Because lower bases produce better sampling uniformity, the lowest prime numbers are used first. As the dimensionality of the problem increases, higher bases are used. Poor equi-distribution of sampling points for higher prime bases results in the breakdown of uniformity after about the fourth dimension. This becomes an issue for higher-dimensional problems. However, QMC is still an attractive alternative to standard MC because the numbers generated are deterministically selected so as to minimize discrepancy. The Halton sequence (Halton 1964) is expressed in terms of the radical inverse function $\phi_b(n)$ and given in Equation (4.16), where the x_i^j's represent the realization for the i^{th} sample of the j^{th} random variable.

$$x_i^j = \phi_{b_j}(i-1)$$

$$x_i^j = \sum_{k=0}^{m} a_k (i-1) b_j^{-k-1} \tag{4.16}$$

4.6.2 Fauré Sequence

To remedy this problem of poor equi-distribution of sampling points in higher dimensions, the Fauré sequence was developed (Fauré 1992). This sequence and other scrambled sequences not included here (Sobol 1967; Tuffin 1996; Warnock 1972), have been based on permutations of the Halton sequence. The numbers are permuted (where π_b represents the permutation) according to the following rules:

For b > 2 and b = even $\quad \pi_b = (2\pi_{b/2}, 2\pi_{b/2} + 1)$

For b > 2 and b = odd $\quad k = (b-1)/2$ $\quad$ k = center value

$\eta_b(j) = (\pi_{b-1}(j))$ $\quad$ when $\pi_{b-1}(j) = 0, \ldots, k-1$

$$\eta_b(j) = (\pi_{b-1}(j)+1) \qquad \text{when } \pi_{b-1}(j) = k,\ldots,b-2$$
$$\pi_b = (\eta_b(0),\ldots,\eta_b(k-1),k,\eta_b(k),\ldots,\eta_{b-1}(b-2))$$

Then the scrambled sequence is given by the following expression, where again the x_i^j's represent the realization for the i^{th} sample of the j^{th} random variable. However, the a's are reordered according to the permutation given in π_b:

$$x_i^j = \sum_{k=0}^{m} \pi_{b_j}(a_k(i-1))b_j^{-k-1} \tag{4.17}$$

Below are sample hypersquares that compare, Halton, Fauré, and LHS samples.

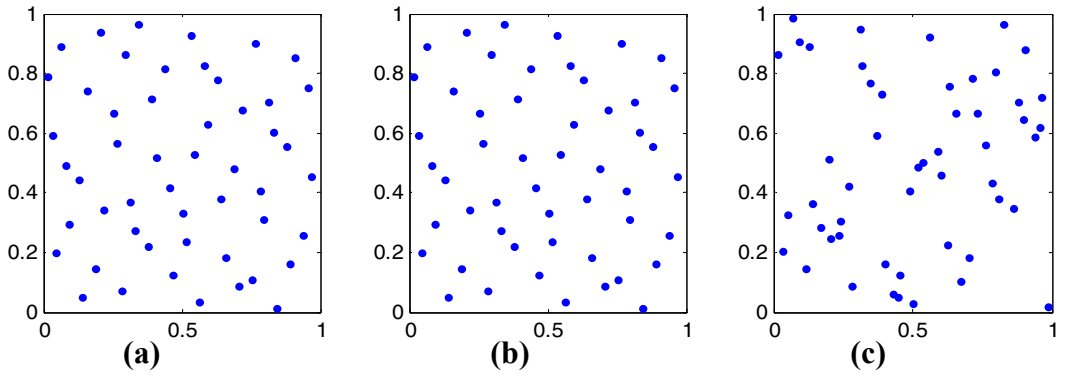

Fig. 4.15 Samples from 1st vs. 2nd dimensions: (a) Halton, (b) Fauré, and (c) LHS.

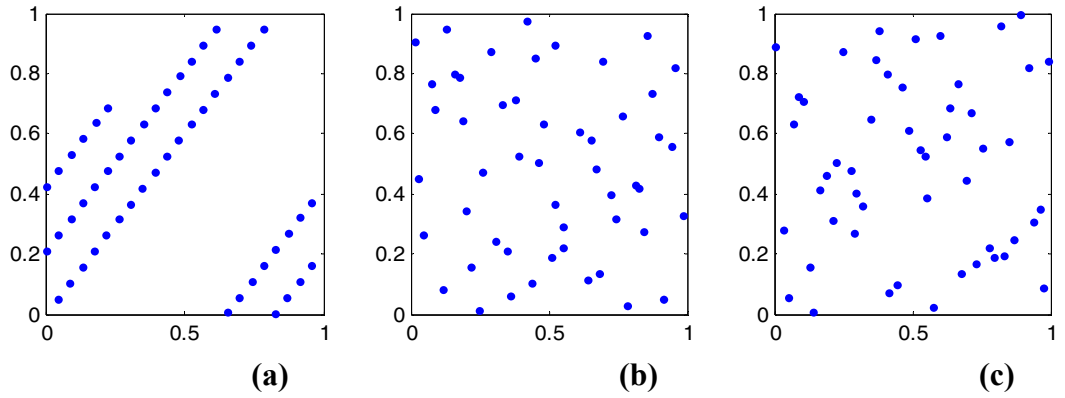

Fig. 4.16 Samples from 8th vs. 9th Dimensions: (a) Halton, (b) Fauré, and (c) LHS.

In Figures 4.15–4.16, the first 50 samples of a Halton sequence, Fauré sequence, and Latin hypercube points were taken and plotted. For small samples sizes (e.g., 50 or less), the LHS samples reveal less uniform coverage of samples points than the Fauré samples.

4.7 DISCUSSION

Modeling dependencies in ground motion and damage for spatially distributed bridges in the network have a significant impact on both the upper tails of the aggregate loss distribution as well as optimal emergency routing configurations for a given origin-destination.

It was demonstrated that for uncorrelated sites, the aggregate distribution is well behaved (i.e., not heavy tailed). As higher levels of both ground motion and damage correlation are introduced, the loss distribution becomes increasingly heavy tailed. The implication is that by ignoring correlation, the chance of higher loss levels is significantly underestimated. While the means of the aggregate loss distributions are approximately equal, the standard deviation of the loss becomes significantly larger.

The upper tails of the empirical PDF curves also highlight the important differences between the damage-factor and replacement cost truncation bounds. These variations reflect a wide range of possible low probability, high consequence losses. The tested damage-factor truncation bounds were such that the mean damage factor from HAZUS (2002) is contained within each of those tested bounds. The suggested HAZUS (2002) truncation bounds were shown to be more conservative than one of the cases tested in these analyses, but less conservative than two other cases considered. Replacement cost truncation bounds were then tested for various ranges. Again, the results point to large differences in the upper tail region of the loss curve.

In the final stage of these scenario-based analyses including correlation effects, the optimal routing configuration for an origin-destination sub-network was evaluated. Previously, optimal paths were found based on the assumption of uncorrelated bridges in the network. Consideration of dependencies between bridges in the network, however, results in link travel times that are dependent. In this research, experiments for each of the link travel time realizations based on the $M_w = 7.0$ event on the Hayward fault resulted in three different adaptive shortest-path configurations. These results highlight the importance of incorporating correlations in the routing decision process.

5 Probabilistic Seismic Risk Analysis for Spatially Distributed Systems: Loss and Reliability

This chapter focuses on ground motion and damage correlation effects in the aggregate loss and in the system reliability risk curves. Retrofit prioritization based on the importance of individual components to overall system reliability is considered. The results indicate that correlation in ground motion and in damage will affect the system risk curve in a significant way.

5.1 INTRODUCTION AND MOTIVATION

For a spatially distributed system such as a transportation network, deterministic scenario-based hazard and risk assessment is often used in favor of a comprehensive probabilistic seismic hazard and risk assessment (PSRA). The PSRA entails identifying all earthquake scenarios that have the potential of affecting a site or region. The catalog of scenarios may then be characterized by uncertainties in magnitude and relative location between rupture and site(s). The computational demands of assessing system risk in a large area and the uncertainties involved in scenario selection can be overwhelming. Thus DSRA approaches are often used for solving spatially distributed system problems.

The annual rate of exceeding an aggregate loss or system performance measure (l) is given by the total probability theorem introduced in Equation (2.1). A disaggregation of risk by ground motion intensity or event magnitude is a useful means of determining the most significant hazard sources that contribute to the risk. For example, losses to drift sensitive or acceleration sensitive nonstructural losses (e.g., damage to lighting or electrical fixtures, nonstructural partitions, water piping), which are caused by more frequently occurring smaller events may dominate the overall loss to a single building over the structure's lifetime (Aslani 2005). In

contrast, the PEER demonstration project by Kiremidjian et al. (2006) illustrated that the large magnitude rare earthquake events contribute more to the mean annual loss to San Francisco Bay Area bridges than smaller more frequently occurring events ($M \leq 6$ or 6.5). This is attributed to the fact that bridges do not contain nonstructural elements. These nonstructural elements are more vulnerable to accumulated damage from smaller events over time.

The assumption of selecting large rare events is verified by considering two checks. First, site hazard curves in the higher IM levels (i.e., $S_a \geq 1.0g$) are compared against published USGS (2002) site hazard curves for an approximate match in the same IM range. Secondly, a disaggregation of expected loss by fault source is used to verify that the events causing the largest damage to the sub-network in question are included in the catalog.

In order to characterize the probabilistic seismic risk, a catalog of earthquake events describing the hazard must be developed. Only characteristic earthquake events contributing to the hazard regime of interest are considered. These characteristic events are identified in the San Francisco Bay Region (SFBR) earthquake model (USGS 2003) to cause large segment ruptures, consistent with geologic, geodetic, and seismic data. They are expected to recur with non-small recurrence probabilities. Background earthquakes, those not identified on one of the seven major fault zones, and aftershock events are excluded from the description of "characteristic" events and are not considered further in the analysis that follows.

Traditionally, Monte Carlo (MC) methods are used to sample probable earthquakes over a finite period of time. Assuming stationarity in the earthquake parameters and arrival processes (Bazzurro and Luco 2005; Wesson and Perkins 2001) reduces the complexity of sampling earthquakes whose stochastic properties will vary over time. The time frame must be sufficiently large to adequately represent the regional hazard. Regional and site hazard maps and their metadata, available for download from the USGS regional hazard maps (USGS 2002), are useful for verifying a MC representation. Alternatively, a method by Chang et al. (2000) associates hazard-consistent probabilities with a small number of characteristic and scenario events. Their research proposed an iterative calibration of these hazard consistent probabilities for each event to approximately match a hazard map for the region and a hazard curve for a single site in the region.

A simple sampling approach based on a USGS (2003) model of SFBR hazard is presented that does not rely on an iterative procedure or a MC sampling of events. The number of (M,R) pairs analyzed can be reduced by using discrete approximations to the parent

distributions via Gaussian quadrature (GQ) techniques. The approach is extremely accurate in matching the statistical properties of the parent distribution with just a few representative discrete value-probability pairs. Thus, the computational burden of the iterative approach or of an exhaustive simple random sampling of magnitudes in time is avoided.

Modeling of the random rupture locations are vastly simplified by considering only characteristic events in the catalog. This is because for characteristic (non-floating) events, the entire fault zone is assumed to rupture. The exclusion of floating events from the earthquake catalog is tested, however, by assessing whether their contributions to the direct loss in the network are relatively small (see Fig. 5.2). Using this catalog of scenarios, seismic risk may be quantified by examining the direct loss and its uncertainty as well as the reliability of a network under varying conditions of ground motion and damage correlation.

5.2 DESCRIPTION OF EARTHQUAKE SCENARIOS

5.2.1 Characterization of Temporal Uncertainty

Earthquake interarrival time is modeled under two cases in this research when characterizing the seismic hazard for a region. First a Weibull interarrival distribution is used to model earthquake occurrence where historic data on the most recent earthquake activity are available. For source zones where historic seismicity data are unavailable, the exponential interarrival model is assumed.

Second, an exponential interarrival distribution is used to model earthquake occurrence. The second model, based on the assumption that earthquake occurrences are described by a Poisson process, requires information only on the mean interarrival times of earthquakes for each rupture source, which is listed in Table 5.1.

5.2.2 Characterization of Fault Rupture

Although a rupture mechanism is generally modeled as random both in rupture length and in rupture location, when considering characteristic events, the entire length of the fault zone is assumed to rupture. Floating rupture events, which are modeled to float with equal likelihood along the fault length, are not considered in this analysis. A disaggregation of loss reveals that floating events contribute far less to the probabilistic risk as compared to non-floating

characteristic events. Floating events result in considerably lower expected losses for bridges in the transportation network than characteristic events (see Figure 5.2). Thus, they are excluded from the earthquake catalog.

5.2.3 Characterization of Seismic Source Zones

The seismic rupture sources in the San Francisco Bay region (SFBR) are identified in the map in Figure 5.1. Associated magnitude-frequency characteristics for the rupture sources are provided in the USGS open file report 03-214 (USGS 2003).

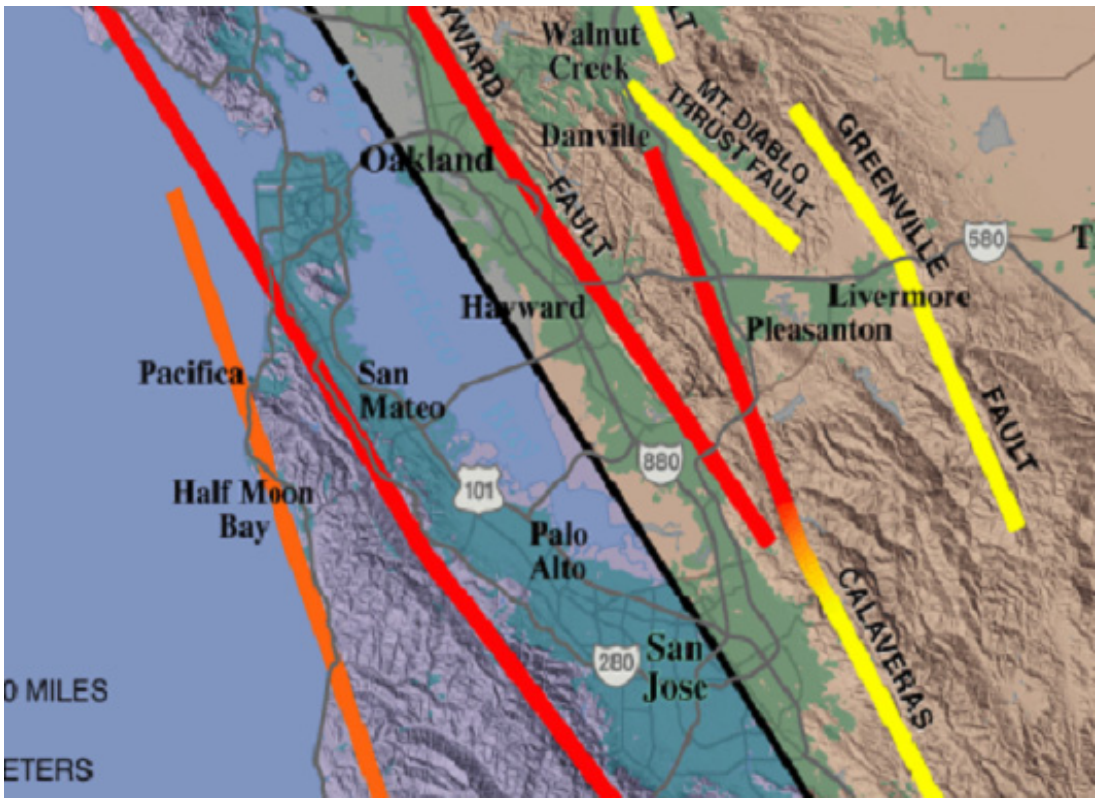

Fig. 5.1 Map of Major fault zones in San Francisco Bay region (SFBR) [USGS 2003]; http://pubs.usgs.gov/of/2003/of03-214/.

Table 5.1 Rupture sources for the San Francisco Bay region (USGS 2003).

ID	Rupture Source	Magnitude			Occurrence Rate (/yr)		
		Mean	2.5%	97.5%	Mean	2.5%	97.5%
1	San Andreas South (SAS)	7.03	6.84	7.22	0.0007	0	0.0015
2	San Andreas Peninsula (SAP)	7.15	6.95	7.32	0.0005	0	0.001
3	San Andreas North (SAN)	7.45	7.28	7.61	0.0001	0	0.0008
4	San Andreas Ocean (SAO)	7.29	7.12	7.44	0.0002	0	0.0011
5	SAS+SAP	7.42	7.26	7.56	0.001	0.0002	0.0029
6	SAP+SAN	7.65	7.48	7.79	0	0	0
7	SAN+SAO	7.7	7.53	7.86	0.0012	0.0004	0.0035
8	SAS+SAP+SAN	7.76	7.59	7.92	0.00002	0	0.0001
9	SAP+SAN+SAO	7.83	7.65	8.01	0.0001	0	0.0004
10	SAS+SAP+SAN+SAO	7.9	7.72	8.1	0.0026	0.0012	0.0042
11	FLOATING	6.9	6.9	6.9	0.0009	0.0001	0.0019
12	Hayward South (HS)	6.67	6.36	6.93	0.0034	0.0012	0.0069
13	Hayward North (HN)	6.49	6.18	6.78	0.0032	0.0011	0.0069
14	HS+HN	6.91	6.68	7.12	0.0024	0.0009	0.0047
15	Rodgers Creek (RC)	6.98	6.81	7.14	0.004	0.0023	0.0063
16	HN+RC	7.11	6.94	7.28	0.0005	0	0.0013
17	HS+HN+RC	7.26	7.09	7.42	0.0003	0.0001	0.0007
18	FLOATING	6.9	6.9	6.9	0.0003	0.0001	0.0006
19	Calaveras South (CS)	5.79	0	6.14	0.0075	0	0.0158
20	Calaveras Central (CC)	6.23	5.75	6.68	0.0054	0.0025	0.0097
21	CS+CC	6.36	5.87	6.75	0.0018	0	0.0065
22	Calaveras North (CN)	6.78	6.58	6.97	0.0035	0.0015	0.0065
23	CC+CN	6.9	6.68	7.11	0.0001	0	0.0011
24	CS+CC+CN	6.93	6.72	7.14	0.0006	0	0.0018
25	FLOATING	6.2	6.2	6.2	0.003	0.0009	0.0077
26	FLOATING CS+CC	6.2	6.2	6.2	0.012	0.0025	0.0285
27	Concord (CON)	6.25	5.75	6.67	0.0014	0.0002	0.0038
28	Green Valley South (GVS)	6.24	5.75	6.65	0.0007	0.0001	0.0018
29	CON+GVS	6.58	6.13	6.91	0.0005	0.00003	0.0016
30	Green Valley North (GVN)	6.02	5.45	6.49	0.0017	0.0002	0.0043
31	GVS+GVN	6.48	6.03	6.81	0.0009	0.0001	0.0024
32	CON+GVS+GVN	6.71	6.34	7	0.0017	0.0003	0.005
33	FLOATING	6.2	6.2	6.2	0.0026	0.0001	0.0126
34	San Gregorio South (SGS)	6.96	6.75	7.17	0.0007	0	0.0023
35	San Gregorio North (SGN)	7.23	7.04	7.41	0.0012	0	0.0034
36	SGS+SGN	7.44	7.27	7.58	0.0008	0	0.0021
37	FLOATING	6.9	6.9	6.9	0.0008	0.0004	0.0014
38	Greenville South (GS)	6.6	6.37	6.83	0.001	0.0004	0.0019
39	Greenville North (GN)	6.67	6.41	6.88	0.001	0.0004	0.0018
40	GS+GN	6.94	6.74	7.13	0.0005	0.0002	0.0009
41	FLOATING	6.2	6.2	6.2	0.0002	0.0001	0.0003
42	Mount Diablo (MTD)	6.65	6.42	6.89	0.0026	0.0006	0.0053

Depending on the location and geographic extent of the network in the SFBR, expected direct loss should be evaluated for all the characteristic and floating rupture sources listed in Table 5.1. For the network consisting of 15 bridges shown in Figure 5.6 and in Figure 5.5, for example, the expected losses for all of the SFBR seismic sources are plotted in Figure 5.2. This

is done to identify seismic sources most damaging to the network, irrespective of their occurrence.

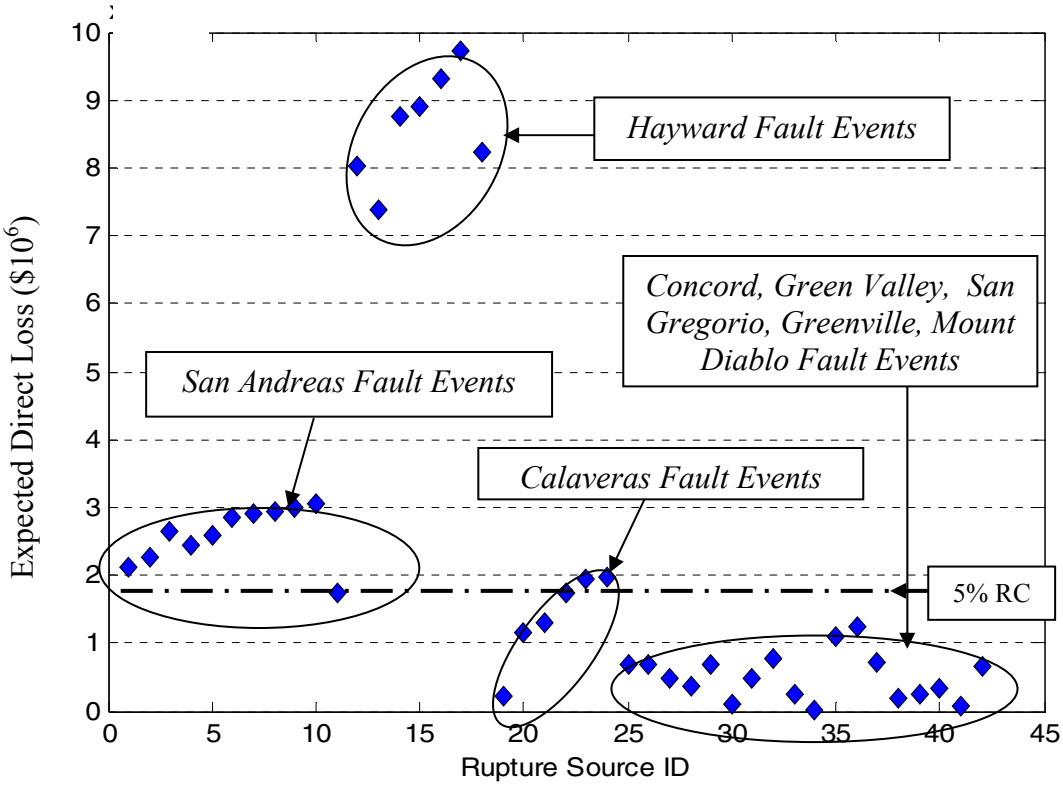

Fig. 5.2 Disaggregation of expected loss, for sub-network consisting of 15 bridges shown in Fig. 5.6, by rupture source ID number listed in Table 5.1.

Expected losses above 5% of the total replacement cost (RC) of the structures are considered to be significant for the sub-network in question. Plotting the expected loss by source as shown below provides a straightforward means of identifying sources contributing the largest risk to bridges in the network. Earthquake sources associated with loss levels above this threshold comprise a catalog of source events to be used for sampling purposes. The total replacement cost for all fifteen structures in the sub-network is equal to $34.4MM.

5.2.4 Characterization of Magnitude Uncertainty

In lieu of standard Monte Carlo simulation, which requires a large number of scenarios to ensure probabilistic accuracy, a simple alternative is presented. Discrete approximations, used to preserve several higher-order statistical moments of the parent (continuous) distribution, are introduced for this purpose.

The characteristic event is modeled as a doubly truncated Gaussian distribution, centered at a mean magnitude given by M_c, and bounded by $\pm 2\sigma_{M_c}$. The discrete approximation to a characteristic event's magnitude is estimated by solving for a few (typically $N \leq 5$) values in the domain of the random variable (m_i) and their associated probability masses (p_i), where i represents the i^{th} discrete value-probability pair. The first ($2N$-1) moments of the continuous distribution must be preserved to arrive at a solution. Together these values constitute a set of representative pairs. In Equation (5.1), $\langle m^k \rangle$ represents the k^{th} moment of M, $f_M(m)$ represents the distribution of M, and the p_i's represent discrete probabilities.

$$\langle m^k \rangle = \int_{m_{\min}}^{m_{\max}} m^k f_M(m)\,dm = \sum_{i=1}^{N} p_i m_i^k \tag{5.1}$$

This involves finding the solution to a set of linear equations as shown in (5.2).

$$\begin{array}{ccccccc}
p_1 & + p_2 & + p_3 & +\cdots & + p_N & = \langle m^0 \rangle \\
p_1 m_1 & + p_2 m_2 & + p_3 m_3 & +\cdots & + p_N m_N & = \langle m^1 \rangle \\
p_1 m_1^2 & + p_2 m_2^2 & + p_3 m_3^2 & +\cdots & + p_N m_N^2 & = \langle m^2 \rangle \\
\vdots & & & & & \vdots \\
p_1 m_1^{2N-1} & + p_2 x_2^{2N-1} & + p_3 m_3^{2N-1} & +\cdots & + p_N m_N^{2N-1} & = \langle m^{2N-1} \rangle
\end{array} \tag{5.2}$$

The m_i's are solved by first defining the polynomial in (5.3) as follows:

$$\psi(m) = (m - m_1)(m - m_2)\cdots(m - m_N) = \sum_{k=0}^{N} C_k m^k \tag{5.3}$$

and noting that $\sum_{i=1}^{N} p_i \psi(m_i) = \sum_{k=0}^{N} C_k \langle m^k \rangle = 0$. After solving for the coefficients C, the m_i's are determined. Given m_i's, the p_i's are solved from the original set of linear Equations (5.2) and (5.3). The procedure is described in detail in Miller and Rice (1983).

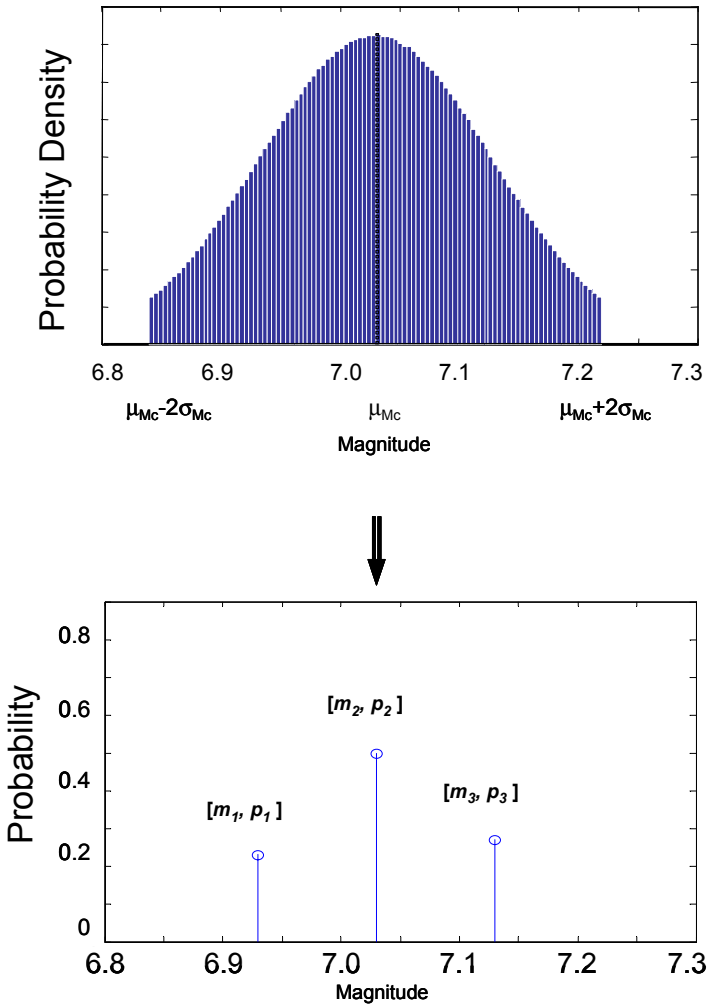

Fig. 5.3 Discrete magnitude-probability pairs for one characteristic rupture source.

For each of the events in the earthquake catalog, the first five moments of the magnitude distributions are matched to solve for three representative pairs. More pairs ensure better higher-order moment matching but offset the computational gains of reducing the overall number of event simulations required. The first five moments, however, are considered to be robust enough for the analysis purposes in this research. Every earthquake event in the catalog is thus disaggregated into three possible (*M, R*) pairs.

5.2.5 Procedure Verification

Site hazard curves for an application network were developed for characteristic earthquakes from 17 rupture sources identified in Figure 5.2. The *(M,R)* disaggregation previously described resulted in an earthquake catalog consisting of a total of 51 earthquakes under consideration.

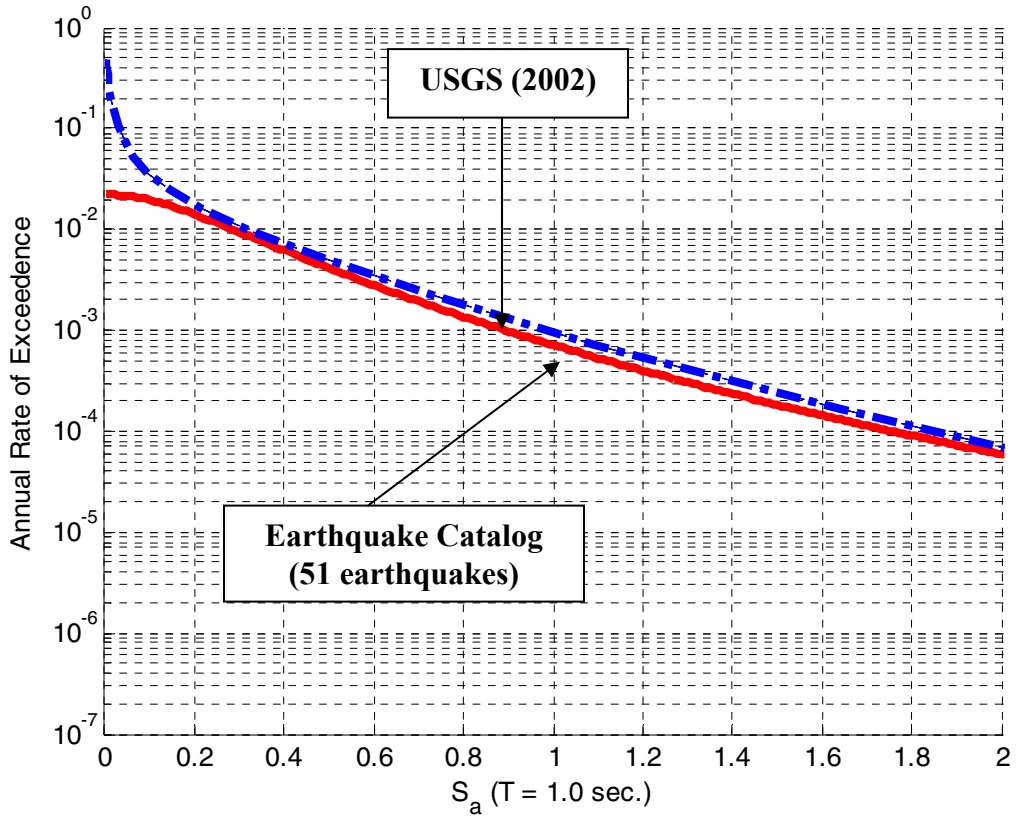

Fig. 5.4 Comparison of USGS (2002) site hazard curve with discrete representation procedure for one site in network.

The hazard curves based on this catalog were then compared against the complete PSHA reported by USGS (2002) hazard data.

From the comparison, the hazard curve diverges significantly in the left lower tail in Figure 5.4. This is a natural result of limiting the earthquakes in the catalog to larger events. It should be noted that the hazard curves reported in http://earthquake.usgs.gov/research/hazmaps correspond to a 1.0 sec spectral acceleration for sites located between latitudes 37.7° to 37.9° and longitudes between -122.1° to -122.3°. Test site locations will not correspond precisely to USGS hazard map data coordinates due to the rough 0.10° increments in USGS (2002). A tenth of a

degree latitude corresponds to approximately 11 km. A tenth of a degree longitude corresponds to approximately 9 km within the coterminous United States.

5.3 SYSTEM DIRECT LOSS EXCEEDANCE, SUB-NETWORK RELIABILITY, AND RETROFIT ACTION FOR A NETWORK

Risk exceedance curves serve as important quantitative aids in identifying acceptable risk tolerances for decision makers or risk insurers in a fully probabilistic setting. This section of research is focused on the development of exceedance curves for two risk metrics and the determination of retrofit prioritization's impact on system risk exceedance curves. Specifically, this research addresses how the network loss and reliability curves shift with the varying influence of uncertainties and correlations in ground motion intensities and in damage. After obtaining system reliability curves for the network, another goal of this research relates to understanding how important individual bridges in the network are to the overall system reliability. The importance of specific bridges is essential for identifying candidate bridges to retrofit. Once these candidate bridges are identified, the impact on system risk curves to varying degrees of retrofit upgrade is observed. A full retrofit consideration involves an assessment of network delays due to improvements in bridge performance, which is beyond the scope of this research.

5.3.1 Assembling Annual Risk Exceedance Curve

The annual rate of exceedance curve is developed by first assessing the decision variable (DV) for each earthquake event, then ranking the DV from lowest (1) to highest (N), where the N^{th} earthquake corresponds to the most damaging earthquake in the catalog. The annual probability of exceeding some DV_i is expressed as:

$$P\left[DV \geq DV_i\right] = P\left[DV_i \cup DV_{i+1} \cup DV_{i+2} \cdots \cup DV_N\right]$$

The DVs in the above equations are collectively exhaustive but not mutually exclusive. This is because the occurrence of more than one DV in a year is possible in the outcome space. Hence, the union of the DVs is not equal to the sum of the probabilities associated with each of

the *DV*s, but rather the result of addition and subtraction of summations of *DV*s. The above can be rewritten more simply as follows:

$$P[DV \geq DV_i] = 1 - P\left[\left(DV_i \cup DV_{i+1} \cup DV_{i+2} \cdots \cup DV_N\right)^*\right]$$

$$= 1 - P\left[DV_i^* \cap DV_{i+1}^* \cap DV_{i+2}^* \cdots \cap DV_N^*\right]$$

In the formulation, $P[DV_i \cup DV_i^*] = 1$ where the asterisk defines a complementary event. The above is consistent with de Morgan's rule. After assuming *DV*s are independent, the equation can be reduced to the following:

$$\begin{aligned} &= 1 - \prod_{j=i}^{N} P[DV_j^*] \\ &= 1 - \prod_{j=i}^{N} \{1 - P[DV_j]\} \\ &= 1 - \prod_{j=i}^{N} \left\{1 - \left(1 - e^{\nu_{m,j}}\right)\right\} = 1 - \prod_{j=i}^{N} \left\{e^{\nu_{m,j}}\right\} \\ &\approx 1 - \prod_{j=i}^{N} \left(1 - \nu_{m,j}\right) \end{aligned} \tag{5.4}$$

In the above expression, $\nu_{m,j}$ is the mean annual rate of the j^{th} ($j = i \ldots N$) most damaging earthquake in the catalog. The expression is approximated after a Taylor series expansion in the last line of Equation (5.4).

5.3.1.1 Annual Exceedance of μ+1σ Direct Loss

The expectation and variance of aggregate loss for a network are evaluated following methods in Chapter 4 for every scenario in the earthquake catalog. Each event is associated with an *annual rate* of *occurrence* (ν_m) (USGS 2003). Conditioned on a seismic event, the $\mu+1\sigma$ loss is ordered according to the ranking definition described in Section 5.3.1.

5.3.1.2 Annual Exceedance of System Failure

The annual exceedance of some level of system failure, denoted P_f, is developed by using the earthquake catalog and the ordering rationale behind Equation (5.4). P_f can be solved approximately for a sub-network via a minimum cut-set formulation. It should be noted that

system failure is hereafter denoted by a capital P_f, while individual bridge failures are denoted by a lowercase p_f. After identifying the minimum cut-sets for the sub-network, each component's limit state function is written as shown in Equation (5.5). The sub-network in question may be analyzed as a series system in parallel (SSP) by identifying the minimum cut-sets on a network between origin and destination. These minimum cut-sets are defined such that failure of any cut-set will result in failure of the system, and failure of any component within a cut-set will make it no longer a cut-set. The SSP formulation is widely referenced in the literature (Yeh and Loh 2001; Augusti et al. 1998).

Each of the bridges on the network act as individual components defined by the limit state function described as follows:

$$\begin{aligned} \{g_i(x) = U_{capacity,i} - U_{demand,i}\} \\ U_{demand,i} = LN(\mu, \sigma)_i \\ U_{capacity,i} = LN(\lambda_{\text{mod}}, \xi_{\text{mod}})_i \end{aligned} \tag{5.5}$$

where U_{demand} is the ground shaking corresponding to spectral acceleration at a period of 1.0 sec which is a lognormally distributed random variable with parameters (μ, σ). $U_{capacity}$ is the bridge fragility function lognormally distributed with parameters (λ_{mod}, ξ_{mod}). These parameters, subscripted *mod*, are associated with a fragility that characterizes exceedance of a moderate damage state. The link is closed to traffic for a bridge in a moderate damage state or higher (Cho 2003). g is the limit state function, where $g \leq 0$ constitutes failure of the component and $g > 0$ constitutes survival of the component. i indicates the component in the network.

Network reliability is defined as the viability of an origin-destination path via major highways and select roadways in the network. The probability of network failure for the same origin-to-destination sub-network is assessed for every event in the catalog. An equi-correlated ground motion model is used to describe the correlation in U_{demand} between each of the sites in a network. Similarly, an equi-correlated damage model is used to describe the correlation in the capacities, $U_{capacity}$. The probability of network failure from origin-to-destination for every event in the catalog is estimated using the first-order system reliability method (Melchers 1999).

5.3.2 System-Reliability Assessment with Correlated Components

This section introduces and outlines the methodology used to assess bridge importance from a system reliability perspective. Current retrofit prioritization decision models for transportation networks typically ignore correlation effects in determining not only system direct loss, but also in determining system performance. Additionally, ranking bridges by most seismically vulnerable to least vulnerable based on a site-specific hazard assessment does not in itself justify a good ranking hierarchy. Minimizing the loss of network performance with respect to upgrade of damaged components, assumed to be independent, was proposed by several researchers in the recent past (Sohn et al. 2003; Basöz and Kiremidjian 1996; Yeh and Loh 2001) and is the topic of more current research by Liu and Fan (2007). Other models address correlation by approximating bounds on system failure (Selcuk and Yücemen 2000; Song and Der Kiureghian 2005).

The reliability of a network for a given origin to a given destination is particularly important for retrofit decision making. Although local roads provide a high degree of redundancy to the transportation system in the SFBR, use of local roads as a fastest path from origin to destination may be unacceptable in some emergency cases.

In a retrofit effort an exhaustive bridge retrofit program is prohibitive because of the expense of retrofit. Thus, where budget constraints restrict the number of bridges that can be retrofitted, a retrofit prioritization framework must be able to identify critical bridges with respect to overall system performance rather than individual bridge performance. These most critical bridges in a network can be identified from a FORM sensitivity analysis. This approach eliminates many bridges from consideration for bridge retrofit. After identifying these most important bridges, cost-benefit analysis or economics of resource allocation must be addressed though they are not addressed in this research.

5.3.2.1 Retrofit Prioritization Methodology

The advantage of using FORM in identifying candidate bridges for retrofit upgrade is that important bridges are selected based on their site ground motion and damage considerations as well as their importance in network resilience. The disadvantage of such an approach, however,

is that its use is prohibitive for very large, complex networks characterized by a high degree of redundancy. This is due to the difficulty of generalizing the cut-set or path-set formulation for such large complex networks. As a result, this kind of procedure is extremely beneficial for studying retrofit upgrade planning for small-scale critical networks where hospitals or distribution centers for relief goods are known to be highly concentrated or in extremely critical regions. This procedure serves as a way of pre-screening candidate bridges for retrofit upgrade before any operational loss studies are undertaken.

The sensitivity of the system failure to small changes in the component reliability indices (β_i) is recorded for each event in the record. Those components whose reliability indices have the greatest influence on system failure are considered most important. The ranking of bridges by $\partial P_f / \partial \beta$ considering different cases of ground motion and damage correlation is observed. Treatment of dependencies such as these in reliability studies is discussed in Section 5.5: Appendices. The impact of correlation in this ordering is tested. A sensitivity study yields several insightful observations about the importance of individual components to the network failure. This is considered by using the following formulation of general system failure based on structural reliability:

For general systems, the probability of system failure is expressed as follows

$$P_f = P\left[\bigcup_m \bigcap_{i \in C_m} \{g_i(x) \le 0\}\right] \tag{5.6}$$

In formulating Equation (5.6), the failure of a given cut-set, C_m, is given by

$$E_m = \bigcap_{i \in C_m} \{g_i(x) \le 0\} \tag{5.7}$$

Then the system probability of failure (P_f) follows from the inclusion-exclusion rule, where n_c is the total number of components in the system and m is the total number of cut-sets:

$$\begin{aligned} P_f &= P\left(\bigcup_m E_m\right) = P(E_1 \cup E_2 \cup E_3 \cup \ldots E_{n_c}) \\ &= \sum_{i=1}^{n_c} P(E_i) - \sum_{j=1}^{n_c} \sum_{i}^{j-1} P(E_i E_j) + \cdots + (-1)^{n_c - 1} P(E_1 E_2 \cdots E_{n_c}) \end{aligned} \tag{5.8}$$

An event failure is a function of the failure of the components in that cut-set (e.g. $E_1 = \{g_C(x) \le 0 \cap g_D(x) \le 0\}$). Equation (5.6) undergoes a standard normal transformation using a Nataf transformation, resulting in Equation (5.9) (Melchers 1999). The result is a first-order approximation that is obtained from the mapping of lognormal variables to standard normal space.

$$P_f \approx P\left[\bigcup_m \bigcap_{i \in C_m} \{G_i(u) \le 0\}\right] \tag{5.9}$$

where $G(u) = 0$ is linearized at the design point u* for each limit state function using a Taylor series expansion as shown in Equation (5.10).

$$G_i(u) \approx \nabla G^T(u_i^*)(u - u_i^*) = \|\nabla G^T(u_i^*)\|[-\alpha_i^T(u - u_i^*)] = \|\nabla G^T(u_i^*)\|[\beta_i - \alpha_i^T u] \tag{5.10}$$

α is the unit vector $\perp$ to $G(u)$ at the design point (u^*). U indicates a variable in standard normal space. u_i^* is the design point determined from the Hasofer-Lind Rackwitz-Fiessler (HL-RF) algorithm, β_i is the bridge reliability index (from the HL-RF algorithm). The sensitivity of system failure (P_f) to β_i is tested by checking the change in P_f with a change in β_i (Rackwitz and Fiessler 1978).

5.3.2.2 HL-RF Algorithm

The HL-RF algorithm is one commonly used method in structural reliability for finding the design point, u^* in Equation (5.10). The design point corresponds to a point on the limit state surface ($G(u) = 0$) that results in the shortest distance between the origin of the standard variate space and the limit state surface. This shortest distance is given by β. This section discusses the search algorithm for finding u^*.

Finding u^* involves solving the constrained optimization problem in Equation (5.11).

$$\begin{aligned} &\text{minimize } \|u\| = \sqrt{u^T u} \\ &\text{subject to } G(u) = 0 \end{aligned} \tag{5.11}$$

From a starting value of u_o, the algorithm iterates to u^* by updating u_k through the following formula:

$$u_{k+1} = \frac{\nabla G(u_k)}{\|\nabla G(u_k)\|^2}[\nabla G^T(u_k)u_k - G(u_k)] \tag{5.12}$$

where $u_k = [u_1, u_2, \ldots, u_n]_k^T$, $\nabla G(u_k) = \left[\frac{\partial G}{\partial u_1}, \frac{\partial G}{\partial u_2}, \ldots, \frac{\partial G}{\partial u_n}\right]$ is the gradient of the limit state function at $u = u_k$, and $G(u_k)$ is the limit state function evaluated at u_k. The estimate of the reliability index at the k^{th} iteration, β_k, is given by Equation (5.13).

$$\beta_k = \left[-\frac{\nabla G(u_k)}{\|\nabla G(u_k)\|}\right]^T u_k \tag{5.13}$$

When $|G(u_k)|<\varepsilon_1$ and $\|u_k-\beta_k\alpha_k\|^2<\varepsilon_2$, the algorithm terminates, ensuring that the design point is on the limit state and that *u** is the origin projection point on a hyper-plane tangent to the limit state surface, respectively. Both ε_1 and ε_2 have very small tolerances.

5.3.2.3 Retrofit Prioritization for a Network in Contra Costa County, California

The following network located in Contra Costa County, California, consists of 15 bridges labeled alphabetically in Table 5.2 with corresponding bridge numbers. The sub-network, which is part of the larger SFBR network, is used to illustrate the goals of this chapter. Hereafter, this sub-network is referred to throughout the remainder of this chapter.

Fig. 5.5 Sub-network location for single origin–single destination viability assessment.

Table 5.2 Caltrans bridge IDs for sub-network bridges and corresponding letter IDs.

Bridge	ID	Bridge	ID	Bridge	ID
33 0162	A	33 0416	F	33 0314	K
33 0227	B	33 0414	G	33 0315	L
33 0159	C	33 0420	H	33 0324	M
33 0318	D	33 0313	I	33 0343	N
33 0359	E	33 0289	J	33 0421	O

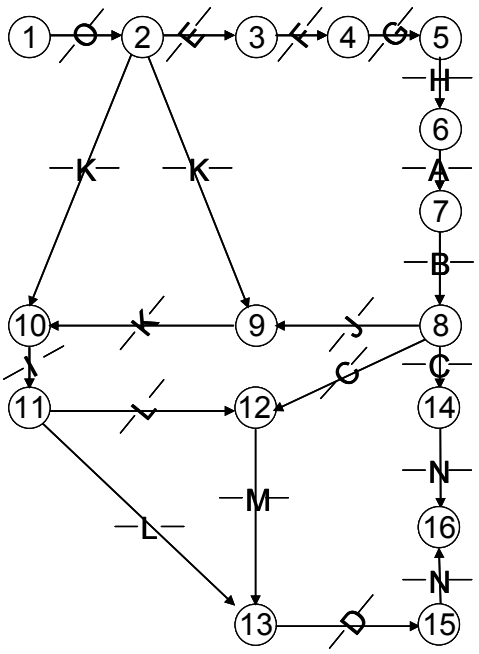

Fig. 5.6 Major roadway configuration for sub-network in Alameda County, California. Nodes indicated by numbers. Links associated with a bridge, indicated by alphabetic ID shown in Fig. 5.5.

The origin (*node 1*) and destination (*node 16*) are both associated with bridges. These bridges are assumed to act as a fictitious source and sink, respectively, of commuter traffic. For clarity, the origin is indicated by bridge *O* (33-0241) while the destination bridge is indicated by bridge *N* (33-0343). Using the alphabetic notation, the minimum cut-sets for the sub-network are indicated in Figure 5.7. The capacities and demands at each of the bridges on the network are treated under three different cases below. The reliability of the network under all three conditions is considered.

5.3.2.3.1 Modeling Assumptions

Modeling assumptions, used to simplify a number of complexities in the network, are described in this section. Bridges are assumed to be located on links, whose status can only be assigned a binary damage state: damaged or undamaged. Nodes, located where two or more links intersect, are assumed to be unaffected or undamaged post-event. Bidirectional traffic, changes in network flow, or traffic redistribution are not considered in assessing system viability. Viability refers in this research to the existence of a viable path from origin to destination via the designated highway and surface road links. Several links map to a single bridge; however each link can map only to a single bridge. Links and nodes are modeled in a directed graph shown in Figure 5.6.

5.3.2.3.2 Modeling the General System

After defining all major links, the sub-network is converted into an equivalent series/parallel system (SSP) as shown in Figure 5.7. The sub-network in Figure 5.6 consists of major expressways and surface roads, characterized by a maximum velocity of 60–70 mph and 25–35 mph, respectively. These surface roads provide redundancy to the system in case of failure on the major expressways. Although transportation networks are highly redundant, it is assumed in this example that access to surface roads is limited to only two major links.

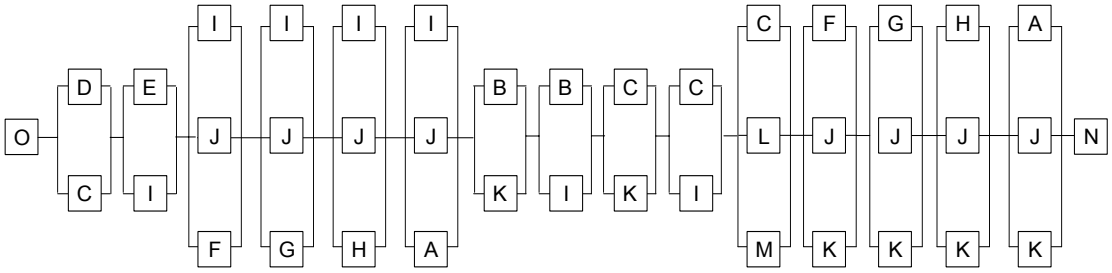

Fig. 5.7 Minimum cut-sets for idealized sub-network.

For the 15 cut-sets (C_m, where $m = 1,\ldots,15$) formulated in this example, let C_1 = {D, C} and C_2 = {E, I}, etc. until C_{15} = {A, J, K}. The failure of cut-set C_1 is denoted by E_1, and is the intersection of two component failures indicated below.

$$E_1 = \{(g_D \le 0) \cap (g_E \le 0)\}$$
$$E_2 = \{(g_E \le 0) \cap (g_I \le 0)\} \quad (5.14)$$

$$\vdots$$

$$E_{15} = \{(g_A \le 0) \cap (g_J \le 0) \cap (g_K \le 0)\}$$

By the inclusion-exclusion rule in Equation (5.8), the failure probability for the system is written below in Equation (5.15).

$$\begin{aligned} P_f = {} & P(E_1) + P(E_2) + \ldots + P(E_{15}) \\ & - [P(E_1E_2) + P(E_1E_3) + P(E_2E_3) + P(E_1E_4) + P(E_2E_4) + \ldots + P(E_{14}E_{15})] \\ & + [P(E_1E_2E_3) + P(E_1E_2E_4) + P(E_1E_2E_5) + P(E_1E_2E_6) + \ldots + P(E_{13}E_{14}E_{15})] \\ & - \ldots + P(E_1E_2 \cdots E_{15}) \end{aligned} \tag{5.15}$$

Table 5.3 Reliability case studies for varying degrees of correlation.

Case 1	Capacities are uncorrelated, Demands are uncorrelated
Case 2	Capacities are correlated ($\rho_D = 0.5$), Demands are correlated ($\rho_G = 0.5$)
Case 3	Capacities are correlated ($\rho_D = 0.9$), Demands are correlated ($\rho_G = 0.9$)

Table 5.4 Sensitivity with respect to component reliability. Results in table based on northern Hayward-Rodgers Creek fault source, $M_w = 7.1$ characteristic event. Most critical bridges (*C, K, I, B, D*) are boxed for this scenario event.

Case 1		Case 2		Case 3	
Component	$dP_f/d\beta$	Component	$dP_f/d\beta$	Component	$dP_f/d\beta$
C	-0.05	K	-0.06	K	-0.07
K	-0.05	C	-0.06	C	-0.05
I	-0.05	I	-0.05	B	-0.05
B	-0.04	B	-0.04	I	-0.03
D	-0.02	D	-0.02	D	-0.02
E	-0.01	J	-0.01	J	0.00
J	-0.01	E	-0.01	L	0.00
G	0.00	L	0.00	E	0.00
L	0.00	M	0.00	M	0.00
F	0.00	G	0.00	F	0.00
M	0.00	F	0.00	G	0.00
A	0.00	A	0.00	A	0.00
H	0.00	H	0.00	H	0.00
$P_f = 0.074$		$P_f = 0.126$		$P_f = 0.133$	

System failure sensitivities to component reliabilities, as described in Section 5.3.2, are indicated by $\partial P_f / \partial \beta_i$. The system failure probability is estimated for each of the three cases from Table 5.3, and shown in the bottom row of Table 5.4. It is worth noting here that the most important bridges on this network were identified for all events in the earthquake catalog. Despite minor

variations in the ordering of importance, five bridges were consistently important across all events in the earthquake catalog. These bridges are thus considered to be the most seismically vulnerable for sub-network viability. After selecting these most vulnerable bridges, the effect of retrofit upgrade on these important bridges to system risk curves is subsequently considered.

5.3.3 Risk Exceedance Curves with Retrofit

The probabilistic seismic risk assessment for the sub-network example incorporates the temporal and spatial uncertainty of earthquake arrivals, while these uncertainties are left untreated in the deterministic seismic risk assessment. Two different risk metrics are evaluated in this section using the earthquake catalog previously developed to characterize the SFBR hazard.

5.3.3.1 Annual $\mu+1\sigma$ Loss Exceedance Curves for Sub-Network

Before considering uncertainty in loss exceedance curves, the mean annual loss exceedance (MLE) is first constructed. The goal of constructing the MLE curve first is to measure the impact of retrofit for the most important bridges on these system risk curves. The mean annual loss exceedance for the application network was plotted under (*i*) currently built conditions, (*ii*) 30% increased capacity and (*iii*) 10% increased capacity of the same targeted bridges. A 30% increase in capacity implies that the fragility function shaking medians are increased by 30%. The plot is shown below in Figure 5.8. As expected, the MLE curves show the greatest shift in loss for the largest (30%) retrofit case. The smaller (10%) retrofit case results in relatively smaller improvements in the network mean annual loss exceedance. Only minor gains may be achieved for small improvements to individual components on the network. For example, a 1% annual rate of exceedance is associated with a total direct loss of 17% of the total replacement cost for components of this sub-network. If the 10% retrofit upgrade is considered for the most important bridges on the network, the same 1% annual rate of exceedance translates into a total direct loss of 15% of the total replacement cost of the components. However, for a 30% retrofit upgrade to the most important bridges, the 1% annual rate of exceedance translates into a total direct loss of 8% of the total replacement cost of components of this system.

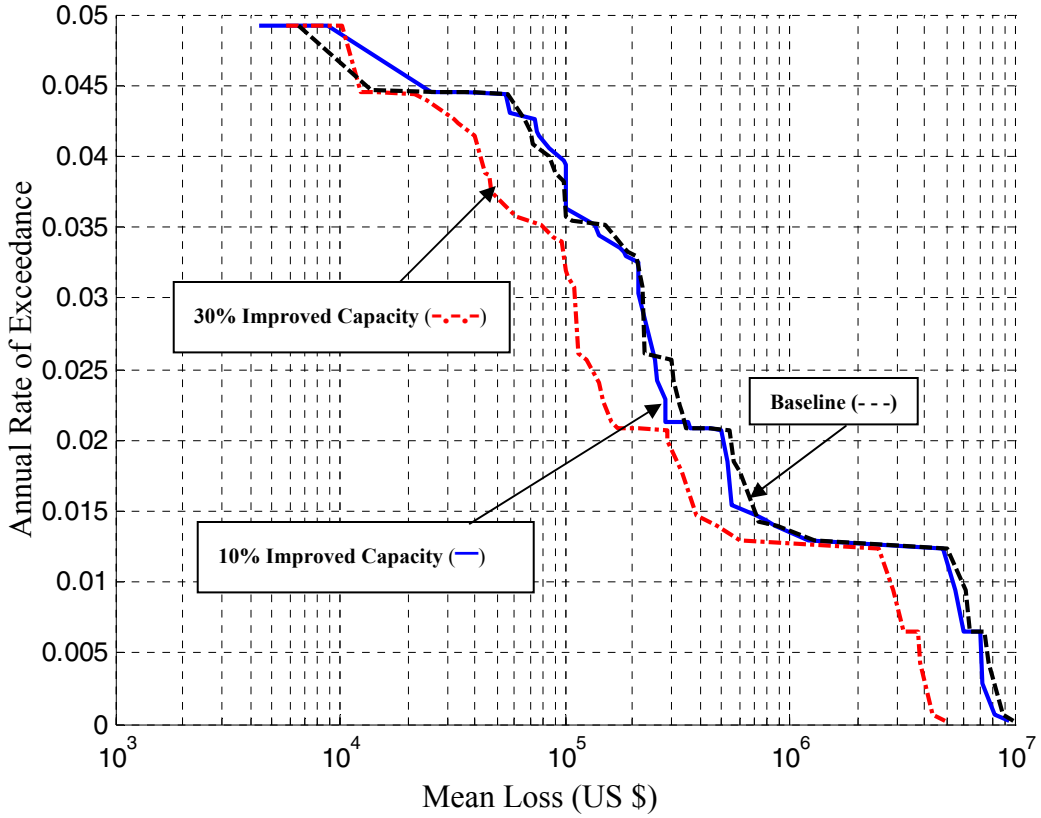

Fig. 5.8 A linear-log plot of annual rate of exceedance of *E*[*Loss*] for (*i*) baseline (--); (*ii*) 30% retrofit (-.); (*iii*) 5% retrofit (—) cases.

When including the uncertainty and correlation in ground motion and in damage, three cases were considered: (*a*) $\rho_G = \rho_D = 0$; (*b*) $\rho_G = \rho_D = 0.5$; and (*c*) $\rho_G = \rho_D = 0.9$. The influence of correlation creates a wide band of uncertainty. In Figure 5.9, the $\mu+1\sigma$ loss curves are plotted for varying cases of correlation (*a*-*c*).

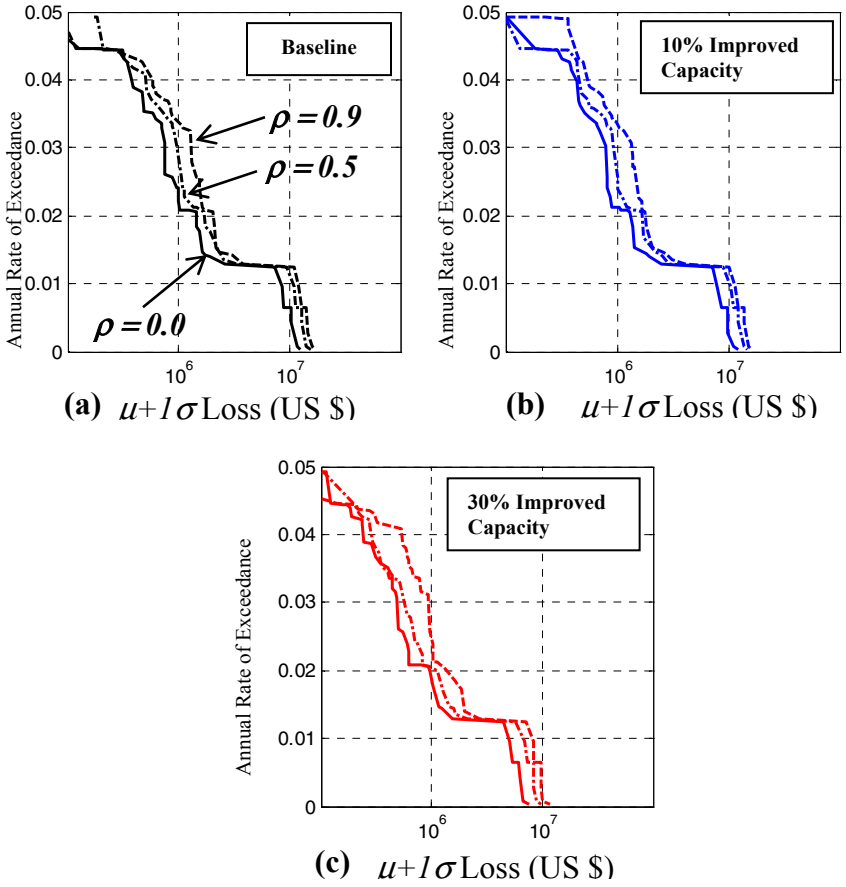

Fig. 5.9 $\mu+1\sigma$ Loss annual exceedance curves for varying levels of retrofit: (a) Baseline case (no retrofit upgrades), (b) 10% retrofit upgrade for important bridges, (c) 30% retrofit upgrade for important bridges.

The importance of damage dependencies and ground motion correlation for the risk to the transportation sub-network are demonstrated in Figure 5.9. The system risk curves provide a basis for understanding the relationship between the degree of bridge retrofit action and the influence of uncertainties and correlations in the determination of tolerable risk acceptance levels.

The non-dotted line in Figure 5.9a shows the annual rate of exceeding the $\mu+1\sigma$ loss without considering correlations or retrofit. After considering correlations, the $\mu+1\sigma$ exceedance curves shift toward the right, indicating that there is an underestimation of risk for a particular $\mu+1\sigma$ loss value. As a result of characterizing system risk curves accordingly, the bounds on the mean annual rate of exceeding a given level of $\mu+1\sigma$ can be quantified. For a given level of

$\mu+1\sigma$ loss, e.g., approximately 3% of the replacement cost of the structures, the exceedance rate varies between 1.7% to 3%. Likewise, for a given risk level, e.g., 1% annual exceedance, the $\mu+1\sigma$ loss can be bounded between 20% and 26% of the replacement cost of the structures.

It should be noted that the operational losses were not considered here. However, these losses, as well as downtime and casualty losses, must be accounted for in a complete decision-making retrofit framework.

5.3.3.2 Annual Exceedance Rate for System Failure Probability, P_f

Assuming components are uncorrelated in the network underestimates the system failure probability (P_f) significantly. The results from the FORM analysis for the system failure probability in a Northern Hayward-Rodgers Creek fault characteristic event of M_w = 7.1 are shown in Table 5.4. The scenario-based results demonstrated the importance of considering correlations in evaluating system reliability. However, the annual exceedance rate of a P_f further emphasizes the significance of considering correlations.

The left-most plots of Figure 5.10 (a, c) highlight the risk of exceeding various levels of network failure before any retrofit actions have taken place. The top figures in Figure 5.10 (a, b) are the system risk exceedance curves for P_f considering all earthquake events in the catalog. The bottom figures in Figure 5.10 (c, d) show the upper tail region of P_f annual rate of exceedance. After retrofitting the most important bridge structures on the network, the improved reliability of the system is shown on the right-most plots of Figure 5.10(b, d). A 10% retrofit upgrade was considered in this study.

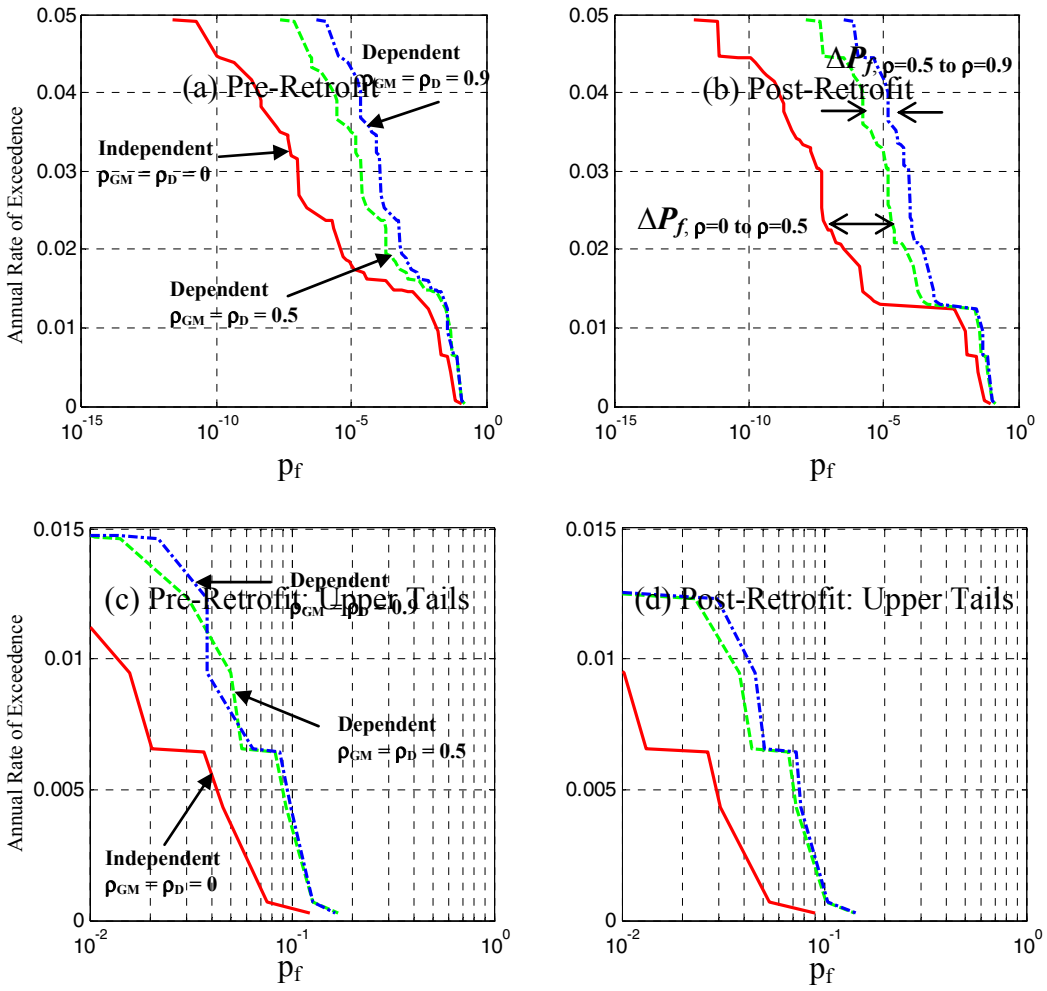

Fig. 5.10 Failure probability (P_f) of system under varying levels of correlation. (a) Pre-retrofit baseline performance, (b) post-retrofit performance, (c) pre-retrofit upper tails of system performance, (d) post-retrofit upper tails of system performance.

Several conclusions are emphasized from this research on system risk exceedance curves. First, mean annual loss exceedance curves in themselves do not adequately describe the risk to the system. Uncertainties and correlations must be incorporated in order to adequately assess bounds on annual loss exceedance. Second, as the level of correlation in ground motion and structural fragility functions increase, the network reliability decreases (e.g., P_f increases from 7% to 13%).

5.4 DISCUSSION

The importance of correlation effects in loss uncertainty, in retrofit prioritization, and in overall system performance is explored. Most notably, correlation in structural capacities and spatial ground motion correlation are demonstrated to have a large impact on the overall system performance and loss exceedance curves. As the $\mu+1\sigma$ loss exceedance plots show in Figure 5.9, the loss uncertainty results in wide error bands across the entire risk curve. In other applications, direct loss coefficients of variation as high as 1.6 were observed (Lee, et al. 2006).

Of interest to city and urban planners are the effects of correlation on retrofit prioritization strategy. Identifying critical bridges as those most vulnerable to structural failure is not adequate from a system point of view. Therefore, this research proposes an importance ordering for critical sub-networks based on the system reliability. The impact of selectively upgrading a limited number of bridge structures on the system reliability and loss curves is shown in Figure 5.10. By increasing capacities of a few of the most important bridges, the risk curves begin to show improved estimates on loss and performance. These methods are effective in bounding system direct loss and P_f for a given risk tolerance level (e.g., 1% annual exceedance). To complete the retrofit framework, the decision maker must address the economic constraints under which a retrofit program would be implemented.

5.5 APPENDIX: TREATMENT OF DEPENDENT RELIABILITY

For a dependent random vector ($\underline{\mathbf{X}} = X_1 \ldots X_n$), which may be the component capacities or the spectral acceleration (demands), for which the marginal cumulative distribution functions ($F_{\underline{\mathbf{x}}}(\underline{\mathbf{x}})$) and correlation matrix ($\underline{\mathbf{R}}$) in x-space are known, transform $\underline{\mathbf{X}}$ into correlated standard normal space ($F_{\mathbf{Z}}(\mathbf{z})$) where the PDF of $\mathbf{Z}$ is jointly normal $\phi_n(\underline{Z}, \underline{R_o})$ with correlation matrix $\underline{\mathbf{R_o}}$. Then the joint distribution of $\mathbf{X}$ is defined by:

$$f_{\underline{X}}(\underline{x}) = \phi_n(\underline{Z}, \underline{R_o}) \left| \frac{\partial z}{\partial x} \right| = \phi_n(\underline{Z}, \underline{R_o}) J_{zx} \tag{5.16}$$

where,

$$J_{zx} = \frac{\partial(z_1, z_2, \ldots z_n)}{\partial(x_1, x_2, \ldots x_n)} = \frac{f_{X_1}(x_1) \cdot f_{X_2}(x_2) \cdots f_{X_n}(x_n)}{\phi(z_1) \cdot \phi(z_2) \cdots \phi(z_n)} \tag{5.17}$$

$$\rho_{ij} = \int_{-\infty}^{\infty}\int_{-\infty}^{\infty}\left(\frac{x_i - \mu_i}{\sigma_i}\right)\left(\frac{x_j - \mu_j}{\sigma_j}\right)\phi_2(z_i, z_j, \rho_{o,ij})dz_i dz_j \tag{5.18}$$

Solving for $\rho_{o,ij}$ from ρ_{ij} involves an iterative procedure that balances the right- and left-hand side of Equation (5.18). Empirical relationships have already been developed for common multivariate distributions to approximate $\rho_{o,ij}$ (Der Kiureghian and Liu 1986). Once the $\underline{\mathbf{R}_o}$ is found from the above procedure, the correlated standard normal distribution $f_{\underline{\mathbf{Z}}}(\underline{\mathbf{z}})$ is known; thus for every pair of ($\mathbf{X_i}$, $\mathbf{X_j}$) an orthogonal transformation is used to obtain independent standard normal random variables to be used in the procedures applied here.

Until recently, solving the dependent reliability problem was a major hindrance to solving non-zero, non-unity dependence problems (no closed-form solution), but an algorithm by Ambartzumian et al. (1988) was used in CARDINAL (Menun 2004) to accurately approximate $\Phi_n(\underline{Z}, \underline{R_o})$.

6 Conclusions

This chapter provides a brief summary and discusses some key features of the probabilistic seismic risk-assessment framework for bridges in a transportation network.

The underlying goals that motivated the development of the framework are as follows:

- Consideration of spatial ground motion correlation and structure-to-structure damage correlation for spatially distributed components in a lifeline system is necessary in a risk modeling framework. Uncertainty in risk is incomplete without addressing and incorporating these sources of correlation.
- Computational demands of modeling risk uncertainty prohibit the modeling of complex dependencies for very large networks or for repeating the analyses for many earthquake scenarios. Thus, efficient simulation techniques for modeling a correlated random field of ground motion and for modeling damage-state dependencies between bridges in the network require special attention, depending upon the application purposes.
- Prior seismic risk assessments for transportation networks have generally relied upon a scenario-based approach. A probabilistic seismic risk assessment requires consideration of a catalog of earthquake events to represent the hazard in a region. Probabilistic seismic risk exceedance curves for system loss and reliability can more adequately describe the occurrence rate, or return period, on risk.

Beyond addressing these goals in further detail, a summary of the major contributions and direction for future work are discussed.

6.1 MAJOR CONTRIBUTIONS

While much of the previous research in seismic risk assessment for transportation networks has considered individual components of the system to be independent, this research demonstrates that risks are underestimated under this assumption. Additionally, previous research for risk assessment of transportation networks is typically based on a scenario-based approach. The scenario-based approach, however, does not provide a sense of the likelihood of assessed risks in time. Thus, the exceedance probability curves, based on risk assessment over many scenarios in space and time, are better suited to describe the risk.

This report focuses on the development of a framework for incorporating the effects of spatial ground motion correlation and structure-to-structure damage correlation in the probabilistic seismic risk assessment for transportation systems. In addition, this research focuses on several important aspects of characterizing hazard and risk for components in the network. The characterization of a correlated random field of ground motion shaking intensities for components in the network is first addressed. This step is followed by characterization of the damage state dependencies between multiple sites in the network. A linear dependency between structural damage states is explored in order to demonstrate the sensitivity of the risk to this source of correlation.

The goal of the next stage of this research was to efficiently solve the analytical formulations using various simulation techniques. These techniques were developed in order to extend modeling capabilities to potentially very large networks and to analyze the risk to these same networks under earthquake uncertainties. For this aim, discrete representation in modeling the uncertainties in earthquake size and occurrences are presented for use in a full probabilistic seismic risk assessment of the spatially distributed network.

In this research, the importance of accounting for uncertainties and correlations between components in the network is illustrated for several types of applications. First, the probability distribution function of the aggregate direct loss for correlated components is characterized in a scenario earthquake event. A sensitivity study of the loss distribution to parameters on structural replacement costs and damage factors is addressed. Second, for a given scenario, optimal post-event routes for sub-networks in the system are identified based on conditional damage data. Third, after identifying a suitable earthquake catalog to describe the hazard for a region of interest, the probabilistic loss exceedance curves for a portfolio of network bridges is assessed.

Fourth, the influence of the two sources of correlation on network reliability for a critical sub-network in the transportation system is quantified in a fully probabilistic approach. The network reliability for a given origin-destination pair is assessed in order to identify the most critical bridges for the system. Fifth, two options for retrofit upgrade of the selected critical bridges are compared on the basis of their influence on probabilistic risk exceedance curves.

This research addresses a methodology and efficient techniques for implementing a fully probabilistic seismic risk assessment for any class of spatially distributed systems, though applications in this report are specific to transportation networks. Furthermore, the framework and modeling approaches can be modified to accommodate a broad class of structural types, hazard types, or system types.

6.2 SUMMARY OF CONCLUSIONS

The expected value of loss to components, while important, does not adequately describe the risk to a spatially distributed system of bridges. In order to accurately assess the uncertainty in the overall risk, it is important to incorporate the effects of both spatial ground motion correlation and structure-to-structure damage correlation.

This research demonstrated that the uncertainty of the direct physical network loss is sensitive to correlations. Neglecting correlation underestimated the CoV of loss for the example networks presented in Section 3.3 by 20%–170%. For example, in subjecting the application network to a magnitude 8.0 event on the San Andreas fault, the loss CoV increases by approximately 30–40% when sites are moderately correlated in their ground motion shaking intensities (ρ_G = 0.5). Thus, the current practice of assuming uncorrelated ground motion intensities may lead to an underestimation of the risk.

The sensitivity study revealed that the two different sources of correlation impact loss CoV differently, however, this difference is not significant. For example, loss CoV increases by as much as 30–60% for moderate levels of damage correlation (ρ_D = 0.5). The results are comparable to those obtained when considering the effect of moderate levels of ground motion correlation (ρ_G = 0.5). Incorporating both sources of correlation resulted in even larger uncertainties for the two applications considered. For example, when considering moderate correlation levels for both sources, the loss CoV increases by 90% for the networks shown in

Section 3.3. Thus, the impact of the two individual sources of correlation and their combined sources of correlation on the loss CoV is potentially large.

A second sensitivity study of loss to varying levels of equi-correlated bridge damage in the network is considered based on a distance-dependent ground motion correlation model. This model was used to assess the ground motion correlation as a function of separation distance between sites. This correlation model yielded a high range of loss CoV values because sites in the application network were closely spaced.

The importance of correlations in assessing the second-order statistics on aggregate loss was thus far addressed. However, the importance of correlation effects in the full loss distribution is considered next in this research. It was observed that modeling dependencies in the network has an impact on the upper tails of the aggregate loss distribution. The aggregate loss distribution under the assumption of uncorrelated sites is well behaved, implying no heavy tails. When ground motion and damage correlation are introduced, the loss distribution becomes increasingly heavy tailed. Thus, by ignoring correlations, the likelihood of high losses is underestimated. In the application presented at the end of Section 4.4, the network is subjected to a $M_w = 7.0$ event on the Hayward fault. It was demonstrated in that example that the differences between ignoring correlation and considering correlation are pronounced for aggregate loss values greater than or equal to 9% of the total replacement cost of the bridge structures. While the means of the aggregate loss distributions are approximately equal, the standard deviation of the loss increases with increasing correlation.

The upper tails of the empirical PDF curves also highlight the important differences between the truncation bounds of the damage factor and the replacement cost. These variations reflect a wide range of possible low-probability, high-consequence losses. The damage-factor truncation bounds were subject to a sensitivity study based on the assumption that the mean damage factor from HAZUS (2002) is contained within each of the tested bounds. Replacement cost truncation bounds were also compared among various tested ranges, with demonstrated variations in the upper tail of the loss distribution.

This research illustrates not only the greater uncertainty in the aggregate loss distribution, but the effect dependencies in the system may have on post-event emergency routing and on system reliability. In prior research, optimal emergency paths were identified based on the assumption that bridges in the network are uncorrelated. A natural result of this assumption is that link travel times are also assumed to be uncorrelated. Consideration of dependencies

between bridges in the network, however, results in link travel times that are dependent. In this research, experiments for each of the link travel time realizations based on a M_w = 7.0 event on the Hayward fault for a network shown in Section 4.5 resulted in three different adaptive shortest-path configurations. These results highlight the importance of incorporating correlations in the routing decision process. In considering the system reliability for a network, it was observed that the network shown in Section 5.3 under the same M_w = 7.0 Hayward event, the failure probability of the network increases from 7.4% to 12.6% to 13.3% as ρ in ground motion and in damage for all sites in the network increases from 0 to 0.5 to 0.95.

A complete probabilistic seismic risk assessment is considered next based on the earthquake catalog representing the hazard in the region of interest. Bounds on the loss exceedance rate, bounds on the direct aggregate loss for a given level of risk, bounds on system reliability, and improvements to the system risk curve as a result of various retrofit efforts are quantified. Before considering uncertainty in loss exceedance curves, the mean or average annual loss exceedance is first constructed. The curves, which are produced after considering correlations and retrofit action, are then compared against the baseline mean annual loss exceedance curve which does not take into account correlations or retrofit upgrades. After considering correlations, the $\mu+1\sigma$ exceedance curves suggest an underestimation of risk for a given $\mu+1\sigma$ loss value. For example, in the application network of Section 5.3, a $\mu+1\sigma$ loss equal to 3% of the replacement cost of the network components corresponds to an annual exceedance rate that varies between 1.7% and 3%. For a 1% annual exceedance, the $\mu+1\sigma$ loss can be bounded between 20% and 26% of the total replacement cost of network components.

Next, the annual loss exceedance curves for the application network were developed for several cases of retrofit consideration. These cases include (a) currently built conditions — baseline, (b) 30% increased capacity and (c) 10% increased capacity of the same critical bridges. An increase in capacity is defined as an increase in the fragility function shaking medians. The greatest improvement in loss was observed for the larger (30%) retrofit case. The smaller (10%) retrofit case resulted in much smaller improvements in the network annual loss exceedance. Thus, minor gains may be achieved for small improvements to individual components on the particular network studied here. For example, a 1% annual rate of exceedance is associated with a loss of 17% of the network replacement cost. If the 10% retrofit upgrade is considered for the most important bridges on the network, the 1% annual rate of exceedance translates into a direct loss of 15% of component replacement cost. However, for a 30% retrofit upgrade to the most

important bridges, the 1% annual rate of exceedance translates into a loss of 8% of the network replacement cost.

6.3 FUTURE RESEARCH DIRECTIONS

In this research, spatial ground motion correlation and damage correlation models were developed and incorporated in a framework for assessing the loss uncertainty and distribution for a portfolio of bridge structures in a transportation network. Several limitations of these models require additional attention in future research. First, the distance-dependent isotropic ground motion correlation model presented here was based on a purely theoretical framework. Experimental validation of correlation distances and the parameters of this model require further attention. Furthermore, only spectral acceleration values at a period of 1 sec are considered for characterizing the site ground motion intensity measure. However, these intensity measures may show variation in their correlations at different spectral accelerations values. This should be investigated through experimental data, which may be collected from extensive recorded ground motions from linear or concentric arrays (Wang and Takada 2005; Harichandran and Vanmarcke 1986; Loh and Yeh 1988). Correlation models that are appropriate for near-fault events or for events which exhibit strong directivity should also be developed upon availability of data.

The dependencies in bridge damage are the result of bridges having been built around the same time by contractors using very similar materials and construction crews. This dependency must be further investigated by considering either a theoretical framework that accounts for these various sources of similarities in bridge construction or by developing expert opinion surveys which would provide data for modeling this correlation. The assumption of linear dependency between structures must also be experimentally validated.

Because the goal of this research was to identify these correlation models and develop the framework for quantifying risk, this research did not fully address the operational and network loss computation. These types of loss are likely to dominate the total loss, depending on several random factors. These difficult to quantify random factors include the time of day in which an earthquake occurs, the resources and relief effort available on-hand to immediately recover the system post-event, and the socio-political decisions that may affect the downtime recovery process.

Future research may involve further application of the correlation models into the risk analysis by (a) treating the transportation system as a stochastic network to model redistribution of traffic after bridge failures and (b) assessing operational, downtime, and casualty losses in the retrofit decision-making framework. The retrofit decision-making framework should ideally be treated as an optimization problem over many different earthquake scenarios describing hazard in a region (Liu and Fan 2007). Complexities in the network such as cascade effects (Dueñas-Osorio 2007) and unpredictable human behavior in the post-event transportation network may add further depth to the risk modeling effort.

Furthermore, other hazards specific to earthquakes and other hazards due to natural and man-made causes should be considered in the risk modeling. A disaggregation of loss by different modes of seismic hazard (i.e., landslide and liquefaction) and other types of hazard must be considered in order to make optimal risk decisions. The retrofit decision under all of these hazard types should be considered in an appropriate decision analysis framework that addresses the decision maker's risk attitude and the financial constraints involved (Porter and Kiremidjian 2001).

REFERENCES

Abramowitz, M. and I.A. Stegun (1964). *Handbook of Mathematical Functions with Formulas, Graphs and Mathematical Tables*. New York: Dover.

Ambartzumian, R., A. Der Kiureghian, V. Ohanian, and H. Sukiasian (1988). "Multinormal Probability by Sequential Conditioned Importance Sampling: Theory and Application." *Probabilistic Engineering Mechanics.* Volume 13, Number 4, pages 299–308.

Aslani, H. (2005). "Probabilistic Earthquake Loss Estimation and Loss Disaggregation in Buildings." *Ph.D. Dissertation, Department of Civil and Environmental Engineering, Stanford University*. Stanford, CA.

Augusti, G., M. Ciampoli, and D.M. Frangopol (1998). "Optimal Planning of Retrofitting Interventions on Bridges in a Highway Network." *Engineering Structures*. Volume 20, Number 11, pages 933–939.

Basöz, N. and A.S. Kiremidjian (1996). *Risk Assessment for Highway Transportation Systems. Technical Report No. 1184.* John A. Blume Earthquake Engineering Center, Department of Civil and Environmental Engineering, Stanford University, Stanford, CA.

Basöz, N. and A.S. Kiremidjian (1998). *Evaluation of Bridge Damage Data from the Loma Prieta and Northridge. California Earthquakes Technical Report MCEER-98-0004.* Multidisciplinary Center for Earthquake Engineering Research, State University of New York at Buffalo, Buffalo, NY.

Basöz, N. and J. Mander (1999). *Enhancement of the Highway Transportation Lifeline Module in HAZUS.* National Institute of Building Sciences, Washington D.C.

Bazzurro, P. and N. Luco (2005). "Accounting for Uncertainty and Correlation in Earthquake Loss Estimation." *Proceedings of 9th International Conference on Structural Safety and Reliability.* Rome, Italy. June 19–23, 2005, pages 2687–2694.

Boore, D.M., W.B. Joyner, and T.E. Fumal (1997). "Equations for Estimating Horizontal Response Spectra and Peak Acceleration from Western North American Earthquakes: A Summary of Recent Work." *Seismological Research Letters*. Volume 68, Number 1, pages 128–153.

California Department of Transportation (1993). *OSMI Coding Guide for SMS.* Division of Structures, Office of Structures Maintenance and Investigations, Sacramento, CA.

California Department of Transportation (2004). *Comparative Bridge Costs*. Division of Engineering Services, Office of Specifications and Estimates, Sacramento, CA.

Campbell, K.W. and H.A. Seligson (2003)."Quantitative Method for Developing Hazard-Consistent Earthquake Scenarios." *Proceedings of the 6th U.S. Conference and Workshop on Lifeline Earthquake Engineering.* Long Beach, CA. August 10–13, 2003, pages 829–838.

Chang, S.E., M. Shinozuka, and J.E. Moore (2000). "Probabilistic Earthquake Scenarios: Extending Risk Analysis Methodologies to Spatially Distributed Systems." *Earthquake Spectra*. Volume 16, Number 3, pages 557–572.

Cho, S., C.K. Huyck, S. Ghosh, and R.T. Eguchi (2003). "REDARS: A Validation Study of the REDARS Earthquake Loss Estimation Software Program." *Advancing Mitigation Technologies and Disaster Response for Lifeline Systems: Proceedings of the Sixth U. S. National Conference on Lifeline Earthquake Engineering,* ed. by James E. Beavers, Reston, VA: ASCE Technical Council on Lifeline Earthquake Engineering Monograph No. 25, pages 878–885.

Clark, K.M. (1986). "A Formal Approach to Catastrophe Risk Assessment and Management." *Proceedings of Casualty Actuarial Society.* Volume 73, Number 139, pages 69–92.

Der Kiureghian, A. and P.L. Liu (1986). "Structural Reliability under Incomplete Probability Information." *Journal of Engineering Mechanics*. Volume 112, Number 1, pages 85–104.

Dijkstra, E.W. (1959). "A Note on Two Problems in Connection with Graphs." *Numerische Mathematik.* Volume 1, pages 269–271.

Ditlevsen, O. (1981). *Uncertainty Modeling with Applications to Multidimensional Civil Engineering Systems.* New York: McGraw-Hill International Book Company.

Dueñas-Osorio, L. (2007). "Risk Assessment of Dynamic Urban Infrastructures." *Proceedings of Risk Acceptance and Risk Communication Workshop*. March 26–27, 2007. Stanford University, Stanford, CA.

Efron, B. and R. Tibshirani (1993). *An Introduction to the Bootstrap.* New York: Chapman & Hall.

Embrechts, P., F. Lindskog, and A. McNeil (2003). Modeling Dependence with Copulas and Applications to Risk Management. *Handbook of Heavy Tailed Distributions in Finance*, ed. S. Rachev. Amsterdam: Elsevier.

Fauré, H. (1992). "Good Permutations for Extreme Discrepancy." *Journal of Number Theory*. Volume 42, pages 47–56.

Ferson, S., R.B. Nelson, J. Hajagos, D. Berleant, J. Zhang, W.T. Tucker, L. Ginzburg, and W.L. Oberkampf (2004). *Dependence in Probabilistic Modeling, Dempster-Shafer Theory, and Probability Bounds Analysis. Sandia Report SAND2004-3072.* Sandia National Laboratories, Albuquerque, NM

Florian, A. (1992). "An Efficient Sampling Scheme: Updated Latin Hypercube Sampling." *Probabilistic Engineering Mechanics*. Volume 7, pages123–130.

Floyd, R.W. (1962). "Algorithm 97: Shortest Path." *Communications of the ACM.* Volume 5, Issue 6, page 345.

Franchin, P., A. Lupoi, and P.E. Pinto (2006). "On the Role of Road Networks in Reducing Human Losses after Earthquakes." *Journal of Earthquake Engineering.* Volume 10, Number 2, pages 195–206.

Friedman, D.M. (1975). *Computer Simulation in Natural Hazard Assessment.* Boulder: Institute of Behavioral Science, University of Colorado.

Halton, J.H. (1964). "Algorithm 247: Radical-Inverse Quasi-Random Point Sequence." *Communications of the ACM.* Volume 7, Number 12, pages 701–702.

Harichandran, S. and E.H. Vanmarcke (1986). "Stochastic Variation of Earthquake Ground Motion in Space and Time." *Ronald Journal of Engineering Mechanics*. Volume 112, Number 2, pages 154–174.

Huntington, D.E. and C.S. Lyrintzis (1998). "Improvements to and Limitations of Latin Hypercube Sampling." *Probabilistic Engineering Mechanics*. Volume 13, Number 4, pages 245–253.

Hill, I.D. (1973). "Algorithm AS66." *Applied Statistics.* Volume 22, Number 3, pages 424–427.

Iman, R.L. and W.J. Conover (1982). "Distribution-Free Approach to Inducing Rank Correlation among Input Variables." *Communications in Statistics: Simulation and Computation*. Volume 11, Number 3, pages 311–334.

Jeon, S.S. and T.D. O'Rourke (2005). "Northridge Earthquake Effects on Pipelines and Residential Buildings." Bulletin of the Seismological Society of America. Volume 95, Number 1, pages 294–318.

Kiremidjian, A.S., J. Moore, Y.Y. Fan, N. Basöz, O. Yazlali, and M. Williams (2006). "Pacific Earthquake Engineering Research Center Highway Demonstration Project." *Report No. PEER 2006/02*, Department of Civil and Environmental Engineering, Stanford University, Stanford, CA. Pacific Earthquake Engineering Research Center, Richmond, CA. 180 pages.

Kramer, S.L. (1996). *Geotechnical Earthquake Engineering*. Upper Saddle River, New Jersey: Prentice Hall, Inc.

Lee, R., A. Kiremidjian, and E. Stergiou (2006). "Uncertainty and Correlation of Losses for a Spatially Distributed System." *Proceedings of 8th National Conference in Earthquake Engineering*. April 18–22, 2006. San Francisco, CA.

Liu, C. Z. and Y.Y. Fan (2007). "A Two-Stage Stochastic Programming Model for Transportation Network Retrofit." *Transportation Research Board Annual Meeting*. Paper #07-0705, Washington D.C.

Loh, C.H. and Y.T. Yeh (1988). "Spatial Variation and Stochastic Modeling of Seismic Differential Ground Movement." *Earthquake Engineering and Structural Dynamics*. Volume 16, Number 4, pages 583–596.

Loh, C.H. and C.Y. Lee (2003). "Seismic Risk Assessment of Transportation Systems: Evaluation Immediately After Earthquake." *Advancing Mitigation Technologies and Disaster Response for Lifeline Systems: Proceedings of the Sixth U. S. National Conference on Lifeline Earthquake Engineering,* ed. by James E. Beavers, Reston, VA: ASCE Technical Council on Lifeline Earthquake Engineering Monograph No. 25, pages 289–299.

McGuire, R. K. (1990). "Effects of Uncertainties in Component Fragilities on Lifeline Seismic Risk Analysis." *Recent Lifeline Seismic Risk Studies*, ed. Anne S. Kiremidjian, Reston, VA: ASCE Technical Council on Lifeline Earthquake Engineering Monograph No 1, pages 14–22.

McKay, M.D., R.J. Beckman, and W.J. Conover (1979). "A Comparison of Three Methods for Selecting Values of Input Variables in the Analysis of Output from a Computer Code." *Technometrics*. Volume 21, Number 2, pages 239–245.

Melchers, R.E. (1999). *Structural Reliability Analysis and Prediction.* New York: John Wiley & Sons, Ltd.

Menun, C. (2004). *CARDINAL Structural Reliability Program*. User's Manual. Stanford, CA.

Miller, A.C. and T.R. Rice (1983). "Discrete Approximations of Probability Distributions." *Management Science*. Volume 29, Number 3, pages 352–363.

Moghtaderi-Zadeh, M. R.K. Wood, A. Der Kiureghian, R.E. Barlow, and T. Sato (1982). "Seismic Reliability of Flow and Communications Networks." *ASCE Journal of Technical Councils*. Volume 108, Number 1, pages 60–78.

Moghtaderi-Zadeh, M. and D. Diamantidis (1986). "Full Probabilistic Seismic Risk Evaluation." *Proceedings of the 8th European Conference on Earthquake Engineering*. Lisbon, Portugal. Volume 1, pages 2.5/1-2.5/8.

Moghtaderi-Zadeh, M. (1990). "Probabilistic Prediction of Losses to Lifeline Systems due to Earthquakes." *Recent Lifeline Seismic Risk Studies,* ed. Anne S. Kiremidjian, San Francisco, CA: ASCE Technical Council on Lifeline Earthquake Engineering Monograph No 1, pages 36–57.

NIBS/FEMA (2002). *HAZUS Earthquake Loss Estimation Methodology*. Service Release 2 (SR2) Technical Manual. Developed by the Federal Emergency Management Agency through agreements with the National Institute of Building Sciences, Washington D.C.

Niederreiter, H. (1992). *Random number generation and quasi-Monte Carlo methods.* CBMS-NSF regional conference series in applied mathematics, 63. Philadelphia, PA: Society for Industrial and Applied Mathematics.

Owen, A. (1998). "Monte Carlo Extension of Quasi-Monte Carlo." *Proceedings of the Winter Simulation Conference*, IEEE Press, pages 571–577.

Owen, A.B. (2005). *Monte Carlo, Quasi Monte Carlo, and Markov Chain Monte Carlo*. Stat 362 Course Reader.

Porter, K.A., and A.S. Kiremidjian (2001). *Assembly-Based Vulnerability and its Uses in Seismic Performance Evaluation and Risk-Management Decision-Making. Report No. 139.* John A. Blume Earthquake Engineering Center, Department of Civil and Environmental Engineering, Stanford University, Stanford, CA.

Rackwitz R. and B. Fiessler (1978). "Structural Reliability under Combined Random Load Sequences." *Computers and Structures.* Volume 9, pages 484–94.

Ripley, B.D. (1981). *Spatial Statistics*. New York: John Wiley & Sons, Inc.

Rubinstein, R.Y. (1981). *Simulation and the Monte Carlo Method*. New York: John Wiley & Sons, Inc.

Selcuk, A.S. and M.S. Yücemen (2000). "Reliability of Lifeline Networks with Multiple Sources under Seismic Hazard." *Natural Hazards*. Volume 12, Number 1, pages 1–18.

Shinozuka, M., T. Koike, and H. Kameda (1988). "Seismic Reliability of Hierarchical Lifeline Systems." *Proceedings of the ASCE Seismic Design and Construction of Complex Civil Engineering Systems,* ed. by Michael A. Cassaro and James D. Cooper, pages 47–64

Shinozuka, M. and G. Deodatis (1996). "Simulation of Multi-dimensional Gaussian Stochastic Fields by Spectral Representation." *Applied Mechanics Review.* Volume 49, pages 49–53.

Shinozuka. M., M.Q. Feng, H.K. Kim, S.H. Kim (2000). "Nonlinear Static Procedure for Fragility Curve Development." *ASCE Journal of Engineering Mechanics.* Volume 126, Number 12, pages 1267–1295.

Shinozuka, M., Y. Murachi, X. Dong, Y. Zhou, and M.J. Orlikowski (2003). "Seismic Performance of Highway Transportation Networks." *Proceedings of China-US Workshop on Protection of Urban Infrastructure and Public Buildings against Earthquakes and Manmade Disasters*. Beijing, China. February 21–22, 2003.

Sohn, J., T. J. Kim, G. J. D. Hewings, J. S. Lee and S.G. Jang (2003). "Retrofit Priority of Transport Network Links under an Earthquake." *Journal of Urban Planning and Development*. Volume 129, Number 4, pages 195–210.

Sobol, I.M. (1967). "The Distribution of Points in a Cube and the Approximate Evaluation of Integrals." *USSR Computational Mathematics and Mathematical Physics*. Volume 7, Issue 4, pages 86–112.

Song, J. and A. Der Kiureghian (2005). "Component Importance Measures by Linear Programming Bounds on System Reliability." *Proceedings of the 9th International Conference on Structural Safety and Reliability*. Rome, Italy. June 19–23, 2005, pages 1431–1438.

Steinbrugge, K.V. (1982). *Earthquakes, Volcanoes, and Tsunamis: An Anatomy of Hazards*. New York: Skandia-America Group.

Taleb-Agha, G. (1977). "Seismic Risk Analysis of Lifeline Networks." Bulletin of the Seismological Society of America. Volume 67, Number 6, pages 1625–1645.

Taylor C.E., M.R. Legg, J.M. Haber, and J.H. Wiggins (1985). "New Lifeline Multi-scenario Seismic Risk Techniques with a Model Application," *Civil Engineering Systems*. Volume 2, pages 77–83.

Taylor C.E., S.D. Werner, and S. Jakubowski (2001). "Walkthrough Method for Catastrophe Decision Making." *Natural Hazards Review.* Volume 2, Issue 4, pages 193–202.

Thomas, G. E. (1986). "Remark ASR65: A remark on algorithm AS 76: An Integral Useful in Calculating Noncentral t and Bivariate Normal Probabilities." *Applied Statistics.* Volume 35, pages 310–312.

Tuffin B. (1996). "A New Permutation Choice in Halton Sequences, in: Monte Carlo and Quasi-Monte Carlo." Volume 127, pages 427–435. New-York: Springer.

USGS (2002). *Interpolated Probabilistic Ground Motion for the Conterminous 48 States by Latitude Longitude, 2002 Data.* Retrieved May 1, 2006, from http://eqint.cr.usgs.gov/eq-men/html/lookup-2002-interp-06.html

USGS (2003). "Earthquake Probabilities in the San Francisco Bay Region: 2002–2031." *Open File Report 03-214*. Menlo Park, CA.

Vanmarcke, E. (1983). *Random Fields: Analysis and Synthesis.* Cambridge, MA: The MIT Press.

Walker, A.J. (1977). "An Efficient Method for Generating Discrete Random Variables with General Distributions." *ACM Transactions on Mathematical Software*. Volume 3, Issue 3, pages 253–256.

Wang, M. and T. Takada (2005). "Macrospatial Correlation Model of Seismic Ground Motions." *Earthquake Spectra.* Volume 21, Issue 4, pages 1137–1156.

Warnock, T.T. (1972). "Computational Investigations of Low-Discrepancy Point Sets." *Applications of Number Theory to Numerical Analysis (Proceedings of the Symposium, University of Montreal, Que., 1971)*, pages 319–343. New York: Academic Press.

Werner, S.D. and C.E. Taylor (1995). *Demonstration Seismic Risk Analysis of Highway-Roadway System in Memphis, Tennessee*. San Francisco, CA: Dames & Moore.

Werner S. D., C.E. Taylor, J.E. Moore (1997). "Loss Estimation due to Seismic Risks to Highway Systems." *Earthquake Spectra.* Volume 13, Number 4, pages 585–605.

Wesson, R.L. and D.M. Perkins (2001). "Spatial Correlation of Probabilistic Earthquake Ground Motion and Loss." *Bulletin of the Seismological Society of America*. Volume 91, Number 6, pages 1498–1515.

Yeh, S.C. and C.H. Loh (2001). "Seismic Reliability Analysis for Highway Network System." *Proceedings of the 8th International Conference on Structural Safety and Reliability*. Newport Beach, CA. June 17–22, 2001.

PEER REPORTS

PEER reports are available from the National Information Service for Earthquake Engineering (NISEE). To order PEER reports, please contact the Pacific Earthquake Engineering Research Center, 1301 South 46th Street, Richmond, California 94804-4698. Tel.: (510) 665-3405; Fax: (510) 665-3420.

PEER 2007/05 *Uncertainty and Correlation in Seismic Risk Assessment of Transportation Systems.* Renee G. Lee and Anne S. Kiremidjian. July 2007.

PEER 2007/02 *Campbell-Bozorgnia NGA Ground Motion Relations for the Geometric Mean Horizontal Component of Peak and Spectral Ground Motion Parameters.* Kenneth W. Campbell and Yousef Bozorgnia. May 2007.

PEER 2007/01 *Boore-Atkinson NGA Ground Motion Relations for the Geometric Mean Horizontal Component of Peak and Spectral Ground Motion Parameters.* David M. Boore and Gail M. Atkinson. May. May 2007.

PEER 2006/12 *Societal Implications of Performance-Based Earthquake Engineering.* Peter J. May. May 2007.

PEER 2006/11 *Probabilistic Seismic Demand Analysis Using Advanced Ground Motion Intensity Measures, Attenuation Relationships, and Near-Fault Effects.* Polsak Tothong and C. Allin Cornell. March 2007.

PEER 2006/10 *Application of the PEER PBEE Methodology to the I-880 Viaduct.* Sashi Kunnath. February 2007.

PEER 2006/09 *Quantifying Economic Losses from Travel Forgone Following a Large Metropolitan Earthquake.* James Moore, Sungbin Cho, Yue Yue Fan, and Stuart Werner. November 2006.

PEER 2006/08 *Vector-Valued Ground Motion Intensity Measures for Probabilistic Seismic Demand Analysis*. Jack W. Baker and C. Allin Cornell. October 2006.

PEER 2006/07 *Analytical Modeling of Reinforced Concrete Walls for Predicting Flexural and Coupled–Shear-Flexural Responses*. Kutay Orakcal, Loenardo M. Massone, and John W. Wallace. October 2006.

PEER 2006/06 *Nonlinear Analysis of a Soil-Drilled Pier System under Static and Dynamic Axial Loading.* Gang Wang and Nicholas Sitar. November 2006.

PEER 2006/05 *Advanced Seismic Assessment Guidelines.* Paolo Bazzurro, C. Allin Cornell, Charles Menun, Maziar Motahari, and Nicolas Luco. September 2006.

PEER 2006/04 *Probabilistic Seismic Evaluation of Reinforced Concrete Structural Components and Systems.* Tae Hyung Lee and Khalid M. Mosalam. August 2006.

PEER 2006/03 *Performance of Lifelines Subjected to Lateral Spreading.* Scott A. Ashford and Teerawut Juirnarongrit. July 2006.

PEER 2006/02 *Pacific Earthquake Engineering Research Center Highway Demonstration Project.* Anne Kiremidjian, James Moore, Yue Yue Fan, Nesrin Basoz, Ozgur Yazali, and Meredith Williams. April 2006.

PEER 2006/01 *Bracing Berkeley. A Guide to Seismic Safety on the UC Berkeley Campus.* Mary C. Comerio, Stephen Tobriner, and Ariane Fehrenkamp. January 2006.

PEER 2005/16 *Seismic Response and Reliability of Electrical Substation Equipment and Systems.* Junho Song, Armen Der Kiureghian, and Jerome L. Sackman. April 2006.

PEER 2005/15 *CPT-Based Probabilistic Assessment of Seismic Soil Liquefaction Initiation.* R. E. S. Moss, R. B. Seed, R. E. Kayen, J. P. Stewart, and A. Der Kiureghian. April 2006.

PEER 2005/14 *Workshop on Modeling of Nonlinear Cyclic Load-Deformation Behavior of Shallow Foundations.* Bruce L. Kutter, Geoffrey Martin, Tara Hutchinson, Chad Harden, Sivapalan Gajan, and Justin Phalen. March 2006.

PEER 2005/13 *Stochastic Characterization and Decision Bases under Time-Dependent Aftershock Risk in Performance-Based Earthquake Engineering*. Gee Liek Yeo and C. Allin Cornell. July 2005.

PEER 2005/12 *PEER Testbed Study on a Laboratory Building: Exercising Seismic Performance Assessment.* Mary C. Comerio, editor. November 2005.

PEER 2005/11 *Van Nuys Hotel Building Testbed Report: Exercising Seismic Performance Assessment.* Helmut Krawinkler, editor. October 2005.

PEER 2005/10 *First NEES/E-Defense Workshop on Collapse Simulation of Reinforced Concrete Building Structures.* September 2005.

PEER 2005/09 *Test Applications of Advanced Seismic Assessment Guidelines.* Joe Maffei, Karl Telleen, Danya Mohr, William Holmes, and Yuki Nakayama. August 2006.

PEER 2005/08 *Damage Accumulation in Lightly Confined Reinforced Concrete Bridge Columns.* R. Tyler Ranf, Jared M. Nelson, Zach Price, Marc O. Eberhard, and John F. Stanton. April 2006.

PEER 2005/07 *Experimental and Analytical Studies on the Seismic Response of Freestanding and Anchored Laboratory Equipment.* Dimitrios Konstantinidis and Nicos Makris. January 2005.

PEER 2005/06 *Global Collapse of Frame Structures under Seismic Excitations.* Luis F. Ibarra and Helmut Krawinkler. September 2005.

PEER 2005//05 *Performance Characterization of Bench- and Shelf-Mounted Equipment.* Samit Ray Chaudhuri and Tara C. Hutchinson. May 2006.

PEER 2005/04 *Numerical Modeling of the Nonlinear Cyclic Response of Shallow Foundations.* Chad Harden, Tara Hutchinson, Geoffrey R. Martin, and Bruce L. Kutter. August 2005.

PEER 2005/03 *A Taxonomy of Building Components for Performance-Based Earthquake Engineering.* Keith A. Porter. September 2005.

PEER 2005/02 *Fragility Basis for California Highway Overpass Bridge Seismic Decision Making.* Kevin R. Mackie and Bozidar Stojadinovic. June 2005.

PEER 2005/01 *Empirical Characterization of Site Conditions on Strong Ground Motion.* Jonathan P. Stewart, Yoojoong Choi, and Robert W. Graves. June 2005.

PEER 2004/09 *Electrical Substation Equipment Interaction: Experimental Rigid Conductor Studies.* Christopher Stearns and André Filiatrault. February 2005.

PEER 2004/08 *Seismic Qualification and Fragility Testing of Line Break 550-kV Disconnect Switches.* Shakhzod M. Takhirov, Gregory L. Fenves, and Eric Fujisaki. January 2005.

PEER 2004/07 *Ground Motions for Earthquake Simulator Qualification of Electrical Substation Equipment.* Shakhzod M. Takhirov, Gregory L. Fenves, Eric Fujisaki, and Don Clyde. January 2005.

PEER 2004/06 *Performance-Based Regulation and Regulatory Regimes.* Peter J. May and Chris Koski. September 2004.

PEER 2004/05 *Performance-Based Seismic Design Concepts and Implementation: Proceedings of an International Workshop.* Peter Fajfar and Helmut Krawinkler, editors. September 2004.

PEER 2004/04 *Seismic Performance of an Instrumented Tilt-up Wall Building.* James C. Anderson and Vitelmo V. Bertero. July 2004.

PEER 2004/03 *Evaluation and Application of Concrete Tilt-up Assessment Methodologies.* Timothy Graf and James O. Malley. October 2004.

PEER 2004/02 *Analytical Investigations of New Methods for Reducing Residual Displacements of Reinforced Concrete Bridge Columns.* Junichi Sakai and Stephen A. Mahin. August 2004.

PEER 2004/01 *Seismic Performance of Masonry Buildings and Design Implications.* Kerri Anne Taeko Tokoro, James C. Anderson, and Vitelmo V. Bertero. February 2004.

PEER 2003/18 *Performance Models for Flexural Damage in Reinforced Concrete Columns.* Michael Berry and Marc Eberhard. August 2003.

PEER 2003/17 *Predicting Earthquake Damage in Older Reinforced Concrete Beam-Column Joints.* Catherine Pagni and Laura Lowes. October 2004.

PEER 2003/16 *Seismic Demands for Performance-Based Design of Bridges.* Kevin Mackie and Božidar Stojadinovic. August 2003.

PEER 2003/15 *Seismic Demands for Nondeteriorating Frame Structures and Their Dependence on Ground Motions.* Ricardo Antonio Medina and Helmut Krawinkler. May 2004.

PEER 2003/14 *Finite Element Reliability and Sensitivity Methods for Performance-Based Earthquake Engineering.* Terje Haukaas and Armen Der Kiureghian. April 2004.

PEER 2003/13 *Effects of Connection Hysteretic Degradation on the Seismic Behavior of Steel Moment-Resisting Frames.* Janise E. Rodgers and Stephen A. Mahin. March 2004.

PEER 2003/12 *Implementation Manual for the Seismic Protection of Laboratory Contents: Format and Case Studies.* William T. Holmes and Mary C. Comerio. October 2003.

PEER 2003/11 *Fifth U.S.-Japan Workshop on Performance-Based Earthquake Engineering Methodology for Reinforced Concrete Building Structures.* February 2004.

PEER 2003/10 *A Beam-Column Joint Model for Simulating the Earthquake Response of Reinforced Concrete Frames.* Laura N. Lowes, Nilanjan Mitra, and Arash Altoontash. February 2004.

PEER 2003/09 *Sequencing Repairs after an Earthquake: An Economic Approach.* Marco Casari and Simon J. Wilkie. April 2004.

PEER 2003/08 *A Technical Framework for Probability-Based Demand and Capacity Factor Design (DCFD) Seismic Formats*. Fatemeh Jalayer and C. Allin Cornell. November 2003.

PEER 2003/07 *Uncertainty Specification and Propagation for Loss Estimation Using FOSM Methods.* Jack W. Baker and C. Allin Cornell. September 2003.

PEER 2003/06 *Performance of Circular Reinforced Concrete Bridge Columns under Bidirectional Earthquake Loading*. Mahmoud M. Hachem, Stephen A. Mahin, and Jack P. Moehle. February 2003.

PEER 2003/05 *Response Assessment for Building-Specific Loss Estimation.* Eduardo Miranda and Shahram Taghavi. September 2003.

PEER 2003/04 *Experimental Assessment of Columns with Short Lap Splices Subjected to Cyclic Loads*. Murat Melek, John W. Wallace, and Joel Conte. April 2003.

PEER 2003/03 *Probabilistic Response Assessment for Building-Specific Loss Estimation.* Eduardo Miranda and Hesameddin Aslani. September 2003.

PEER 2003/02 *Software Framework for Collaborative Development of Nonlinear Dynamic Analysis Program.* Jun Peng and Kincho H. Law. September 2003.

PEER 2003/01 *Shake Table Tests and Analytical Studies on the Gravity Load Collapse of Reinforced Concrete Frames.* Kenneth John Elwood and Jack P. Moehle. November 2003.

PEER 2002/24 *Performance of Beam to Column Bridge Joints Subjected to a Large Velocity Pulse.* Natalie Gibson, André Filiatrault, and Scott A. Ashford. April 2002.

PEER 2002/23 *Effects of Large Velocity Pulses on Reinforced Concrete Bridge Columns.* Greg L. Orozco and Scott A. Ashford. April 2002.

PEER 2002/22 *Characterization of Large Velocity Pulses for Laboratory Testing.* Kenneth E. Cox and Scott A. Ashford. April 2002.

PEER 2002/21 *Fourth U.S.-Japan Workshop on Performance-Based Earthquake Engineering Methodology for Reinforced Concrete Building Structures*. December 2002.

PEER 2002/20 *Barriers to Adoption and Implementation of PBEE Innovations.* Peter J. May. August 2002.

PEER 2002/19 *Economic-Engineered Integrated Models for Earthquakes: Socioeconomic Impacts.* Peter Gordon, James E. Moore II, and Harry W. Richardson. July 2002.

PEER 2002/18 *Assessment of Reinforced Concrete Building Exterior Joints with Substandard Details.* Chris P. Pantelides, Jon Hansen, Justin Nadauld, and Lawrence D. Reaveley. May 2002.

PEER 2002/17 *Structural Characterization and Seismic Response Analysis of a Highway Overcrossing Equipped with Elastomeric Bearings and Fluid Dampers: A Case Study.* Nicos Makris and Jian Zhang. November 2002.

PEER 2002/16 *Estimation of Uncertainty in Geotechnical Properties for Performance-Based Earthquake Engineering.* Allen L. Jones, Steven L. Kramer, and Pedro Arduino. December 2002.

PEER 2002/15 *Seismic Behavior of Bridge Columns Subjected to Various Loading Patterns.* Asadollah Esmaeily-Gh. and Yan Xiao. December 2002.

PEER 2002/14 *Inelastic Seismic Response of Extended Pile Shaft Supported Bridge Structures.* T.C. Hutchinson, R.W. Boulanger, Y.H. Chai, and I.M. Idriss. December 2002.

PEER 2002/13 *Probabilistic Models and Fragility Estimates for Bridge Components and Systems.* Paolo Gardoni, Armen Der Kiureghian, and Khalid M. Mosalam. June 2002.

PEER 2002/12 *Effects of Fault Dip and Slip Rake on Near-Source Ground Motions: Why Chi-Chi Was a Relatively Mild M7.6 Earthquake.* Brad T. Aagaard, John F. Hall, and Thomas H. Heaton. December 2002.

PEER 2002/11 *Analytical and Experimental Study of Fiber-Reinforced Strip Isolators*. James M. Kelly and Shakhzod M. Takhirov. September 2002.

PEER 2002/10 *Centrifuge Modeling of Settlement and Lateral Spreading with Comparisons to Numerical Analyses***.** Sivapalan Gajan and Bruce L. Kutter. January 2003.

PEER 2002/09 *Documentation and Analysis of Field Case Histories of Seismic Compression during the 1994 Northridge, California, Earthquake.* Jonathan P. Stewart, Patrick M. Smith, Daniel H. Whang, and Jonathan D. Bray. October 2002.

PEER 2002/08 *Component Testing, Stability Analysis and Characterization of Buckling-Restrained Unbonded Braces™.* Cameron Black, Nicos Makris, and Ian Aiken. September 2002.

PEER 2002/07 *Seismic Performance of Pile-Wharf Connections.* Charles W. Roeder, Robert Graff, Jennifer Soderstrom, and Jun Han Yoo. December 2001.

PEER 2002/06 *The Use of Benefit-Cost Analysis for Evaluation of Performance-Based Earthquake Engineering Decisions*. Richard O. Zerbe and Anthony Falit-Baiamonte. September 2001.

PEER 2002/05 *Guidelines, Specifications, and Seismic Performance Characterization of Nonstructural Building Components and Equipment*. André Filiatrault, Constantin Christopoulos, and Christopher Stearns. September 2001.

PEER 2002/04 *Consortium of Organizations for Strong-Motion Observation Systems and the Pacific Earthquake Engineering Research Center Lifelines Program: Invited Workshop on Archiving and Web Dissemination of Geotechnical Data, 4–5 October 2001*. September 2002.

PEER 2002/03 *Investigation of Sensitivity of Building Loss Estimates to Major Uncertain Variables for the Van Nuys Testbed.* Keith A. Porter, James L. Beck, and Rustem V. Shaikhutdinov. August 2002.

PEER 2002/02 *The Third U.S.-Japan Workshop on Performance-Based Earthquake Engineering Methodology for Reinforced Concrete Building Structures*. July 2002.

PEER 2002/01 *Nonstructural Loss Estimation: The UC Berkeley Case Study.* Mary C. Comerio and John C. Stallmeyer. December 2001.

PEER 2001/16 *Statistics of SDF-System Estimate of Roof Displacement for Pushover Analysis of Buildings.* Anil K. Chopra, Rakesh K. Goel, and Chatpan Chintanapakdee. December 2001.

PEER 2001/15 *Damage to Bridges during the 2001 Nisqually Earthquake.* R. Tyler Ranf, Marc O. Eberhard, and Michael P. Berry. November 2001.

PEER 2001/14 *Rocking Response of Equipment Anchored to a Base Foundation.* Nicos Makris and Cameron J. Black. September 2001.

PEER 2001/13 *Modeling Soil Liquefaction Hazards for Performance-Based Earthquake Engineering.* Steven L. Kramer and Ahmed-W. Elgamal. February 2001.

PEER 2001/12 *Development of Geotechnical Capabilities in OpenSees.* Boris Jeremi . September 2001.

PEER 2001/11 *Analytical and Experimental Study of Fiber-Reinforced Elastomeric Isolators*. James M. Kelly and Shakhzod M. Takhirov. September 2001.

PEER 2001/10 *Amplification Factors for Spectral Acceleration in Active Regions.* Jonathan P. Stewart, Andrew H. Liu, Yoojoong Choi, and Mehmet B. Baturay. December 2001.

PEER 2001/09 *Ground Motion Evaluation Procedures for Performance-Based Design.* Jonathan P. Stewart, Shyh-Jeng Chiou, Jonathan D. Bray, Robert W. Graves, Paul G. Somerville, and Norman A. Abrahamson. September 2001.

PEER 2001/08 *Experimental and Computational Evaluation of Reinforced Concrete Bridge Beam-Column Connections for Seismic Performance*. Clay J. Naito, Jack P. Moehle, and Khalid M. Mosalam. November 2001.

PEER 2001/07 *The Rocking Spectrum and the Shortcomings of Design Guidelines.* Nicos Makris and Dimitrios Konstantinidis. August 2001.

PEER 2001/06 *Development of an Electrical Substation Equipment Performance Database for Evaluation of Equipment Fragilities*. Thalia Agnanos. April 1999.

PEER 2001/05 *Stiffness Analysis of Fiber-Reinforced Elastomeric Isolators.* Hsiang-Chuan Tsai and James M. Kelly. May 2001.

PEER 2001/04 *Organizational and Societal Considerations for Performance-Based Earthquake Engineering.* Peter J. May. April 2001.

PEER 2001/03 *A Modal Pushover Analysis Procedure to Estimate Seismic Demands for Buildings: Theory and Preliminary Evaluation.* Anil K. Chopra and Rakesh K. Goel. January 2001.

PEER 2001/02 *Seismic Response Analysis of Highway Overcrossings Including Soil-Structure Interaction.* Jian Zhang and Nicos Makris. March 2001.

PEER 2001/01 *Experimental Study of Large Seismic Steel Beam-to-Column Connections.* Egor P. Popov and Shakhzod M. Takhirov. November 2000.

PEER 2000/10 *The Second U.S.-Japan Workshop on Performance-Based Earthquake Engineering Methodology for Reinforced Concrete Building Structures.* March 2000.

PEER 2000/09 *Structural Engineering Reconnaissance of the August 17, 1999 Earthquake: Kocaeli (Izmit), Turkey.* Halil Sezen, Kenneth J. Elwood, Andrew S. Whittaker, Khalid Mosalam, John J. Wallace, and John F. Stanton. December 2000.

PEER 2000/08 *Behavior of Reinforced Concrete Bridge Columns Having Varying Aspect Ratios and Varying Lengths of Confinement.* Anthony J. Calderone, Dawn E. Lehman, and Jack P. Moehle. January 2001.

PEER 2000/07 *Cover-Plate and Flange-Plate Reinforced Steel Moment-Resisting Connections.* Taejin Kim, Andrew S. Whittaker, Amir S. Gilani, Vitelmo V. Bertero, and Shakhzod M. Takhirov. September 2000.

PEER 2000/06 *Seismic Evaluation and Analysis of 230-kV Disconnect Switches.* Amir S. J. Gilani, Andrew S. Whittaker, Gregory L. Fenves, Chun-Hao Chen, Henry Ho, and Eric Fujisaki. July 2000.

PEER 2000/05 *Performance-Based Evaluation of Exterior Reinforced Concrete Building Joints for Seismic Excitation.* Chandra Clyde, Chris P. Pantelides, and Lawrence D. Reaveley. July 2000.

PEER 2000/04 *An Evaluation of Seismic Energy Demand: An Attenuation Approach.* Chung-Che Chou and Chia-Ming Uang. July 1999.

PEER 2000/03 *Framing Earthquake Retrofitting Decisions: The Case of Hillside Homes in Los Angeles.* Detlof von Winterfeldt, Nels Roselund, and Alicia Kitsuse. March 2000.

PEER 2000/02 *U.S.-Japan Workshop on the Effects of Near-Field Earthquake Shaking.* Andrew Whittaker, ed. July 2000.

PEER 2000/01 *Further Studies on Seismic Interaction in Interconnected Electrical Substation Equipment.* Armen Der Kiureghian, Kee-Jeung Hong, and Jerome L. Sackman. November 1999.

PEER 1999/14 *Seismic Evaluation and Retrofit of 230-kV Porcelain Transformer Bushings.* Amir S. Gilani, Andrew S. Whittaker, Gregory L. Fenves, and Eric Fujisaki. December 1999.

PEER 1999/13 *Building Vulnerability Studies: Modeling and Evaluation of Tilt-up and Steel Reinforced Concrete Buildings.* John W. Wallace, Jonathan P. Stewart, and Andrew S. Whittaker, editors. December 1999.

PEER 1999/12 *Rehabilitation of Nonductile RC Frame Building Using Encasement Plates and Energy-Dissipating Devices.* Mehrdad Sasani, Vitelmo V. Bertero, James C. Anderson. December 1999.

PEER 1999/11 *Performance Evaluation Database for Concrete Bridge Components and Systems under Simulated Seismic Loads.* Yael D. Hose and Frieder Seible. November 1999.

PEER 1999/10 *U.S.-Japan Workshop on Performance-Based Earthquake Engineering Methodology for Reinforced Concrete Building Structures.* December 1999.

PEER 1999/09 *Performance Improvement of Long Period Building Structures Subjected to Severe Pulse-Type Ground Motions.* James C. Anderson, Vitelmo V. Bertero, and Raul Bertero. October 1999.

PEER 1999/08 *Envelopes for Seismic Response Vectors.* Charles Menun and Armen Der Kiureghian. July 1999.

PEER 1999/07 *Documentation of Strengths and Weaknesses of Current Computer Analysis Methods for Seismic Performance of Reinforced Concrete Members.* William F. Cofer. November 1999.

PEER 1999/06 *Rocking Response and Overturning of Anchored Equipment under Seismic Excitations.* Nicos Makris and Jian Zhang. November 1999.

PEER 1999/05 *Seismic Evaluation of 550 kV Porcelain Transformer Bushings.* Amir S. Gilani, Andrew S. Whittaker, Gregory L. Fenves, and Eric Fujisaki. October 1999.

PEER 1999/04 *Adoption and Enforcement of Earthquake Risk-Reduction Measures.* Peter J. May, Raymond J. Burby, T. Jens Feeley, and Robert Wood.

PEER 1999/03 *Task 3 Characterization of Site Response General Site Categories.* Adrian Rodriguez-Marek, Jonathan D. Bray, and Norman Abrahamson. February 1999.

PEER 1999/02 *Capacity-Demand-Diagram Methods for Estimating Seismic Deformation of Inelastic Structures: SDF Systems.* Anil K. Chopra and Rakesh Goel. April 1999.

PEER 1999/01 *Interaction in Interconnected Electrical Substation Equipment Subjected to Earthquake Ground Motions.* Armen Der Kiureghian, Jerome L. Sackman, and Kee-Jeung Hong. February 1999.

PEER 1998/08 *Behavior and Failure Analysis of a Multiple-Frame Highway Bridge in the 1994 Northridge Earthquake.* Gregory L. Fenves and Michael Ellery. December 1998.

PEER 1998/07 *Empirical Evaluation of Inertial Soil-Structure Interaction Effects.* Jonathan P. Stewart, Raymond B. Seed, and Gregory L. Fenves. November 1998.

PEER 1998/06 *Effect of Damping Mechanisms on the Response of Seismic Isolated Structures.* Nicos Makris and Shih-Po Chang. November 1998.

PEER 1998/05 *Rocking Response and Overturning of Equipment under Horizontal Pulse-Type Motions.* Nicos Makris and Yiannis Roussos. October 1998.

PEER 1998/04 *Pacific Earthquake Engineering Research Invitational Workshop Proceedings, May 14–15, 1998: Defining the Links between Planning, Policy Analysis, Economics and Earthquake Engineering.* Mary Comerio and Peter Gordon. September 1998.

PEER 1998/03 *Repair/Upgrade Procedures for Welded Beam to Column Connections.* James C. Anderson and Xiaojing Duan. May 1998.

PEER 1998/02 *Seismic Evaluation of 196 kV Porcelain Transformer Bushings.* Amir S. Gilani, Juan W. Chavez, Gregory L. Fenves, and Andrew S. Whittaker. May 1998.

PEER 1998/01 *Seismic Performance of Well-Confined Concrete Bridge Columns.* Dawn E. Lehman and Jack P. Moehle. December 2000.

ONLINE REPORTS

The following PEER reports are available by Internet only at http://peer.berkeley.edu/publications/peer_reports.html

PEER 2007/101 *Generalized Hybrid Simulation Framework for Structural Systems Subjected to Seismic Loading.* Tarek Elkhoraibi and Khalid M. Mosalam. July 2007.

PEER 2007/100 *Seismic Evaluation of Reinforced Concrete Buildings Including Effects of Masonry Infill Walls.* Alidad Hashemi and Khalid M. Mosalam. July 2007.